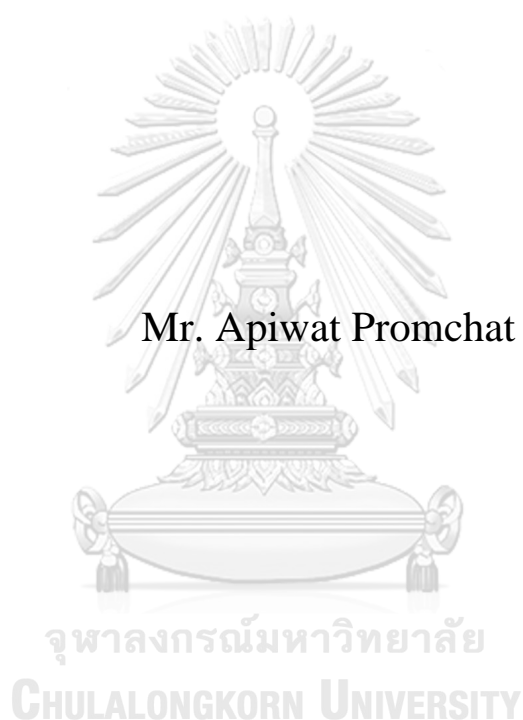


CELLULOSE-SUPPORTED FLUOROPHORE AS METAL ION SENSORS



A Dissertation Submitted in Partial Fulfillment of the Requirements
for the Degree of Doctor of Philosophy in Chemistry
Department of Chemistry
FACULTY OF SCIENCE
Chulalongkorn University
Academic Year 2021
Copyright of Chulalongkorn University

ฟลูออโรโพรบีนเซตลูโลสสำหรับเป็นตัวรับรู้อิออนโลหะ



วิทยานิพนธ์นี้เป็นส่วนหนึ่งของการศึกษาตามหลักสูตรปริญญาวิทยาศาสตรดุษฎีบัณฑิต
สาขาวิชาเคมี ภาควิชาเคมี
คณะวิทยาศาสตร์ จุฬาลงกรณ์มหาวิทยาลัย
ปีการศึกษา 2564
ลิขสิทธิ์ของจุฬาลงกรณ์มหาวิทยาลัย

Thesis Title	CELLULOSE-SUPPORTED FLUOROPHORE AS METAL ION SENSORS
By	Mr. Apiwat Promchat
Field of Study	Chemistry
Thesis Advisor	Professor MONGKOL SUKWATTANASINITT, Ph.D.
Thesis Co Advisor	Associate Professor THANIT PRANEENARARAT, Ph.D.

Accepted by the FACULTY OF SCIENCE, Chulalongkorn University in
Partial Fulfillment of the Requirement for the Doctor of Philosophy

..... Dean of the FACULTY OF
SCIENCE
(Professor POLKIT SANGVANICH, Ph.D.)

DISSERTATION COMMITTEE

..... Chairman
(Professor VUDHICHAJ PARASUK, Ph.D.)
..... Thesis Advisor
(Professor MONGKOL SUKWATTANASINITT, Ph.D.)
..... Thesis Co-Advisor
(Associate Professor THANIT PRANEENARARAT,
Ph.D.)
..... Examiner
(Professor PAITON RASHATASAKHON, Ph.D.)
..... Examiner
(Associate Professor KANET WONGRAVEE, Ph.D.)
..... External Examiner
(Gamolwan Tumcharern, Ph.D.)

CHULALONGKORN UNIVERSITY

อภิวัฒน์ พรหมชาติ : ฟลูออโรฟอร์บนเซลลูโลสสำหรับเป็นตัวรับรู้ไอออนโลหะ. (CELLULOSE-SUPPORTED FLUOROPHORE AS METAL ION SENSORS) อ.ที่ปรึกษาหลัก : ศ. ดร.มงคล สุขวัฒนาลินิทธิ์, อ.ที่ปรึกษาร่วม : รศ. ดร.ธนัญชฎี ปรานีนรารัตน์

ฟลูออเรสเซนต์ลิแกนด์จากสารอินทรีย์เป็นที่สนใจสำหรับการวิเคราะห์ไอออนโลหะทั้งในเชิงคุณภาพและเชิงปริมาณ การติดตัวรับรู้ฟลูออเรสเซนต์บนวัสดุเซลลูโลสเช่นกระดาษกรองเป็นแพลตฟอร์มที่ประหยัดและใช้งานง่ายในการวิเคราะห์ ณ จุดเก็บตัวอย่าง และสามารถสังเกตการเปลี่ยนแปลงได้ด้วยตาเปล่า ในงานวิจัยนี้ได้สังเคราะห์อนุพันธ์ของอะมิโดควิโนลีนชนิดใหม่เพื่อใช้เป็นฟลูออเรสเซนต์ลิแกนด์และพัฒนาตัวรับรู้บนกระดาษเพื่อใช้ในการตรวจวัดที่ใช้สะดวกโดยสามารถวิเคราะห์ผลด้วยตาเปล่าหรือซอฟต์แวร์ประมวลผลภาพ ในส่วนแรกของวิทยานิพนธ์ได้ใช้วิธีการสังเคราะห์แบบคู่ขนานบนของแข็ง เพื่อให้ได้มาโครอาร์เรย์กระดาษที่ใช้ในการคัดกรองและศึกษาความสัมพันธ์ระหว่างโครงสร้างของตัวรับรู้และชนิดของไอออนโลหะ การสังเคราะห์นี้ทำให้ได้ตัวรับรู้แบบอาร์เรย์ที่มีลิแกนด์ติดอยู่บนพื้นผิวของวัสดุเซลลูโลสด้วยพันธะโควาเลนต์ที่สามารถตรวจคัดกรองชนิดของไอออนโลหะอย่างรวดเร็ว ใช้งานได้ และวิเคราะห์ไอออนสังกะสีเชิงปริมาณได้ ส่วนที่สองของวิทยานิพนธ์ได้ศึกษาการปรับเปลี่ยนความไม่ชอบน้ำของอนุพันธ์ไกลซิลอะมิโดควิโนลีนอย่างเป็นระบบ และนำอนุพันธ์ที่ได้มาพัฒนาเป็นตัวรับรู้บนกระดาษที่สามารถวิเคราะห์ปริมาณไอออนโลหะจากกระดาษฟลูออเรสเซนต์ โดยระยะทางของเส้นฟลูออเรสเซนต์สัมพันธ์โดยตรงกับปริมาณของไอออนสังกะสี และมีช่วงการตรวจวัดที่เป็นเส้นตรง ทั้งนี้ช่วงการตอบสนองที่เป็นเส้นตรงต่อปริมาณของไอออนโลหะขึ้นอยู่กับความไม่ชอบน้ำของตัวรับรู้ไกลซิลอะมิโดควิโนลีน การวิเคราะห์ปริมาณไอออนสังกะสีในตัวอย่างน้ำดื่ม ผลิตภัณฑ์อาหารเสริม และปัสสาวะด้วยตัวรับรู้บนกระดาษโดยการวัดระยะทางเส้นฟลูออเรสเซนต์ ให้ผลลัพธ์ที่เปรียบเทียบกับวิธีมาตรฐานที่ใช้อะตอมมิคแอบซอร์ปชันสเปกโทรสโกปี

สาขาวิชา เคมี

ลายมือชื่อนิติศ

ปีการศึกษา 2564

.....
ลายมือชื่อ อ.ที่ปรึกษาหลัก

ลายมือชื่อ อ.ที่ปรึกษาร่วม

5972845023 : MAJOR CHEMISTRY

KEYWORD: metal ion sensor, paper-based sensor, Zn(II) sensor, quinoline derivatives
Apiwat Promchat : CELLULOSE-SUPPORTED FLUOROPHORE AS METAL ION SENSORS. Advisor: Prof. MONGKOL SUKWATTANASINITT, Ph.D.
Co-advisor: Assoc. Prof. THANIT PRANEENARARAT, Ph.D.

Organic fluorescent ligands are attractive for qualitative and quantitative analysis of metal ions. Cellulose substrates, especially for filter paper, have been demonstrated as one of the most economical and easy to use platform for fluorescent sensors applied in on-site analysis with naked-eye observation. In this work, new series of amidoquinoline derivatives were synthesized and investigated as the fluorescent ligands for developing paper-based sensors. The sensors are used for convenient analysis either by simple naked-eye observation or an image processing software. In the first part of this dissertation, parallel solid-state synthesis on filter paper macroarray was used for rapid discovery and structure-property relationships of metal ion fluorescent sensors. The ligands covalently bound on the cellulose surface was used as an array of functional substrate-supported sensors which offer rapid sensing screening, reusability, and enhanced sensitivity for metal ion identification and quantitative analysis of Zn^{2+} . The second part of the dissertation deals with a systematic modification of hydrophobicity of glyceryl amidoquinoline derivatives for development of paper-based sensors having distance-based quantification capability. The distance of the fluorescent lines created in the sensor showed linear relationships with the amount of Zn^{2+} . The linear dynamic ranges depended on the hydrophobicity of the amidoquinoline probes. The distance-based quantification of Zn^{2+} in drinking water, dietary supplement, and fertilizer samples by these paper-based sensors gave the results comparable with the standard method using the atomic absorption spectroscopy.

Field of Study: Chemistry
Academic Year: 2021

Student's Signature
Advisor's Signature
Co-advisor's Signature

ACKNOWLEDGEMENTS

First of all, I wish to express my sincere gratitude to my advisor, Professor Dr. Mongkol Sukwattanasinitt, for giving me a generous guidance, kind supervision, persistent support, and encouragement throughout this research.

My sincere thanks are also extended to my co-advisor, Associate Professor Dr. Thanit Praneenarat for giving me unparalleled knowledge, valuable advice, support, helpful suggestion throughout the entire course of this research. This thesis research would not be completed without their advice and support.

I am also grateful to Associate Professor Dr. Kanet Wongravee for giving suggestion and considerable helps in chemometrics.

My appreciation is also given to thesis defense committees, Professor Dr. Vudhichai Parasuk, Professor Dr. Paitoon Rashatasakhon, and Associate Professor Dr. Kanet Wongravee, and Dr. Gamolwan Tumcharern for their kind attention, beneficial suggestion and recommendations.

My sincere thanks also go to Professor Dr. Paitoon Rashatasakhon, Professor Dr. Sumrit Wacharasindhu, Assistant Professor Dr. Anawat Ajavakom, and Assistant Professor Dr. Sakulsuk Unarunotai for their attention and suggestion during our research group meeting. Furthermore, I appreciatively thank to my friends, Dr. Kanokthorn Boonkitpatarakul, Dr. Nattawut Yotapan, Dr. Waroton Paisuwan, Dr. Jutawat Hojitsiriyonont Jadetapong Klahan, Chakrit Yimsukanan, Atchareeporn Smata, Trin Saetan, Pawittra Chaibuth, Yuthana Sanpradit, Phoom Sangsuwan, and everyone in Material Advancement via Proficient Synthesis (MAPS group) for their honesty, spirit, good wish and help during my graduate research.

I would like to thank (1) Thailand Research Fund (RTA6180007) and Nanotechnology Center (NANOTECH), NSTDA, Ministry of Science and Technology, Thailand, through its program of Research Network NANOTECH (RNN) for the financial support of this work. I must also thank to Science Achievement Scholarship of Thailand (SAST) for great opportunity and scholarships.

Finally, I would like to express my thankfulness to my parents who always stand by my side during both of my pleasant and hard time.

Apiwat Promchat

TABLE OF CONTENTS

	Page
.....	iii
ABSTRACT (THAI)	iii
.....	iv
ABSTRACT (ENGLISH).....	iv
ACKNOWLEDGEMENTS	v
TABLE OF CONTENTS.....	vi
LIST OF TABLES	ix
LIST OF FIGURES	x
LIST OF ABBREVIATIONS.....	xvi
CHAPTER I INTRODUCTION.....	16
1.1. Background and literature survey	16
1.1.1. Fluorescent chemosensors	16
1.1.2. Colorimetric and fluorescent sensor on cellulose substrate	19
1.1.3. Distance-based sensors.....	24
1.2. Objectives	29
CHAPTER II Macroarray Synthesis on Filter Paper for Rapid Discovery and Structure-Property Relationships of Metal Ion Fluorescent Sensors.....	31
2.1. Introduction.....	31
2.2. Experiment.....	33
2.2.1. General information	33
2.2.2. Generation of aldehyde functional groups on paper	33
2.2.3. Reductive amination with reagent X.....	34
2.2.4. Carbodiimide coupling with reagent Y	34
2.2.5. Final finishing with wax printing	34
2.2.6. Probing fluorescence response with various metal ions.....	34

2.2.7. Digital conversion and quantitative analysis of fluorescence signals	35
2.2.8. Chemometrics.....	35
2.2.9. Synthesis of representative fluorophores	36
2.2.9.1. Synthesis of (2-amino- <i>N</i> -(quinolin-8-yl)acetamide) (Gly.8AQ).36	
2.2.9.2. Synthesis of (2-amino- <i>N</i> -(quinolin-6-yl)acetamide) (TFA salt of Gly.6AQ).	37
2.2.9.3. Synthesis of (2-amino- <i>N</i> -(quinolin-3-yl)acetamide) (Gly.3AQ).37	
2.2.9.4. Synthesis of 2-amino- <i>N</i> ^l -(quinolin-8-yl)succinamide) (Asn.8AQ)	38
2.3. Results and Discussion	40
2.4. Conclusions.....	58
CHAPTER III Synthesis of Quinoline Ligands with Tunable Hydrophobicity for Distance-Based Quantification of Metal Ion on Paper-Based Fluorescent Sensors	59
3.1. Introduction.....	59
3.2. Experimental section.....	60
3.2.1. General information	60
3.2.2. Synthetic procedures	61
3.2.2.1. 2-amino- <i>N</i> -(quinolin-8-yl)acetamide (Q1).....	61
3.2.2.2. 2-(methylamino)- <i>N</i> -(quinolin-8-yl)acetamide (Q2)	62
3.2.2.3. 2-(dimethylamino)- <i>N</i> -(quinolin-8-yl)acetamide (Q3).....	62
3.2.2.4. 2-(pyrrolidin-1-yl)- <i>N</i> -(quinolin-8-yl)acetamide (Q4)	63
3.2.2.5. 2-(piperidin-1-yl)- <i>N</i> -(quinolin-8-yl)acetamide (Q5).....	64
3.2.3. Measurement of photophysical properties	64
3.2.4. Preparation of the paper-based fluorescent sensing platform and analysis performance.....	64
3.3. Results and Discussion	65
3.3.1. Synthesis and characterization	65
3.3.2. Metal ion sensing study	66
3.3.3. Preparation and optimization of paper-based sensors	68
3.3.4. Real sample analysis	74

3.4. Conclusion	75
CHAPTER IV CONCLUSION	77
APPENDIX.....	78
REFERENCES	93
VITA.....	101



จุฬาลงกรณ์มหาวิทยาลัย
CHULALONGKORN UNIVERSITY

LIST OF TABLES

Table 2.1. A Jackknife (leave one out cross-validation) classification table for the ions based on the discrimination performance of the combined sensors (Asn.8AQ, Gly.3AQ, Gly.6AQ, Gly.8AQ) in discriminating 17 metal ions and a blank. The prediction accuracy was determined to be 72.35%.....	47
Table 2.2. A Jackknife (leave one out cross-validation) classification table for the ions based on the discrimination performance of the combined sensors (Asn.8AQ, Gly.3AQ, Gly.6AQ, Gly.8AQ) in discriminating 12 metal ions and a blank. The prediction accuracy was determined to be 93.64%.....	48
Table 2.3. Numerical data of graphs shown in Figure 2.7.	49
Table 2.4. Comparison of paper-based, fluorescent sensors for Zn ²⁺ ion.....	51
Table 3.1. Determination of Zn ²⁺ with distance-based sensor (Q3-Q5) in real samples.....	75

LIST OF FIGURES

- Figure 1.1.** Jablonski energy diagram describing fluorescence processes..... 17
- Figure 1.2.** Modes of fluorescence responses. 17
- Figure 1.3.** (a) Proposed complexation between **1** and Cu^{2+} ion and (b) bar chart of relative fluorescence intensity of **1** in the present of various metal ions (1×10^{-5} M).
..... 18
- Figure 1.4.** (a) Proposed complexation between **2** and metal ions, fluorescence spectra and pictures of (b) Zn^{2+} detection and (c) Cd^{2+} detection by using cysteine as an auxiliary reagent..... 18
- Figure 1.5.** (a) Proposed complexation between **3** and a metal ion, (b) photographic image of metal ion (0.1 mM) detected by **3** (1 mM) on wax patterned filter paper, (c) photographic image for simultaneous detection of Zn^{2+} and Cd^{2+} (1 nmol) by **3** (1 mM) after paper chromatographic separation and (d) images and normalized emission spectra of the fluorophores **3** and **3E** in the presence of Zn^{2+} in ethanol. 19
- Figure 1.6.** Schematic representation of activation and functionalization of PCB (**4**) modified cellulose paper with specific proteins (anti-BSA and anti-Fb) and the visualization of immobilized proteins via the detection of a fluorometric antigen probe. 20
- Figure 1.7.** Surface modification of CNCs with fluorescent label (**5**) and folic acid for improved cellular uptake demonstrated by fluorescent microscopic picture of immunofluorescence staining on DBTRG-05MG cells..... 21
- Figure 1.8.** (a) Synthetic steps involved in the surface modification of cellulose with imidazole ligands for **QD** immobilization. (b) Proposed multiplexed nucleic acid hybridization working mechanism for simultaneous detection of multiple DNA sequences. 22
- Figure 1.9.** Synthesis of Cellulose–Lysine–Schiff base (**6**). Pictures and proposed complexation between **6** and Hg^{2+} ion..... 23
- Figure 1.10.** (a) Synthesis of the chemosensor library and L-amino acid and acyl end cap library components and representative solid-phase chemosensors for Hg^{2+} and (b) images of solid-phase chemosensors (**7k-cc**) before and after addition of HgCl_2 24
- Figure 1.11.** Scheme of the theophylline detection based on competitive immunoassay on enzyme immunochromatographic test strip. 25
- Figure 1.12.** (a) Silver nanoparticles aggregated in the presence of glutathione. Reaction kinetics were slow, so wax baffles were used to reroute flow in a twisting

pattern through the channel. Detection of glutathione within the concentration range tested took approximately 10 min. (b) Formation of a brown precipitate product for glucose detection in approximately five minutes. (c) Formation of a bright red precipitate product from complexation of Ni^{2+} in approximately 15 min.26

Figure 1.13. (a) Schematic of distance-based sensor with a multi-layer device. Masking and sensing agents were inkjet printed in the pretreatment and detection zones. Passive timer was printed on the back of the device. Metal was quantified from a complex of ligand-metal precipitated on the substrate that generated a band of color with a length proportional to the amount of metal. Detection time in single and multi-channel devices were accomplished in ~30 and ~40 min, respectively. (b) Ni^{2+} , (c) Cu^{2+} , and (d) Fe^{2+} distance-based detection in single channel devices.27

Figure 1.14. (a) Schematic of distance-based sensor designs and analytical methods. (b) Distance-based sensor showed the increasing of white color band toward concentration of Cl^- . (c) Linear correlation in log scale of Cl^- concentration between 25 and 1000 ppm, $n = 3$28

Figure 1.15. Schematic of the (a) linear and (b) radial devices. Calibration plots presenting the linear range, working range (inset), and photographic images (inset) of (c) linear devices ($n = 8$) and (d) radial devices ($n = 8$) illuminated with a UV flashlight with selected concentrations to highlight the changes in signal length. Inset plot's axes and units are the same as the enlarged plot.29

Figure 2.1. Macroarray synthesis of fluorescent sensors and a subsequent sensing process. DIC = *N,N'*-diisopropylcarbodiimide; HOBt = 1-hydroxybenzotriazole; DMF = *N,N'*-dimethylformamide; HEPES = *N*-(2-hydroxyethyl)piperazine-*N'*-(2-ethanesulfonic acid)40

Figure 2.2. Structures of **Reagent X** and **Reagent Y** used in this study.41

Figure 2.3. Bar graphs representing intensities of each color channel from a) **Asn.8AQ**, b) **Gly.3AQ**, c) **Gly.6AQ**, d) **Gly.8AQ** in responding to Milli-Q water, Cr^{3+} , and Zn^{2+} over the period of two weeks.42

Figure 2.4. Preliminary fluorescence screening of all scaffolds synthesized via macroarray synthesis against selected metal ions.44

Figure 2.5. Structures and sensing profiles of four selected fluorophores discovered from the macroarray synthesis against a variety of metal ions.45

Figure 2.6. Three-dimensional LDA score plots of the combination of four fluorophores (**Asn.8AQ**, **Gly.3AQ**, **Gly.6AQ**, **Gly.8AQ**) in discriminating a) 17

analytes and one blank, and b) 12 analytes with one blank. Ten replicates were performed for each analyte.	46
Figure 2.7. Representative images, along with scattered plots, of fluorescence changes of Gly.8AQ when incubated with different concentrations of Zn^{2+} ion via one spotting (a, b) and 10-time repeated spotting (c, d) of each solution. Calibration plots are also shown as insets in each graph.	49
Figure 2.8. Fluorescence responses of Gly.8AQ in sensing Zn^{2+} after ten times. The sensor was recovered by sequestering Zn^{2+} with EDTA, a known chelator for Zn^{2+} ..	50
Figure 2.9. Response curves for Asn.8AQ in sensing (a) Zn^{2+} and (b) Cd^{2+}	50
Figure 2.10. Fluorescence spectra of surface-free Gly.8AQ (10 μ M with/without 50- μ M Zn^{2+} – excited at 300 nm) and Gly.6AQ (10 μ M with/without 50- μ M Cr^{3+} – excited at 365 nm). Inset: the images of the cuvettes containing the same solutions (but with 100- μ M fluorophores with/without 500- μ M metal ions) under the illumination of 365-nm light. Note: the photos of Gly.6AQ solutions were taken with 1-s longer exposure time than that of Gly.8AQ due to lower fluorescence intensities.	52
Figure 2.11. Fluorescence titration of Gly.8AQ with Zn^{2+} (excited at 300 nm)	53
Figure 2.12. UV-vis titration of Gly.8AQ with Zn^{2+}	53
Figure 2.13. Fluorescence titration of Gly.6AQ with Cr^{3+} (excited at 365 nm).....	54
Figure 2.14. UV-vis titration of Gly.6AQ with Cr^{3+}	54
Figure 2.15. Fluorescence titration of Gly.6AQ with Al^{3+} (excited at 365 nm).....	55
Figure 2.16. UV-vis titration of Gly.6AQ with Al^{3+}	55
Figure 2.17. MS titration between surface-free Gly.8AQ and Zn^{2+}	56
Figure 2.18. MS titration between surface-free Gly.6AQ and Cr^{3+}	57
Figure 2.19. NMR titration between surface-free Gly.8AQ and Zn^{2+}	58
Figure 3.1. Synthesis scheme of target aminoquinoline derivatives (Q1-Q5).....	66
Figure 3.2. Fluorescence spectra and photographic images of Q1-Q5 (10 μ M in 20 mM Tris-HCl solution) tested with various metal ions (100 μ M) and their fluorescence intensity enhancement ratios (I/I_0 measured @500 nm, excited @340 nm).....	67

Figure 3.3. Fluorescence intensity (@500 nm) of **Q1-Q5** solution (10 μM in 20 mM Tris-HCl buffer solution) in the absence (—) and presence (---) of Zn^{2+} (100 μM) at various pH.68

Figure 3.4. Absorption spectra of (a) **Q1**, (b) **Q2**, (c) **Q3**, (d) **Q4** and (e) **Q5** (40 μM) with gradual increment of Zn^{2+} concentration (0-800 μM) in Tris-HCl solution (20 mM) and (f) association constants of **Q1-Q5** with Zn^{2+}68

Figure 3.5. Experimental process for distance-based quantification of Zn^{2+} by paper-based sensor, a) drawing of paper-based channel sensing platform showing deposited point for ligand (L) and sample (S), (b) photographic image of paper-based sensor dipped into a Tris-HCl buffer solution (pH 7.4) in a closed chamber, (c) drying method of paper-based sensor after the solvent was reached the top of the platform (d) photographic images under black light illumination of paper-based sensor **Q4** (100 nmol) tested with various metal ions (20 nmol) eluted with Tris-HCl buffer solution pH 7.4 (0.20 M).69

Figure 3.6. Photographic images of **Q1-Q5** (100 nmol) deposited on wax barrier printed filter paper channel tested with various amounts of Zn^{2+} deposited from $\text{Zn}(\text{NO}_3)_2$ solutions eluted with Tris-HCl buffer pH 7.4 solution (0.20 M). Images were taken under black light illumination.70

Figure 3.7. Photographic images under black light illumination of **Q4** paper-based channel sensors tested with various amounts of Zn^{2+} (• 0, • 5, • 10, • 20, • 40, • 80 nmol) and their mean gray values measured at various distances along the channel. Deposited amounts of **Q4** are a) 1.0, b) 10, c) 100 and d) 1000 nmol. Mean gray values were averaged from 10 pixels across each channel of 3 sensor replicates.71

Figure 3.8. Photographic images under black light illumination of **Q4** (100 nmol) paper-based channel sensors tested with various amounts of Zn^{2+} (• 0, • 5, • 10, • 20, • 40, • 80 nmol) and their mean gray values measured at various distances along the channel. Eluent pH were a) 5.0, b) 6.0, c) 7.0 d) 7.4 and e) 8.0. Mean gray values were averaged from 10 pixels across each channel of 3 replicates.....72

Figure 3.9. Photographic images under black light illumination of **Q4** paper-based channel sensors tested with various amounts of Zn^{2+} (• 0, • 5, • 10, • 20, • 40, • 80 nmol) and their mean gray values plotted as a function distance along the channel. Channel width are a) 1.5 mm, b) 3.0 mm and c) 4.5 mm. Mean gray values were averaged from 10 pixels across each channel of 3 sensor replicates.73

- Figure 3.10.** The scatter plots of fluorescent distance observed by naked eye against a ruler scale (Δ) and image analysis using a threshold line at the 10 times of noises (\square), 3 replicates. 73
- Figure 3.11.** Photographic images under black light illumination of a) **Q3**, b) **Q4** and c) **Q5** (100 nmol) paper-based channel sensors tested with various amounts of Zn^{2+} eluted with Tris-HCl buffer pH 7.4 solution (0.20 M) and their calibration plots obtained from fluorescent distance that have mean gray value more than threshold level ($10 \times SD$ of mean gray value of controlled images, $n = 10$) 3 replicates. 74
- Figure A1.** 1H NMR spectrum of 2-amino-*N*-(quinolin-8-yl)acetamide (**Gly.8AQ**) in DMSO- d_6 78
- Figure A2.** ^{13}C NMR spectrum of 2-amino-*N*-(quinolin-8-yl)acetamide (**Gly.8AQ**) in DMSO- d_6 78
- Figure A3.** HRMS (ESI) spectrum of 2-amino-*N*-(quinolin-8-yl)acetamide (**Gly.8AQ**)..... 79
- Figure A4.** 1H NMR spectrum of 2-amino-*N*-(quinolin-6-yl)acetamide (unbound, TFA salt of **Gly.6AQ**) in DMSO- d_6 79
- Figure A5.** ^{13}C NMR spectrum of 2-amino-*N*-(quinolin-6-yl)acetamide (unbound, TFA salt of **Gly.6AQ**) in DMSO- d_6 80
- Figure A6.** HRMS (ESI) spectrum of 2-amino-*N*-(quinolin-6-yl)acetamide (unbound, TFA salt of **Gly.6AQ**)..... 80
- Figure A7.** 1H NMR spectrum of 2-amino-*N*-(quinolin-3-yl)acetamide (**Gly.3AQ**) in DMSO- d_6 81
- Figure A8.** ^{13}C NMR spectrum of 2-amino-*N*-(quinolin-3-yl)acetamide (**Gly.3AQ**) in DMSO- d_6 81
- Figure A9.** HRMS (ESI) spectrum of 2-amino-*N*-(quinolin-3-yl)acetamide (**Gly.3AQ**)..... 82
- Figure A10.** 1H NMR spectrum of 2-amino-*N*-(quinolin-8-yl)succinamide (**Asn.8AQ**) in DMSO- d_6 82
- Figure A11.** ^{13}C NMR spectrum of 2-amino-*N*-(quinolin-8-yl)succinamide (**Asn.8AQ**) in DMSO- d_6 83
- Figure A12.** HRMS (ESI) spectrum of 2-amino-*N*-(quinolin-8-yl)succinamide (**Asn.8AQ**) in DMSO- d_6 83
- Figure A13.** A heat map showing classification accuracies of four fluorophores (and their various combinations) for predicting 18 analytes, where the same colors between

each cell to its reference color on the right panel means the system predicted the metal ion correctly. Any different color means the system predicted it to be some other metal ions as shown exactly in each color.	84
Figure A14. ^1H NMR spectrum of 2-amino- <i>N</i> -(quinolin-8-yl)acetamide (Q1) in DMSO- <i>d</i> ₆	85
Figure A15. ^{13}C NMR spectrum of 2-amino- <i>N</i> -(quinolin-8-yl)acetamide (Q1) in DMSO- <i>d</i> ₆	85
Figure A16. HRMS (ESI) spectrum of 2-amino- <i>N</i> -(quinolin-8-yl)acetamide (Q1)...	86
Figure A17. ^1H NMR spectrum of 2-(methylamino)- <i>N</i> -(quinolin-8-yl)acetamide (Q2) in DMSO- <i>d</i> ₆	86
Figure A18. ^{13}C NMR spectrum of 2-(methylamino)- <i>N</i> -(quinolin-8-yl)acetamide (Q2) in DMSO- <i>d</i> ₆	87
Figure A19. HRMS (ESI) spectrum of 2-(methylamino)- <i>N</i> -(quinolin-8-yl)acetamide (Q2).....	87
Figure A20. ^1H NMR spectrum of 2-(dimethylamino)- <i>N</i> -(quinolin-8-yl)acetamide (Q3) in DMSO- <i>d</i> ₆	88
Figure A21. ^{13}C NMR spectrum of 2-(dimethylamino)- <i>N</i> -(quinolin-8-yl)acetamide (Q3) in DMSO- <i>d</i> ₆	88
Figure A22. HRMS (ESI) spectrum of 2-(dimethylamino)- <i>N</i> -(quinolin-8-yl)acetamide (Q3).	89
Figure A23. ^1H NMR spectrum of 2-(pyrrolidin-1-yl)- <i>N</i> -(quinolin-8-yl)acetamide (Q4) in DMSO- <i>d</i> ₆	89
Figure A24. ^{13}C NMR spectrum of 2-(pyrrolidin-1-yl)- <i>N</i> -(quinolin-8-yl)acetamide (Q4) in DMSO- <i>d</i> ₆	90
Figure A25. HRMS (ESI) spectrum of 2-(pyrrolidin-1-yl)- <i>N</i> -(quinolin-8-yl)acetamide (Q4).....	90
Figure A26. ^1H NMR spectrum of 2-(piperidin-1-yl)- <i>N</i> -(quinolin-8-yl)acetamide (Q5) in DMSO- <i>d</i> ₆	91
Figure A27. ^{13}C NMR spectrum of 2-(piperidin-1-yl)- <i>N</i> -(quinolin-8-yl)acetamide (Q5) in DMSO- <i>d</i> ₆	91
Figure A28. HRMS (ESI) spectrum of 2-(piperidin-1-yl)- <i>N</i> -(quinolin-8-yl)acetamide (Q5).....	92

LIST OF ABBREVIATIONS

Asn	asparagine
BOC	<i>tert</i> -butoxycarbonyl
calcd	calculated
¹³ C NMR	carbon-13 nuclear magnetic resonance
CDCl ₃	deuterated chloroform
DIC	diisopropylcarbodiimide
DMF	dimethylformamide
DMSO- <i>d</i> ₆	deuterated dimethyl sulfoxide
DMSO	dimethylsulfoxide
DNA	deoxyribonucleic acid
<i>d</i>	doublet (NMR)
<i>dd</i>	doublet of doublet (NMR)
EDC·HCl	<i>N</i> -(3-Dimethylaminopropyl)- <i>N'</i> -ethylcarbodiimide hydrochloride
ESIMS	electrospray ionization mass spectrometry
ESIPT	emission induced proton transfer
equiv	equivalent(s)
FT-IR	fourier transform infrared spectroscopy
g	gram (s)

Gly	glycine
^1H NMR	proton nuclear magnetic resonance
HEPES	4-(2-hydroxyethyl)-1-piperazineethanesulfonic acid
HOBt	hydroxybenzotriazole
HRMS	high resolution mass spectrum
Hz	hertz
h	hour (s)
ICT	intramolecular charge transfer
IR	infrared
J	coupling constant
K_a	association constant
LOD	limit of detection
MeOH	methanol
mg	milligram (s)
mL	milliliter (s)
mmol	millimole (s)
m/z	mass per charge
m	multiplet (NMR)
M.W.	molecular weight
M	molar

MHz	megahertz
nM	nanomolar
nmol	nanomole (s)
PET	photoinduced electron transfer
ppm	parts per million
rt	room temperature
s	singlet (NMR)
TFA	trifluoroacetic acid
TLC	thin layer chromatography
UV	ultraviolet
δ	chemical shift
$^{\circ}\text{C}$	degree Celsius
μg	microgram (s)
μL	microliter (s)
μM	micromolar (s)
Φ	quantum yield
% yield	percentage yield

CHAPTER I

INTRODUCTION

A fluorescent sensor is attractive for chemical, biological, and environmental analyses due to its high sensitivity and selectivity with capability in visualization and imaging. The sensor requires a chemical component of which emission intensity or wavelength can be altered upon interaction with an analyte. For metal ion sensor, the fluorescence changes are related to a certain set of general mechanisms such as photoinduced electron transfer (PET), intramolecular charge transfer (ICT) and emission induced proton transfer (ESIPT). Our previous study found that an aminoquinoline derivatized with a glycine unit was an efficient probe for Zn^{2+} with turn-on fluorescence signal. In this dissertation work, the amidoquinoline derivatives were studied as chemosensing probes and utilized in development of paper-based sensors. Along this line, background and literature survey are focused on fluorescent chemosensors, especially for those related to amidoquinoline derivatives, colorimetric and fluorescent sensors on cellulose substrate, and distance-based sensors.

1.1. Background and literature survey

1.1.1. Fluorescent chemosensors

Fluorescence spectroscopy has become one of the most sensitive analytical techniques. It also allows simple visualization for detecting and monitoring chemical and biological targets. The fluorescence processes that occur between the absorption and emission of light are generally described by a Jablonski diagram as shown in Figure 1.1. A photon absorption of a molecule, in UV or visible range, can induce electronic transition of the molecule from its ground state to one of its excited states (e.g. S₂). After the initial excitation, the molecule rapidly and nonradiatively relaxes to the lowest excited state (S₁) by changing its geometry via vibration and rotation. The following radiative relaxation from the lowest S₁ state to the ground state is called fluorescence. The length of time is often in the order of 10^{-9} to 10^{-8} seconds.

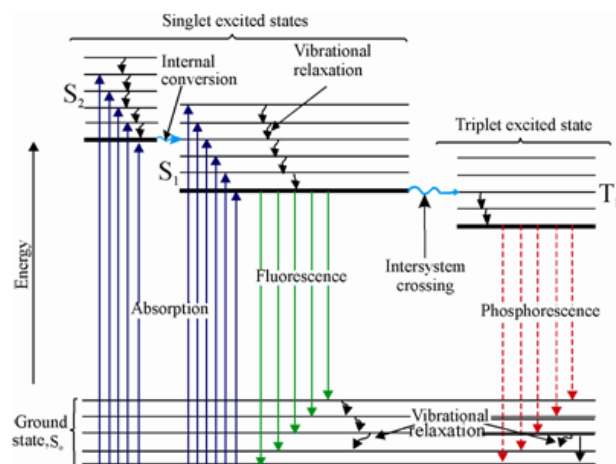


Figure 1.1. Jablonski energy diagram describing fluorescence processes. ¹

Most of the fluorescent chemosensors are composed of two main components: one is a receptor part for selective binding with the analytes, the other is a fluorophore for transducing the binding result into fluorescence signal, whether by fluorescence enhancement, quenching or wavelength shift (Figure 1.2). Besides, geometrical relaxation, some known mechanisms creating the fluorescence responses include PET², ICT³ and ESIPT. In addition, a chemosensor may be designed by using more than one sensing mechanism in order to enhance the fluorescent response. Quinoline derivative are one of the most versatile fluorophores that their fluorescence signals can be created via several mechanisms upon binding with metal ions.

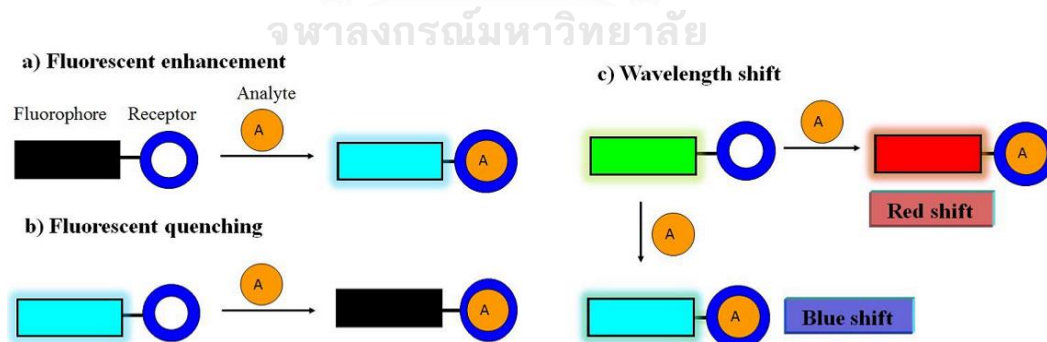


Figure 1.2. Modes of fluorescence responses.

In 2009, Dong and coworkers⁴ reported Cu²⁺ ion sensor **1** from glycine-*N*-8-quinolyamide which was grafted on multi-walled carbon nanotubes. This sensor showed fluorescent quenching for the Cu²⁺ ion with high selectivity and sensitivity and significant fluorescence enhancement for Zn²⁺ and Cd²⁺ ions. From Figure 1.3, the

fluorescence intensity of sensor **1** was gradually dropped with increasing Cu^{2+} concentration. The fluorescence intensity quenched by 95% with $10\ \mu\text{M}$ of Cu^{2+} . The detection limit for Cu^{2+} was claimed at $0.1\ \mu\text{M}$ in 30% methanol aqueous solution.

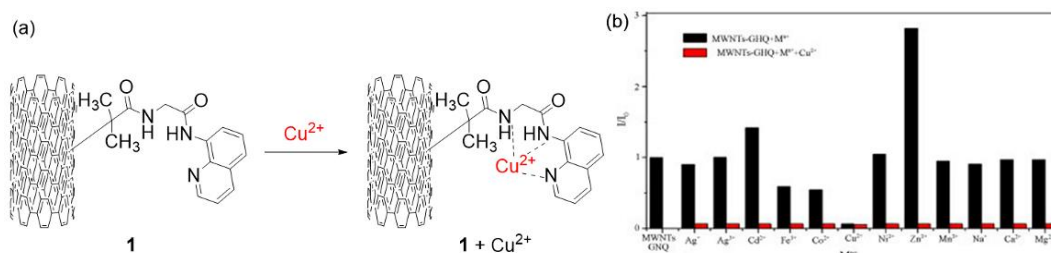


Figure 1.3. (a) Proposed complexation between **1** and Cu^{2+} ion and (b) bar chart of relative fluorescence intensity of **1** in the presence of various metal ions ($1 \times 10^{-5}\ \text{M}$).

In 2013, Ma and coworkers⁵ reported a simultaneous detection of Zn^{2+} and Cd^{2+} in aqueous solution by using 2-((pyridin-2-ylmethyl)amino)-*N*-(quinolin-8-yl)acetamide (**2**) as a turn-on fluorescent chemosensor. Cysteine was used as an auxiliary reagent for distinguishing Cd^{2+} from Zn^{2+} ions by selective fluorescence quenching of the solution containing the sensor and Cd^{2+} (Figure 1.4).

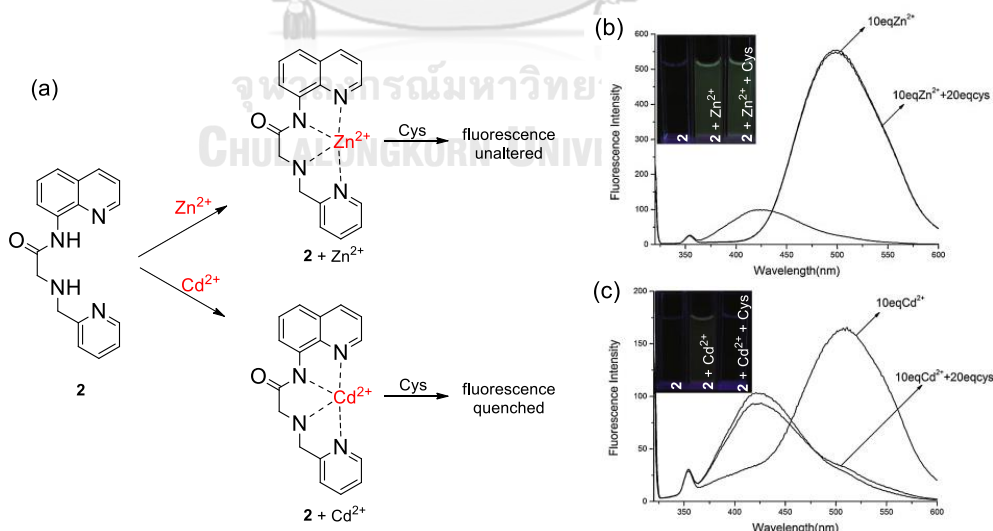


Figure 1.4. (a) Proposed complexation between **2** and metal ions, fluorescence spectra and pictures of (b) Zn^{2+} detection and (c) Cd^{2+} detection by using cysteine as an auxiliary reagent.

In 2018, our research group⁶ reported simple and effective amide derivative sensor (**3**) from 8-aminoquinoline and glycine for Zn^{2+} and Cd^{2+} possessing distinct fluorescence turn-on signal. The sensor showed selective fluorescence enhancement with Zn^{2+} with the limit of detection at $1.6 \mu\text{M}$ in aqueous solution. However, the sensor exhibited fluorescence enhancement with both Zn^{2+} and Cd^{2+} ions in ethanol solution and in solid form deposited on paper substrate. In Figure 1.5, the sensor was thus used as a visualizing agent for simultaneous detection of Zn^{2+} and Cd^{2+} after paper chromatographic separation. Moreover, the emissive color of the sensor is effectively tunable by the extension of π -conjugation from the quinoline ring (**3E**).

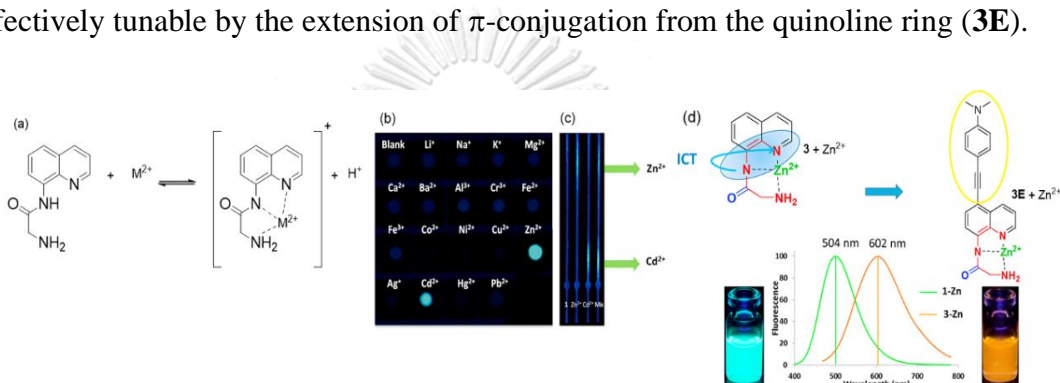


Figure 1.5. (a) Proposed complexation between **3** and a metal ion, (b) photographic image of metal ion (0.1 mM) detected by **3** (1 mM) on wax patterned filter paper, (c) photographic image for simultaneous detection of Zn^{2+} and Cd^{2+} (1 nmol) by **3** (1 mM) after paper chromatographic separation and (d) images and normalized emission spectra of the fluorophores **3** and **3E** in the presence of Zn^{2+} in ethanol.

1.1.2. Colorimetric and fluorescent sensor on cellulose substrate

Cellulose is an attractive supporting material for optical chemosensors due to its white color and chemically modifiable surface. Furthermore, cellulose is commercially and economically available in various forms such as flat sheet and elongated threads. Physical adsorption is the simplest methodology for sensor immobilization on cellulose. Physical adsorption using simple deposition such as dip-coating or drop-casting however often gives sensors with moderate sensing consistency properties and lower sensitivity, when comparing to the solution-based sensors, due to aggregation and dissolution upon usage. Reproducibility and sensitivity can be significantly improved by covalent attachment of the sensing probes because a more uniform monolayer is usually formed. The hydroxyl group at C6 of

cellulose is the most accessible point for covalent attachment via esterification or alkylation.

In 2014, Jiang and coworkers⁷ reported a method for modification of cellulose paper via ester linkage between poly(carboxybetaine) (**4**) by using surface-initiated atom transfer radical polymerization. Specific proteins such as anti-BSA and anti-Fb were then immobilized to the poly(carboxybetaine) modified cellulose by EDC/NHS coupling agent. In Figure 1.6, the functionalized cellulose paper was used as a paper-based microfluidic device and gave very low background signal because super hydrophilic property of poly(carboxybetaine) minimized non-specific protein binding.

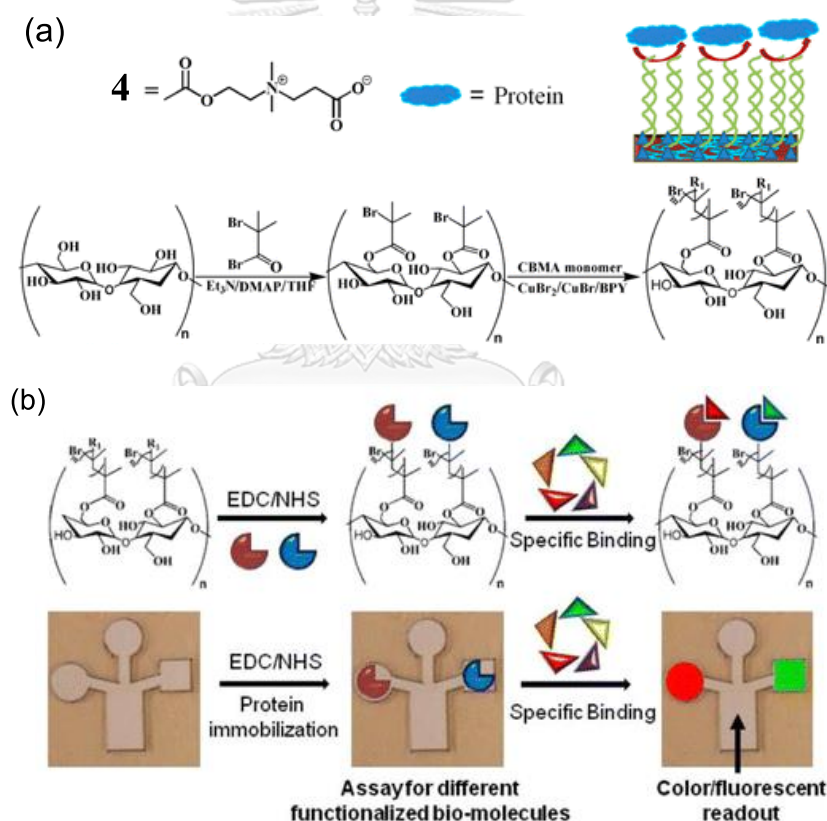


Figure 1.6. Schematic representation of activation and functionalization of PCB (**4**) modified cellulose paper with specific proteins (anti-BSA and anti-Fb) and the visualization of immobilized proteins via the detection of a fluorometric antigen probe.

In 2014, Roman and coworkers⁸ reported the synthesis of covalently attached folic acid and a fluorophore (**5**) on cellulose nanocrystals (CNCs). The hydroxyl group on surface of the cellulose nanocrystals was first converted to amino group by

reacting with an excess of epichlorohydrin in ammonium hydroxide aqueous solution. In this step, grafting of polymerized epichlorohydrin might occur but it is not expected to hinder further functionalization as long as it does not lead to cross-linking. A fluorescein fluorophore (**5**) and folic acid were consecutively attached to the amino groups. The modified cellulose nanocrystals showed excellent cellular uptake and was used for the targeted delivery of chemotherapeutic agents to folate receptor-positive cancer cells demonstrated by immunofluorescence staining on human and rat brain tumor cells (Figure 1.7).

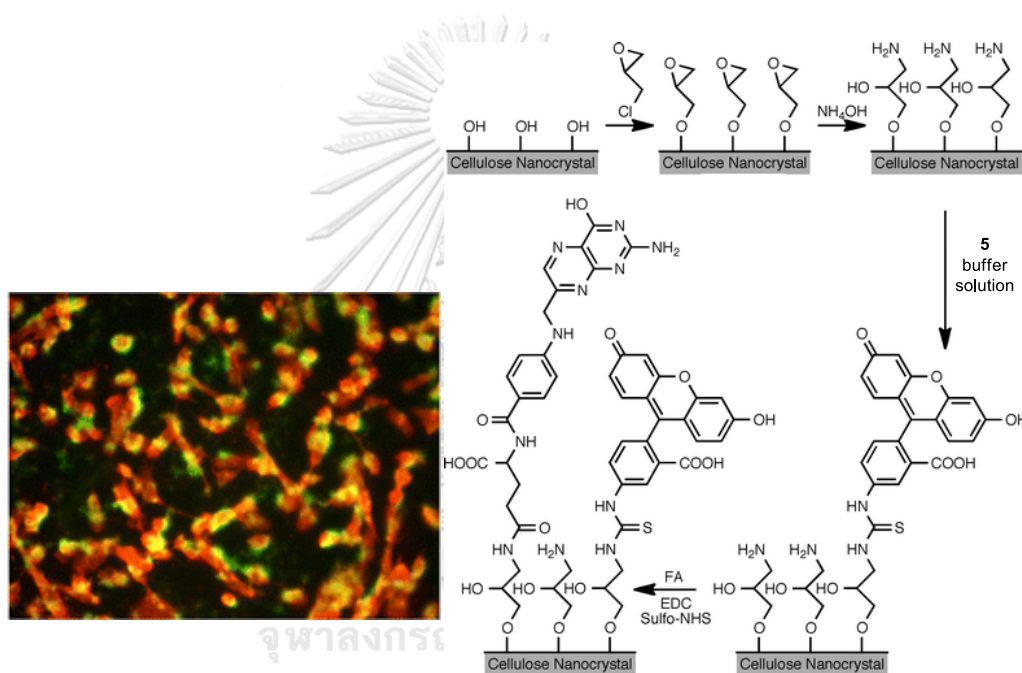


Figure 1.7. Surface modification of CNCs with fluorescent label (**5**) and folic acid for improved cellular uptake demonstrated by fluorescent microscopic picture of immunofluorescence staining on DBTRG-05MG cells.

The esterification and alkylation of native cellulose usually gives low degree of functionalization due to its extensive intramolecular and intermolecular hydrogen bonds restricting its solubility in all common organic solvents. Another alternative reaction involves oxidative cleavage of C3-C4 bond to produce aldehydes. The oxidized cellulose is more reactive than the native cellulose surface due to its reduced hydrogen bonds and lower crystallinity. Periodate is a reagent of choice as it gives high chemoselectivity and can be used in water media.

In 2011, Hormi and coworkers⁹ reported effective oxidation of cellulose to the dialdehyde cellulose with sodium periodate at elevated temperatures. The efficiency of the periodate oxidation can be further improved by using LiCl and other metal chlorides supposedly via a reduction of inter and intra molecular hydrogen bonds between the cellulose polymers. By using LiCl at elevated temperatures, sufficient aldehyde contents can be achieved within short oxidation times with reduced amount of periodate.

In 2013, Krull and coworkers¹⁰ reported a multiplexed solid-phase QD-FRET nucleic acid hybridization assay on a paper-based platform in Figure 1.8. The surface modification of filter paper was prepared by using Hormi's oxidation method followed by functionalization with imidazole groups via reductive amination. Subsequent immersion of the modified filter paper into a solution of green and red quantum dots (QD) successfully immobilized the quantum dot on the paper surface via imidazole binding. The QD immobilized filter paper was demonstrated for FRET nucleic acid hybridization assays for simultaneous detection of multiple DNA sequences.

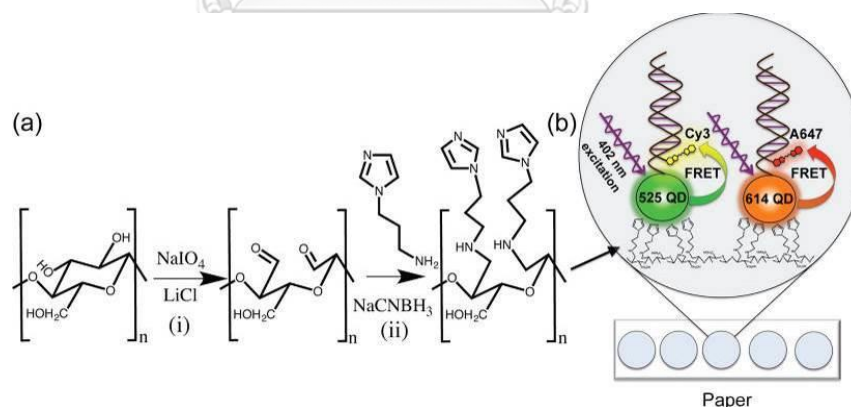


Figure 1.8. (a) Synthetic steps involved in the surface modification of cellulose with imidazole ligands for QD immobilization. (b) Proposed multiplexed nucleic acid hybridization working mechanism for simultaneous detection of multiple DNA sequences.

In 2014, Chauhan and Kumari¹¹ reported the new Schiff bases of oxidized cellulose (**6**) as Hg²⁺ sensor in Figure 1.9. Cellulose filaments were first alkylated with different alkyl bromides in basic condition followed by periodate oxidation to

generate dialdehyde moiety. Finally, imination between aldehyde moiety and *L*-lysine monohydrochloride in buffer solution pH 7.2 to give the desired modified cellulose. The synthesized material was investigated as a sensor-adsorbent for simple, rapid, highly selective, and simultaneous detection and removal of Hg^{2+} ion in aqueous solution. Hg^{2+} sensing was analyzed with naked-eye detection and fluorescence spectroscopy. The sensing material were regenerated by treatment with HCl solution and reused for 8 cycles.

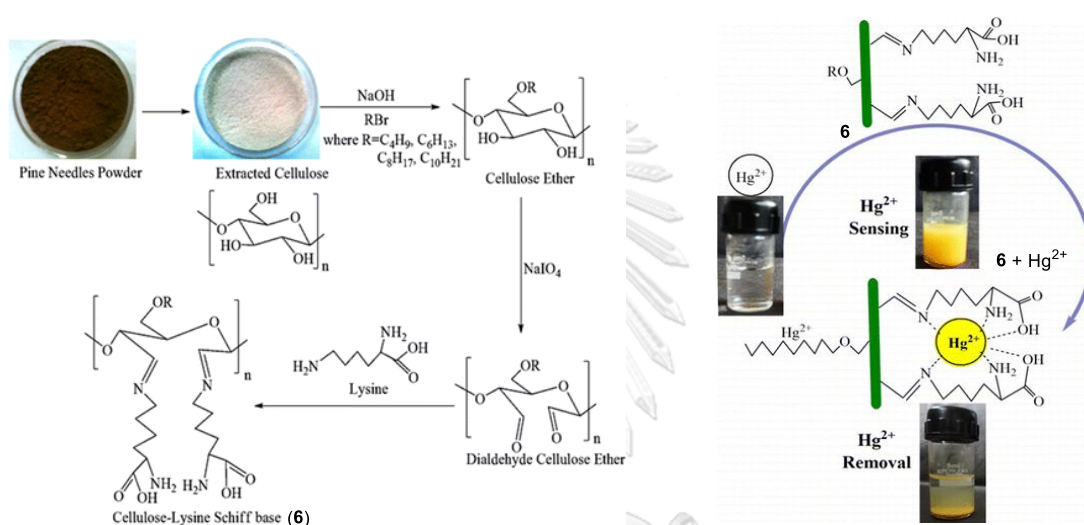


Figure 1.9. Synthesis of Cellulose–Lysine–Schiff base (6). Pictures and proposed complexation between 6 and Hg^{2+} ion.

In 2005, Finney and coworkers¹² reported a new and broadly applicable approach for identification of new fluorescent chemosensors by using reversing discovery paradigm via combinatorial search in Figure 1.10. The library of 198 spatially arrayed was created from solid synthesis between PEG-derivatized aminomethyl polystyrene resin which was synthesized from ArgogelTM-NH₂ resin coupling with 2,6-biarylpyridine-4-carboxaldehyde (7) as a core sensor and various amino acids with acylating end cap as a receptor. Library members were transferred to 96-well plates and evaluated in parallel for their response to 11 metal ions, as evaluated with a microscope in a dark room using a hand-held TLC lamp as the illumination source. A new class of chemosensors (7a - 7cc) for Hg^{2+} detection was found from this array.

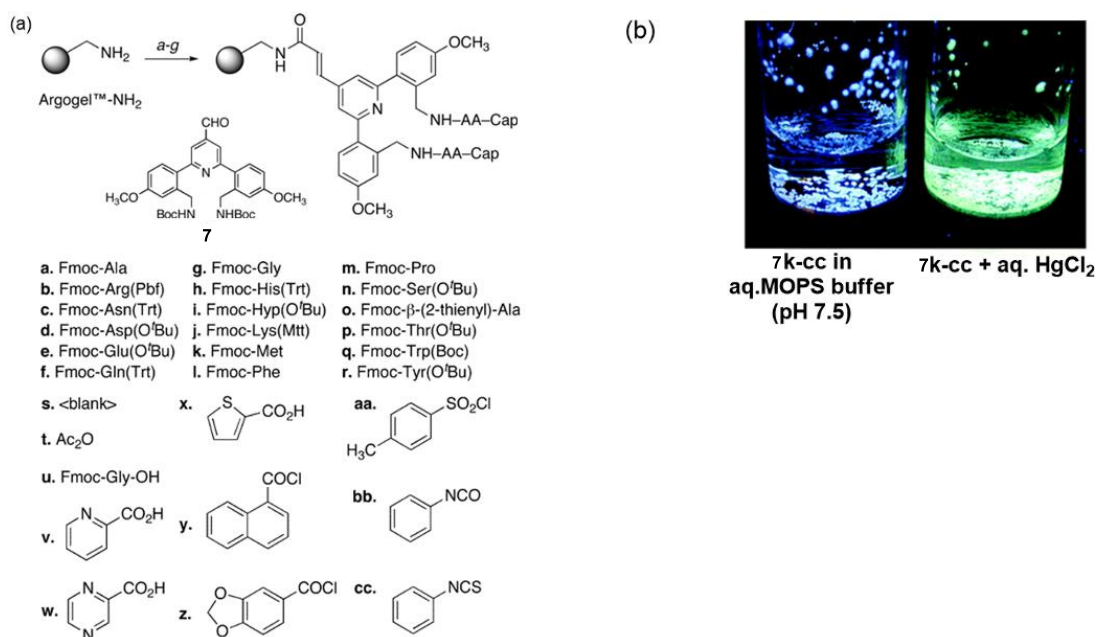


Figure 1.10. (a) Synthesis of the chemosensor library and L-amino acid and acyl end cap library components and representative solid-phase chemosensors for Hg²⁺ and (b) images of solid-phase chemosensors (**7k-cc**) before and after addition of HgCl₂.

1.1.3. Distance-based sensors

Distance-based sensors become intensively developed during the past decades with potential application for on-site analysis due to its easy readout and instrument-free quantification. Mostly, sensors were produced from cellulose substrate which can carry and transport liquid via patterned channels using simple fabrications such as hydrophobic barrier printing or paper cutting. The hydrophilicity and porosity of the cellulose generate flow through capillary effect which allow the interaction between an analyte and sensor occurs over a distance without a need of external pumps or power sources.¹³ The length of visual signal corresponding with an amount of analyte can be measured by either naked eye or photographic image, thus eliminating the need for complicated instruments. The distance-based sensing device is low-cost, easy to operate and can be developed into portable analytical devices for point-of-care testing for example clinical diagnostics, environmental monitoring, and food safety assurance at an exponential rate.

The development of distance-based sensing device was dated back at least since 1985 reported by Litman and coworkers¹⁴ for determination of theophylline

antiasthmatic drug in biological fluid via competitive immunoassay (Figure 1.11). The mixture of sample and enzyme reagents was allowed to be developed on a paper strip coated with antibody. The blue-grey color was generated on the paper strip by the enzymatically catalyzed oxidation of 4-chloro-1-naphthol. The sample containing higher amount of theophylline showed the longer distances of the color band due to the antibody displayed stronger interaction with theophylline than the enzyme reagents. Using this competitive immunoassay device, the theophylline in blood were quantified within 15 min and reduced the effect of enzyme stability by determining the distance of the enzyme dispersion instead of enzyme activity.

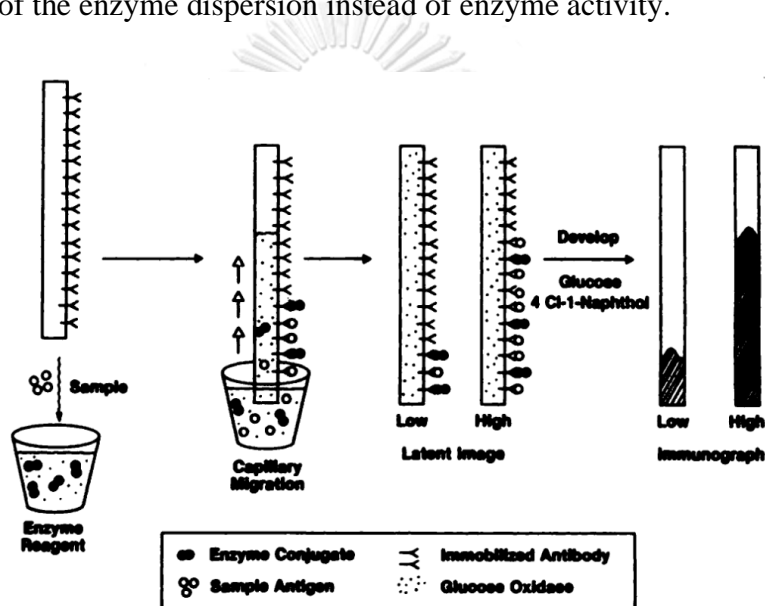


Figure 1.11. Scheme of the theophylline detection based on competitive immunoassay on enzyme immunochromatographic test strip.

In 2013, Henry and coworkers¹⁵ reported a portable paper-based device for simple quantitative analysis of glucose, nickel, and glutathione using different coloring reagents via enzymatic reactions, metal complexation, and nanoparticle aggregation, respectively (Figure 1.12). The coloring reagents were coated in the wax-printed fluidic channels. A lateral flow of the liquid sample in the fluidic channel created coloring distance depended on the analyte concentration. The results showed excellent quantitative agreement with certified standards in complex sample matrices. The linear dynamic ranges against the semi-log scale of the analyte concentration can

be tuned by varying the amounts of coloring reagents coated in the wax-printed fluidic channel.

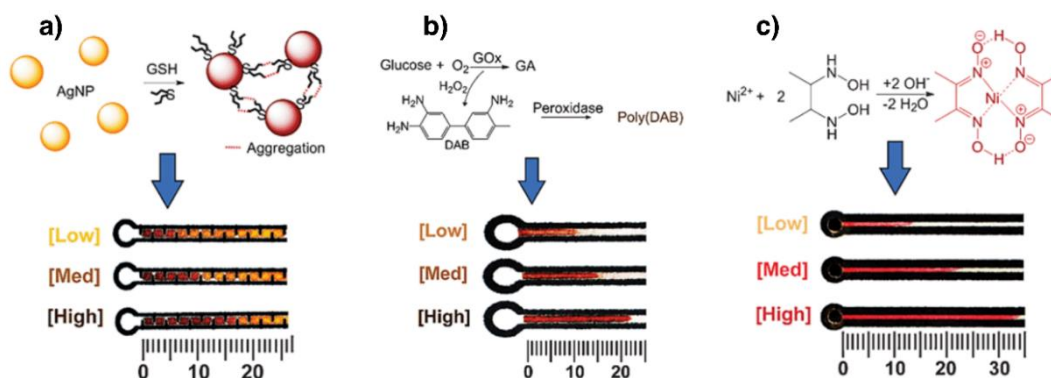


Figure 1.12. (a) Silver nanoparticles aggregated in the presence of glutathione. Reaction kinetics were slow, so wax baffles were used to reroute flow in a twisting pattern through the channel. Detection of glutathione within the concentration range tested took approximately 10 min. (b) Formation of a brown precipitate product for glucose detection in approximately five minutes. (c) Formation of a bright red precipitate product from complexation of Ni^{2+} in approximately 15 min.

In 2015, Henry and coworkers¹⁶ reported a distance-based quantification of Ni^{2+} , Cu^{2+} , and Fe^{2+} in aerosolized particulate matter using wax-printed microfluidic paper-based analytical devices (Figure 1.13). Colorimetric reagents, chelating ligands, were printed by inkjet printing for quantifying metals. Distance of colorimetric response depended on the concentration of the metal ion. Limit of detections for Ni^{2+} , Cu^{2+} , and Fe^{2+} in single and multi-channel devices were 0.10, 0.05, 0.10 μg and 5.0, 1.0, 5.0 μg , respectively. Distance-based device offered convenient and instrument-free quantification, but it usually gave significant error at near the detection limit level.

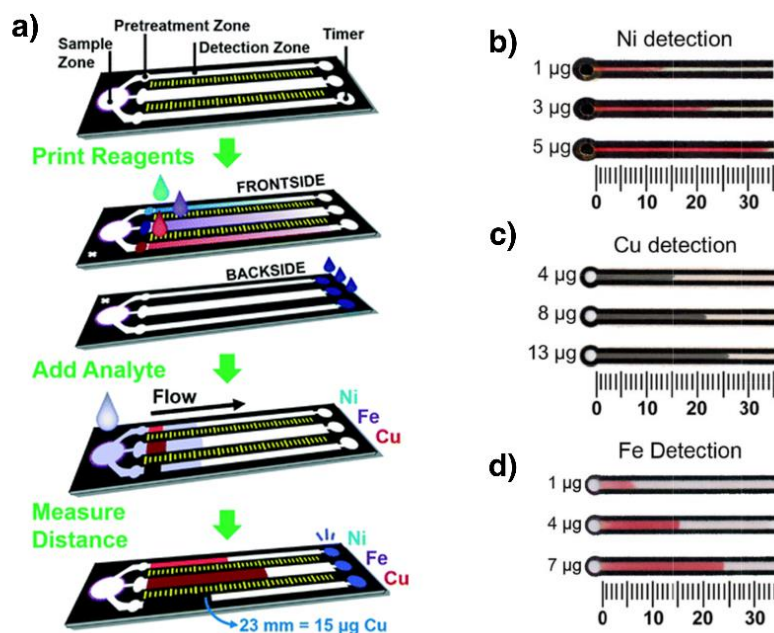


Figure 1.13. (a) Schematic of distance-based sensor with a multi-layer device. Masking and sensing agents were inkjet printed in the pretreatment and detection zones. Passive timer was printed on the back of the device. Metal was quantified from a complex of ligand-metal precipitated on the substrate that generated a band of color with a length proportional to the amount of metal. Detection time in single and multi-channel devices were accomplished in ~ 30 and ~ 40 min, respectively. (b) Ni^{2+} , (c) Cu^{2+} , and (d) Fe^{2+} distance-based detection in single channel devices.

In 2018, Dungchai and coworkers¹⁷ reported a wax-printed distance-based sensor for rapid determination of Cl^- . The quantitative analysis is based on the oxidative etching of red silver nanoparticles (AgNPs) to create a white color band of AgCl in the presence of Cl^- and H_2O_2 (Figure 1.14). The concentration of Cl^- was determined from the length of the white band using a ruler printed on the side of the channel. This device showed reproducible and acceptable results comparing to a commercial chloride test kit for measurement of Cl^- in real water samples without external instrument. However, carbonate ion was a major interference when the concentration ratio of Cl^- and CO_3^{2-} ion is $\leq 1:3$.

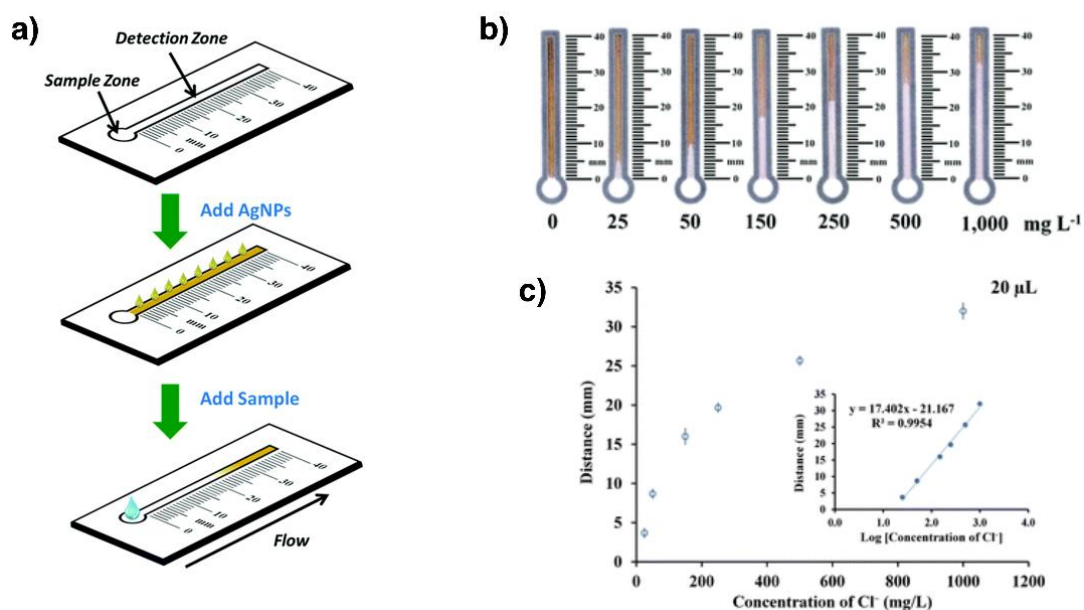


Figure 1.14. (a) Schematic of distance-based sensor designs and analytical methods. (b) Distance-based sensor showed the increasing of white color band toward concentration of Cl^- . (c) Linear correlation in log scale of Cl^- concentration between 25 and 1000 ppm, $n = 3$.

In 2020, Henry and coworkers¹⁸ reported the distance-based sensors using turn-on fluorescence for Al^{3+} quantification. The devices were designed in a linear format, measured the length of a fluorescent band, and a radial format, measured fluorescent diameter, to determine the Al^{3+} concentration (Figure 1.15). The detection limit and dynamic range of two devices cover concentrations in ppm level. The authors suggested a use of portable digital calipers for providing accurate measurements of single digit ppm. These devices could determine the concentration of Al^{3+} in real water sample from a gold mine despite some interference from Fe^{3+} and Cu^{2+} which turn-off the fluorescence response due to a stronger binding affinity to the ligand.

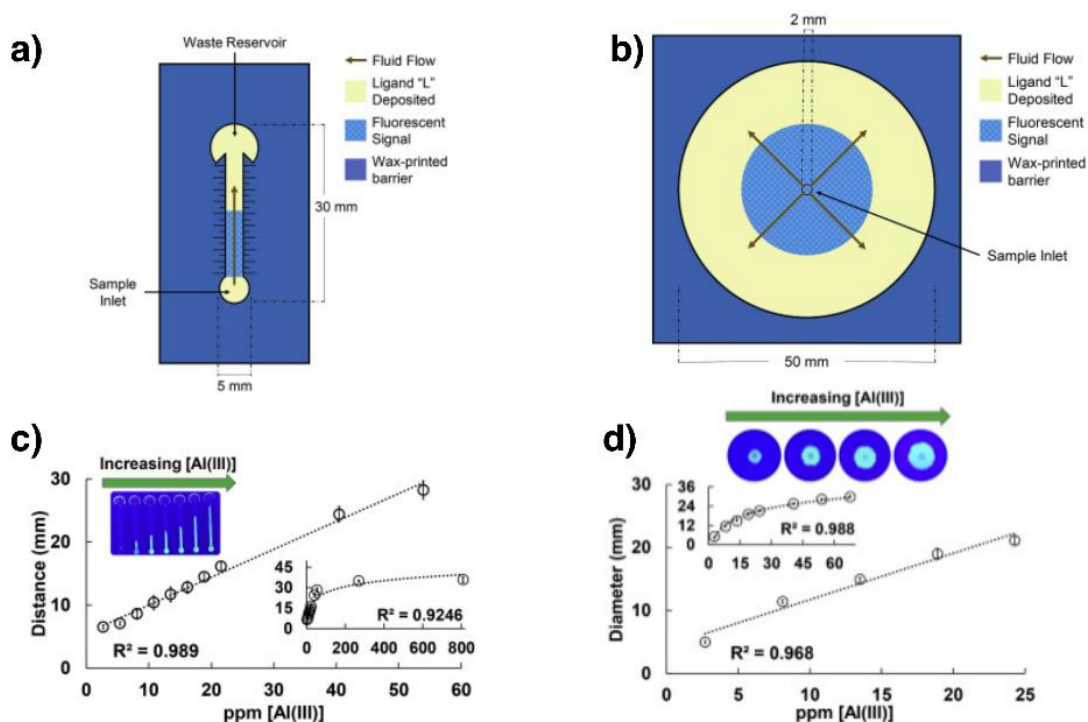


Figure 1.15. Schematic of the (a) linear and (b) radial devices. Calibration plots presenting the linear range, working range (inset), and photographic images (inset) of (c) linear devices ($n = 8$) and (d) radial devices ($n = 8$) illuminated with a UV flashlight with selected concentrations to highlight the changes in signal length. Inset plot's axes and units are the same as the enlarged plot.

1.2. Objectives

From the above literature survey, three summaries maybe drawn; 1) quinoline derivatives have been demonstrated to be versatile and effective as sensing probe and parts of binding sites for metal ion chemosensors; 2) combinatorial synthesis and screening on cellulose surface maybe used to speed up discovery of new chemosensors; 3) distance-based sensors allow simple naked-eye readout for quantitative analysis. However, structure tuning of quinoline derivatives toward development of metal ion sensor have not been systematically explored. Therefore, the structure tuning of quinoline derivatives in this work was performed by varying the substituents, on C2, C3, C6 and C8 position, using different types of amino acids. The parallel combinatorial approach was used to speed up the synthesis and screening of sensing properties. The aim for the first part of this dissertation is to generate a macroarray sensor on filter paper to identify metal ion. The second part of the

dissertation deals with a systematic modification of glycyI amidoquinoline derivative having varied hydrophobic substituents. The objective for this second part is to develop paper-based sensors with distance-based quantification capability. The variation of hydrophobic properties of the ligands should provide systematic modulation of the sensitivity and dynamic range of the sensors.



CHAPTER II

Macroarray Synthesis on Filter Paper for Rapid Discovery and Structure-Property Relationships of Metal Ion Fluorescent Sensors

A macroarray synthesis of ligands on filter papers for metal ions sensor by in-situ reductive amination and amide coupling reactions is reported. Chemometric approaches exhibited a rapid discovery of array sensor that can synergistically distinguish 12 metal ions with high prediction accuracies. Covalently bound of ligands on filter paper can be developing to a practical paper-based sensors with great reusability and sensitivity and achieving the limit of detection at low nanomolar level with some repeating spotting method. Moreover, the discovered ligands were also confirmed to be functional as unbound molecules, thus giving the faster way of screening for sensing applications.

2.1. Introduction

The development of sensing ligands for metal ions detection is one of the most active research subjects in chemical science due to its impact on several fields¹⁹⁻²². Recent publication is aimed to detection methods that suitable for field testing, with rapidness, simplicity and low cost detection are desired²³. Several steps of a sensor development have been geared towards achieving these properties. For example, microfluidic paper-based analytical devices (μ PAD)^{24, 25} are a good platform that extremely reduces the cost of detection by the economic cost of filter paper substrate. Nevertheless, the readout methods for chemical or biochemical reactions achieved from the paper support is also challenging to the success of the analysis. Those methods that require sophisticated instrumentation or complicated interpretation are less likely to be widely accepted and in fact contradict to the low-cost nature of the paper-based platform. Among available methods, fluorescence detection remains an attractive measurement, mainly due to its high sensitivity^{26, 27}. To use this detection method, sensing ligands which change in either intensity or emission wavelength are required. In the case of complexation with metal ion, some known mechanisms are generally utilized for observing fluorescence changes. Examples include PET and

ICT²⁸⁻³¹. Anyway, to effectively enhance the paper-based format, sensing ligands that can provide naked-eye visualization from excitation by commercial black lights with visible-region emissions are essential. Aminoquinoline is a class of compounds that can fit well with these requirements. With additional pendants, this type of molecules can accommodate a metal ion, resulting in a change in fluorescence due to PET or ICT³²⁻³⁸. Besides, this change is usually a “turn-on” fluorescence, which can theoretically allow unlimited enhancement, thereby having potential to be very sensitive. Hence, various research groups have developed a variety of quinoline derivatives capable of sensing metal ions^{4, 39-49}. These usually revealed Zn²⁺ as the main binding partner although some other metal ions were also discovered^{4, 47}. Interestingly, these studies did not contain much information about structure-property relationships. Our recent study thus aimed to retrace back to investigate the essential core of binding and found that a mere glycine unit was sufficient to achieve clear turn-on fluorescence sensing with Zn²⁺ ion⁶.

In the current study, we aimed to synthesize an expansion set of quinoline probes from the aforementioned essential core by “reversing the discovery paradigm”⁵⁰ and thus anticipated to discover some new fluorescent probes in a systematic and rapid manner. Notably, while solid-phase synthesis on polymer beads is a well-established field, our current study was made possible by the use of a carefully-planned macroarray synthesis⁵¹. This type of technique, originated from the peptide-only synthesis (SPOT synthesis)^{52, 53}, is a synthesis strategy for small molecules performed on cellulose support. With the spatially addressable nature, macroarray synthesis allows for the rapid synthesis of multiple compounds on one paper sheet without complex deconvolution. In addition, as similar to other solid-phase techniques, macroarray synthesis was relatively rapid due to the fact that unreacted molecules can be easily washed away without any purification steps. With these unique advantages, previous works have showcased various applications⁵⁴⁻⁵⁷ that were directly benefitted from this rapid, low-cost, and reliable method.

Importantly, our current work highlights the first example of how macroarray synthesis can be used to both get access to diverse molecular scaffolds and to perform

metal ion sensing on-support without extra cleavage or post-synthesis steps. This accelerated the discovery of sensing molecules even further, and resulted in a set of compounds that, with an aid of chemometrics, can complementarily sense various metal ions, a finding of which would otherwise be improbable or tedious to attain with traditional synthesis. Last but not least, we also demonstrated the utilization of a Zn^{2+} -selective scaffold as a ready-to-use paper-based sensor with great sensitivity and reusability. This was all made possible thanks to the permanent binding nature of the compound to the cellulose support.

2.2. Experiment

2.2.1. General information

All reagents were purchased from commercial sources and used without further purification. All metal ions used in this study were in the form of nitrate salts except Fe^{2+} , where the acetate salt was used instead. Paper used in this study was Whatman™ Grade 1 Qualitative Filter Paper, which was used without further treatment. Solutions were made with Milli-Q water from ultrapure water systems with a Millipak 40 filter unit (0.22 μm , Millipore, USA). NMR spectra were acquired on a Bruker NMR spectrometer at 400 MHz (^1H) and 100 MHz (^{13}C). The high-resolution mass spectra were obtained from an electrospray ionization MS (microTOF, Bruker Daltonics). Absorption spectra were measured by using Varian Cary 50 UV-vis spectrophotometer. Fluorescence spectra were recorded on a Varian Cary Eclipse spectrofluorometer. Mass titration spectra were obtained from an electrospray ionization MS (Thermo Scientific TSQ Quantum EMR triple quadrupole MS) with the following parameters: positive mode; spray voltage at 3000 V; capillary temperature at 300 °C; tube lens offset at 84 V).

2.2.2. Generation of aldehyde functional groups on paper

Paper sheets were washed with a series of solvents (DMF, 10 min, 3x, then MeOH, 10 min, 3x) prior to chemical functionalization. Thereafter, paper sheets were immersed into a solution of NaIO_4 (10 mM) and LiCl (100 mM) premixed in 10 mL H_2O at 55 °C for 1 h. This was followed by washing with Milli-Q water (10 min, 3x), MeOH (10 min, 3x), and air-dried.

2.2.3. Reductive amination with reagent X

A solution of each reagent X (amino acids or dipeptides, 1 mmol) with $\text{NaBH}(\text{OAc})_3$ (212 mg, 1 mmol) was prepared by adding 1 mL of 10-mM HEPES pH 8 solution into pre-weighed reagents, resulting in a 1 M solution. In the case of incompletely soluble reagents (judged by observing precipitate after 20-min sonication), only supernatant was withdrawn and used. The resulting solution was spotted (2 μL) onto desired areas on aldehyde-terminated papers (surface 1 in the main article). The sheet was incubated at room temperature for 10 min, and the spotting was repeated two more times. After washing (Milli-Q water (10 min, 3x), then MeOH (10 min, 3x)), the paper sheets were immersed into a solution of NaBH_4 (100 mM) for 20 min at room temperature. This again was followed by a series of washing (Milli-Q water (10 min, 3x), then MeOH (10 min, 3x)).

2.2.4. Carbodiimide coupling with reagent Y

A solution of each reagent Y (aminoquinolines or an aminonaphthalimide, 1 mmol) with HOBt (154 mg, 1 mmol) was prepared by adding 1 mL of DMF into pre-weighed reagents. The resulting solution was mixed with DIC (126 μL , 1 mmol) and the new mixture was immediately used for spotting (2 μL) onto desired areas on carboxyl-terminated papers (surface 2 in the main article). The sheet was incubated at room temperature for 5 min, and the spotting was repeated two more times. The process ended by washing the sheets with HEPES buffer pH 5 solution (10 min, 1x), HEPES buffer pH 7 solution (10min, 1x), DMF (10 min, 5x), and then MeOH (10 min, 3x). After air drying, the paper sheets were ready for metal ion sensing.

2.2.5. Final finishing with wax printing

If desired, finished sensors can be patterned with hydrophobic wax as shown in our studies. This was done by a Xerox ColorQube 8870 wax printer to create circular patterns (diameter at 7 mm) on paper (which was designed by Adobe Photoshop). Heating at 110 °C for 30 sec on a hotplate was then performed to melt the wax and create the final hydrophobic patterns (diameter of around 5 mm).

2.2.6. Probing fluorescence response with various metal ions

First option (immersion method), each finished paper sheet was immersed in a solution of a metal ion (10 μM in HEPES buffer pH 7). The solution was incubated for 30 min. The sheet was air-dried and exposed to UV light. A handheld UV lamp was used to illuminate directly on the paper for fluorescence observation.

Second option (spotting method), each desired area on a finished paper sheet was spotted (2 μL) with a solution of a metal ion (10 μM in HEPES buffer pH 7). The sheet was incubated for 10 min. The sheet was air-dried and exposed to UV light. A handheld UV lamp was used to illuminate directly on the paper for fluorescence observation.

2.2.7. Digital conversion and quantitative analysis of fluorescence signals

Fluorescence signals were captured by using a digital camera (model Panasonic DMC-GF7) with the following camera setting: ISO-200, f/5.0, and 2 s exposure time. The illuminator (TCP-20.LM, Vilber Lourmat, Germany) provided the source of 365-nm light. Similar to other reaction steps, photos were taken under ambient condition, with a handmade cardboard box with a hole to fit the front lens of the camera. These images were then extracted for their RGB values and analyzed with ImageJ (<http://imagej.nih.gov/ij/>). Since the areas to be analyzed were usually circular, we employed the circular region of interest (ROI) to measure the signal intensity. Note that the area was smaller than the average size of each signal area (by 78%) to ensure that all measured area contained some signal intensity. The integrated density as calculated by ImageJ can then be obtained. For chemometric experiments, all raw R, G, and B values were used, while the LOD experiment instead made use of mean grey values and their difference values.

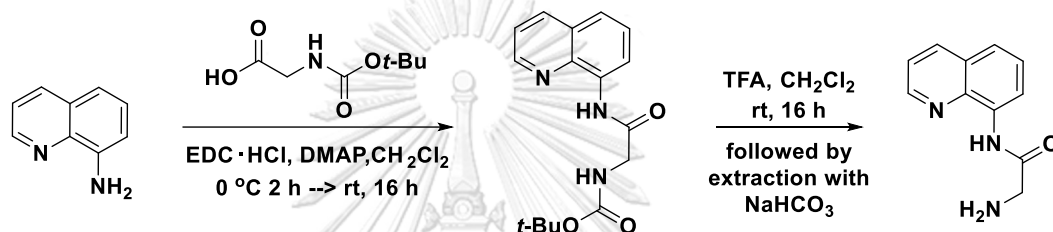
2.2.8. Chemometrics

ImageJ software was used to extract all red, green, and blue color intensity from each reaction data points. These RGB values were then used to calculate for percentage of each color by using the formula: $\%R = (R/(R+G+B)) \times 100$. The same can be done for %G and %B.

Linear discriminant analysis (LDA) was used with a data set consisting of 180 samples (17 metal ions and blank \times 10 replicates) and 12 variances (3 sets of %RGB \times 4 fluorophores). The calculation and plotting were performed using in-house codes based on MATLAB R2018a. Linear discriminant analysis (LDA) for the Jackknife classification provided percent classification accuracies. This is represented in the tables below (Table S1 and S2).

2.2.9. Synthesis of representative fluorophores

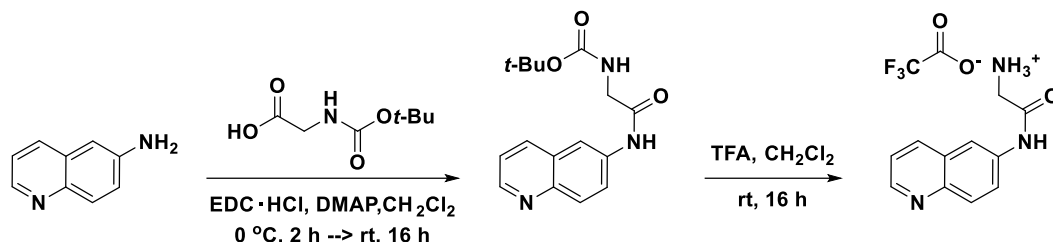
2.2.9.1. Synthesis of (2-amino-*N*-(quinolin-8-yl)acetamide) (Gly.8AQ).



A mixture of 8-aminoquinoline (500 mg, 3.47 mmol), DMAP (21.18 mg, 0.17 mmol) and Boc-Gly-OH (1.22 g, 6.94 mmol) in dichloromethane (30 mL) was stirred in ice bath (~ 0 °C) for 30 minutes, followed by an addition of EDC·HCl (1.33 g, 6.94 mmol). The reaction mixture was stirred at 0 °C for 2 hours and stirred overnight at room temperature. The crude was extracted with NH_4Cl (aq). The organic layer was dried over MgSO_4 , filtered and concentrated under vacuum. The crude product was purified on a column chromatography using ethyl acetate: hexane (2:3) as an eluent to afford (2-Boc-amino-*N*-(quinolin-8-yl)acetamide) as a white solid (910 mg, 3 mmol, 87%). This compound was stirred overnight with trifluoroacetic acid (0.46 mL, 6 mmol) in dichloromethane 20 mL at room temperature. The crude was extracted with saturated NaHCO_3 . The organic layer was dried over MgSO_4 , filtered and concentrated under vacuum. The crude product was purified on a column chromatography using ethyl acetate as an eluent to afford (2-amino-*N*-(quinolin-8-yl)acetamide) as a yellow solid (free base form, 437 mg, 2.2 mmol, 72%). ^1H NMR (400 MHz, $\text{DMSO-}d_6$) δ 11.62 (s, 1H), 8.92 (dd, $J = 4.0, 1.1$ Hz, 1H), 8.75 (d, $J = 7.5$ Hz, 1H), 8.39 (d, $J = 8.2$ Hz, 1H), 7.67 – 7.54 (m, 3H), 3.41 (s, 2H), 2.40 (s, 2H). ^{13}C NMR (100 MHz, $\text{DMSO-}d_6$) δ 172.2, 148.9, 138.1, 136.4, 134.2, 127.8, 127.0, 122.0, 121.5, 115.3, 45.6, 39.5. MS (ESI); m/z calculated for $[\text{C}_{11}\text{H}_{11}\text{N}_3\text{O} + \text{Na}]^+$ is

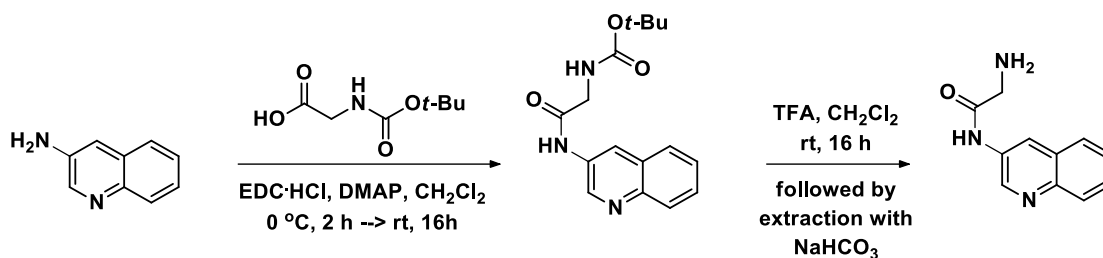
224.07943; found 224.07959 $[M + Na]^+$. The spectra images of 1H , ^{13}C NMR and HRMS can also be found in Appendix Figure A1-3.

2.2.9.2. Synthesis of (2-amino-*N*-(quinolin-6-yl)acetamide) (TFA salt of **Gly.6AQ**).



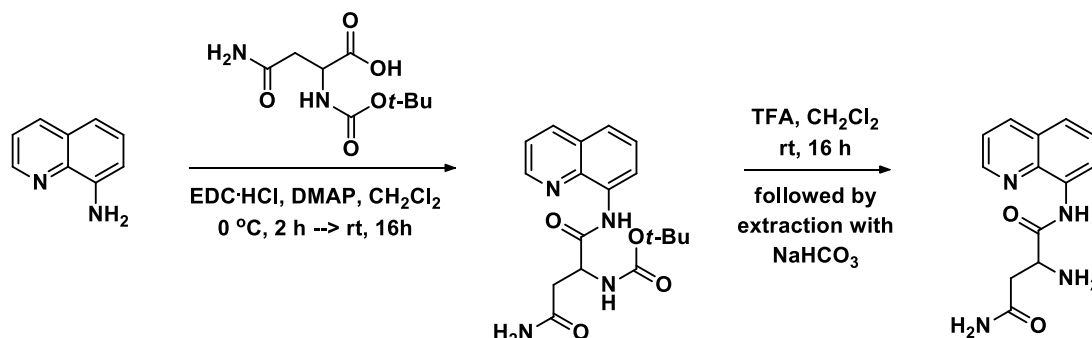
A mixture of 6-aminoquinoline (500 mg, 3.47 mmol), DMAP (21.18 mg, 0.17 mmol) and Boc-Gly-OH (1.22 g, 6.94 mmol) in dichloromethane (30 mL) was stirred in ice bath (~0 °C) for 30 minutes, followed by an addition of EDC·HCl (1.33 g, 6.94 mmol). The reaction mixture was stirred at 0 °C for 2 hours and stirred overnight at room temperature. The crude was extracted with NH₄Cl (aq). The organic layer was dried over MgSO₄, filtered and concentrated under vacuum. The crude product was purified on a column chromatography using ethyl acetate as an eluent to afford (2-Boc-amino-*N*-(quinolin-6-yl)acetamide) as a white solid (700 mg, 2.32 mmol, 67%). Thereafter, this compound was stirred overnight with trifluoroacetic acid (0.36 mL, 4.64 mmol) in dichloromethane 20 mL at room temperature. The crude product was left under vacuum for about 2 hours at 60 °C to afford 2-oxo-2-(quinolin-6-ylamino)ethan-1-aminium 2,2,2-trifluoroacetate as a yellow solid (400 mg, 1.27 mmol, 55%). 1H NMR (400 MHz, DMSO-*d*₆) δ 11.20 (s, 1H), 9.09 (d, $J = 4.7$ Hz, 1H), 8.92 (d, $J = 8.2$ Hz, 1H), 8.58 (d, $J = 1.2$ Hz, 1H), 8.35 (s, 3H), 8.22 (d, $J = 9.2$ Hz, 1H), 8.05 (dd, $J = 9.2, 1.6$ Hz, 1H), 7.89 (dd, $J = 7.5, 5.6$ Hz, 1H). ^{13}C NMR (100 MHz, DMSO-*d*₆) δ 165.9, 159.0 (q, $J = 36.5$ Hz, TFA), 145.3, 143.0, 138.2, 137.5, 129.3, 126.6, 124.4, 122.4, 116.1 (q, $J = 292.2$ Hz, TFA), 115.4, 41.4. MS (ESI); m/z calculated for $[C_{11}H_{11}N_3O]^+$ is 202.09749; found 202.09820 $[M + H]^+$. The spectra images of 1H , ^{13}C NMR and HRMS can also be found in Appendix Figure A4-6.

2.2.9.3. Synthesis of (2-amino-*N*-(quinolin-3-yl)acetamide) (**Gly.3AQ**)



A mixture of 3-aminoquinoline (500 mg, 3.47 mmol), DMAP (21.18 mg, 0.17 mmol) and Boc-Gly-OH (1.22 g, 6.94 mmol) in dichloromethane (30 mL) was stirred in ice bath (~ 0 °C) for 30 minutes, followed by an addition of EDC·HCl (1.33 g, 6.94 mmol). The reaction mixture was stirred at 0 °C for 2 hours and stirred overnight at room temperature. The crude was extracted with NH_4Cl (aq). The organic layer was dried over MgSO_4 , filtered and concentrated under vacuum. The crude product was purified on a column chromatography using ethyl acetate as an eluent to afford (2-Boc-amino-*N*-(quinolin-3-yl)acetamide) as a white solid (420 mg, 1.39 mmol, 40%). Thereafter, this compound was stirred overnight with trifluoroacetic acid (0.22 mL, 2.78 mmol) in dichloromethane 20 mL at room temperature. The crude was extracted with saturated NaHCO_3 . The organic layer was dried over MgSO_4 , filtered and concentrated under vacuum. The crude product was purified on a column chromatography using ethyl acetate as an eluent to afford (2-amino-*N*-(quinolin-3-yl)acetamide) as a yellow solid (free base form, 193 mg, 0.97 mmol, 70%). ^1H NMR (400 MHz, $\text{DMSO}-d_6$) δ 9.00 (d, $J = 2.5$ Hz, 1H), 8.73 (d, $J = 2.4$ Hz, 1H), 7.98 – 7.86 (m, 2H), 7.66 – 7.50 (m, 2H), 3.39 (s, 2H). ^{13}C NMR (100 MHz, $\text{DMSO}-d_6$) δ 173.2, 144.7, 144.2, 132.6, 128.6, 127.9, 127.8, 127.7, 127.1, 122.0, 45.6. MS (ESI); m/z calculated for $[\text{C}_{11}\text{H}_{12}\text{N}_3\text{O}]^+$ is 202.0975; found 202.0972 $[\text{M} + \text{H}]^+$. The spectra images of ^1H , ^{13}C NMR and HRMS can also be found in Appendix Figure A7-9.

2.2.9.4. Synthesis of 2-amino-*N*^l-(quinolin-8-yl)succinamide) (**Asn.8AQ**)



A mixture of 8-aminoquinoline (500 mg, 3.47 mmol), DMAP (21.18 mg, 0.17 mmol) and Boc-Asn-OH (1.61 g, 6.94 mmol) in dichloromethane (30 mL) was stirred in ice bath (~0 °C) for 30 minutes, followed by an addition of EDC·HCl (1.33 g, 6.94 mmol). The reaction mixture was stirred at 0 °C for 2 hours and stirred overnight at room temperature. The crude was extracted with NH₄Cl (aq). The organic layer was dried over MgSO₄, filtered and concentrated under vacuum. The crude product was purified on a column chromatography using ethyl acetate as an eluent to afford *tert*-butyl(4-amino-1,4-dioxo-1-(quinolin-8-ylamino)butan-2-yl)carbamate as a white solid (995 mg, 2.78 mmol, 80%). Thereafter, this compound was stirred overnight with trifluoroacetic acid (0.43 mL, 5.56 mmol) in dichloromethane 20 mL at room temperature. The crude was extracted with saturated NaHCO₃. The organic layer was dried over MgSO₄, filtered and concentrated under vacuum. The crude product was purified on a column chromatography using ethyl acetate as an eluent to afford 2-amino-*N*¹-(quinolin-8-yl)succinimide as a yellow solid (free base form, 890 mg, 3.45 mmol, 62%). ¹H NMR (400 MHz, DMSO-*d*₆) δ 11.61 (s, 1H), 8.94 (dd, *J* = 4.2, 1.7 Hz, 1H), 8.72 (dd, *J* = 7.6, 1.4 Hz, 1H), 8.40 (dd, *J* = 8.3, 1.7 Hz, 1H), 7.71 – 7.55 (m, 3H), 3.90 (dd, *J* = 7.4, 4.8 Hz, 1H), 3.37 (s, 2H), 3.07 (ddd, *J* = 16.8, 4.8, 0.8 Hz, 1H), 2.90 (ddd, *J* = 16.8, 7.5, 0.8 Hz, 1H), 2.74 (s, 2H). ¹³C NMR (100 MHz, DMSO-*d*₆) δ 171.3, 149.1, 138.1, 136.6, 133.9, 127.9, 127.0, 122.2, 122.1, 119.1, 115.5, 52.6, 23.2. MS (ESI); *m/z* calculated for [C₁₃H₁₅N₄O₂]⁺ is 259.1190; found 259.1191 [M + H]⁺. The spectra images of ¹H, ¹³C NMR and HRMS can also be found in Appendix Figure A10-12.

2.3. Results and Discussion

The synthesis, after some optimizations and/or consideration based on previous other works, can be summarized as follows (Figure 2.1). The first step was the treatment of cellulose with NaIO_4 and LiCl ^{9, 10}. This reaction resulted in the conversion of diol at position 2 and 3 of the glucose repeating unit into the dialdehyde **A1**.

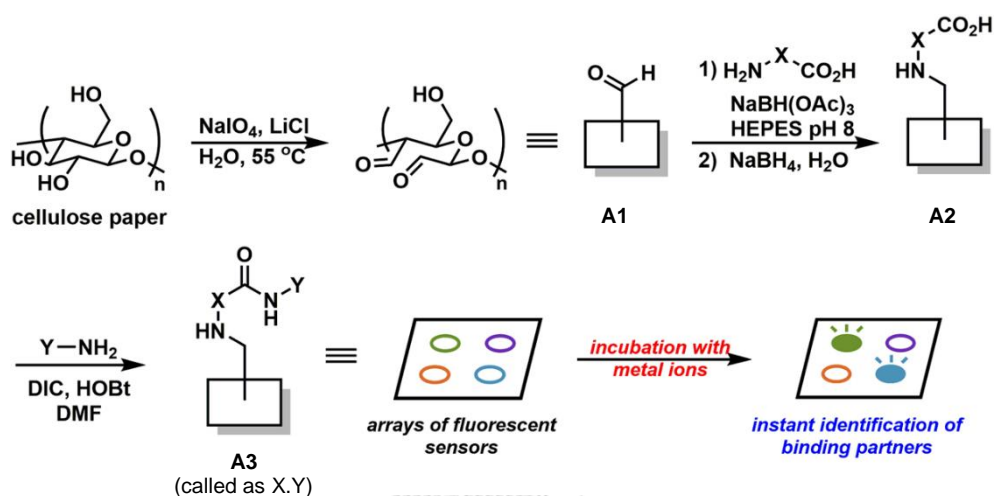


Figure 2.1. Macroarray synthesis of fluorescent sensors and a subsequent sensing process. DIC = *N,N'*-diisopropylcarbodiimide; HOBt = 1-hydroxybenzotriazole; DMF = *N,N'*-dimethylformamide; HEPES = *N*-(2-hydroxyethyl)piperazine-*N'*-(2-ethanesulfonic acid)

Thereafter, **A1** was subject to reductive amination with a variety of amino acids (**reagent X**, see Figure 2.2), followed by NaBH_4 treatment to reduce unreacted surface-bound aldehydes to alcohols. This library X consists of readily available amino acids along with some variations to also probe other effects such as chirality or steric effect due to extended carbon skeletons. The resulting modified surfaces **A2** with free carboxyl groups then under-went carbodiimide-mediated couplings with various aminoquinolines and an aminonaphthalimide (**reagent Y**, Figure 2.2).

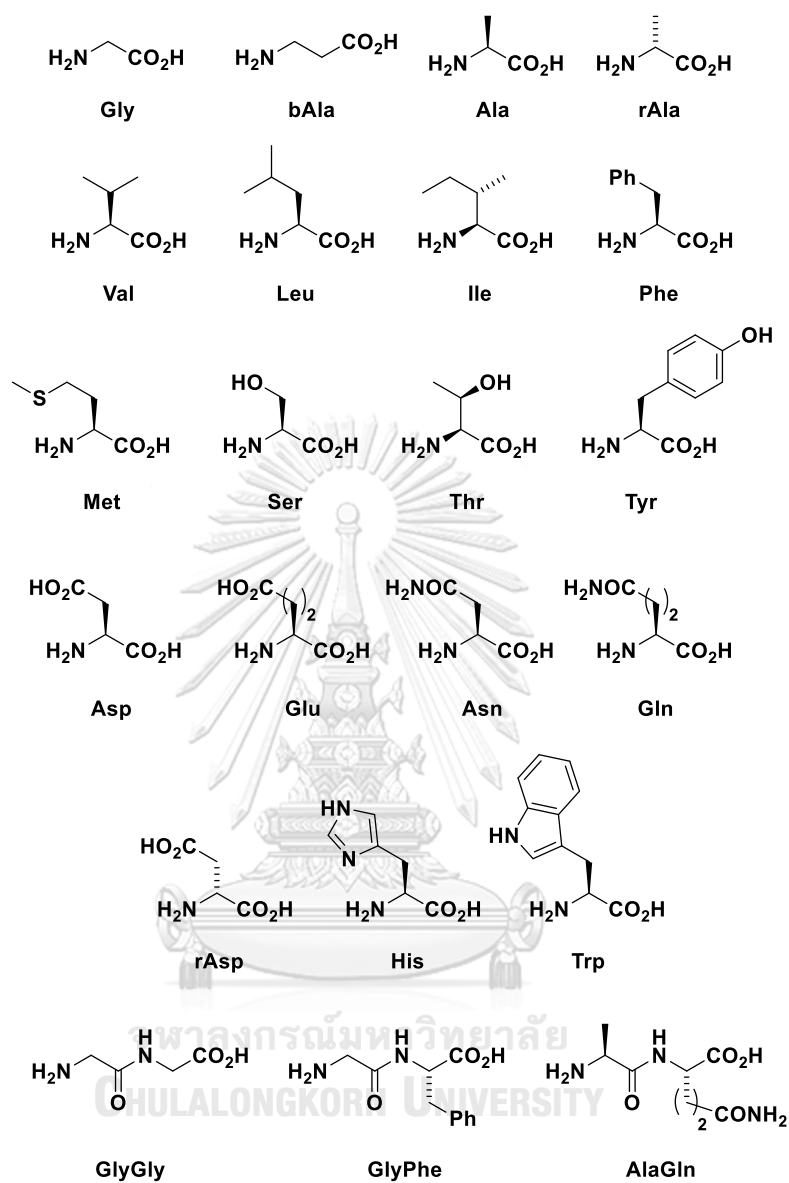
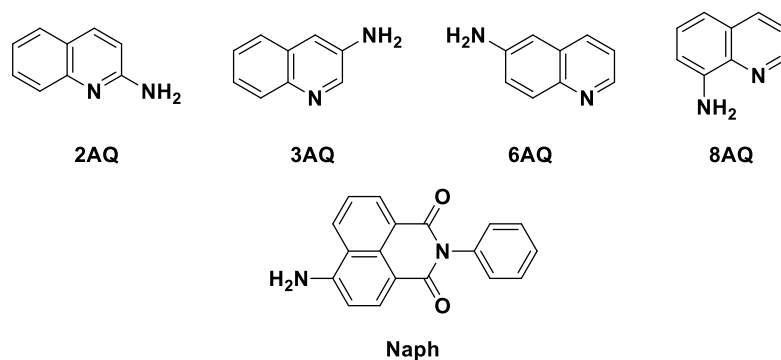
Reagent X**Reagent Y**

Figure 2.2. Structures of **Reagent X** and **Reagent Y** used in this study.

After washing unbound materials off, **A3** can be directly incubated with a solution of a metal ion of interest. Fluorescence response of each surface-bound compound with a metal ion can be easily probed by subjecting the paper sheet with direct illumination from a handheld UV lamp or a transilluminator, thereby revealing active compounds by comparing fluorescence intensity and color hue with the controls. Also, while the exemplary synthesis in Figure 16 utilized the spotting method for synthetic steps with the whole-sheet immersion in the sensing step, this overall process can be swapped. This may be more suitable and efficient in certain cases, *e.g.*, the screening for metal ion partners (by spotting) within a single sheet containing only one sensing scaffold of interest. An example of the exact protocol for the sensing step can be found in the method section. Notably, all synthesis steps could be performed at ambient condition, and the finished cellulose sheets could be kept under a desiccator at ambient temperature for up to at least 2 weeks without deterioration in sensing performance (

a) Figure 2.3). This reflected a fairly high versatile and durable nature of the whole methodology. b)

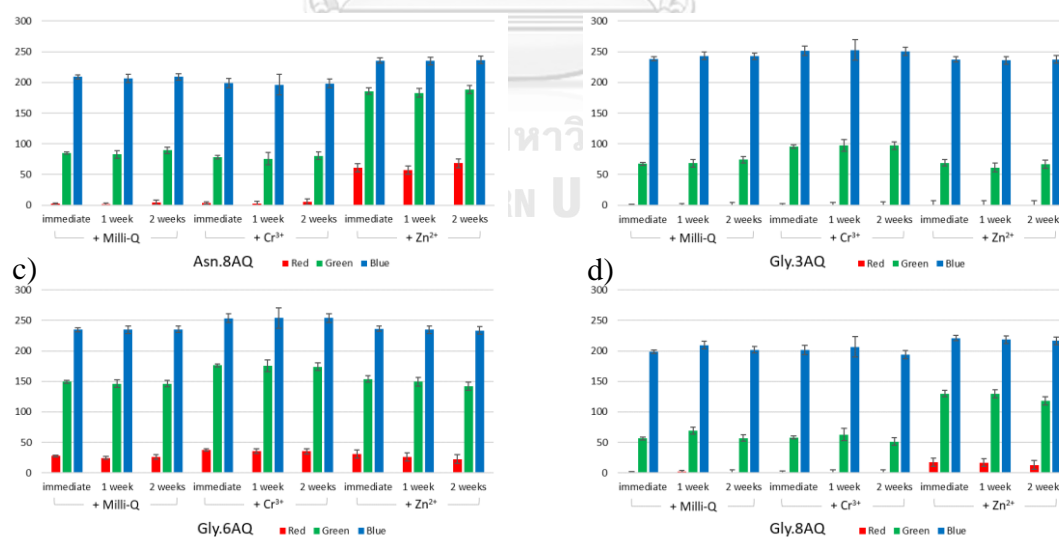
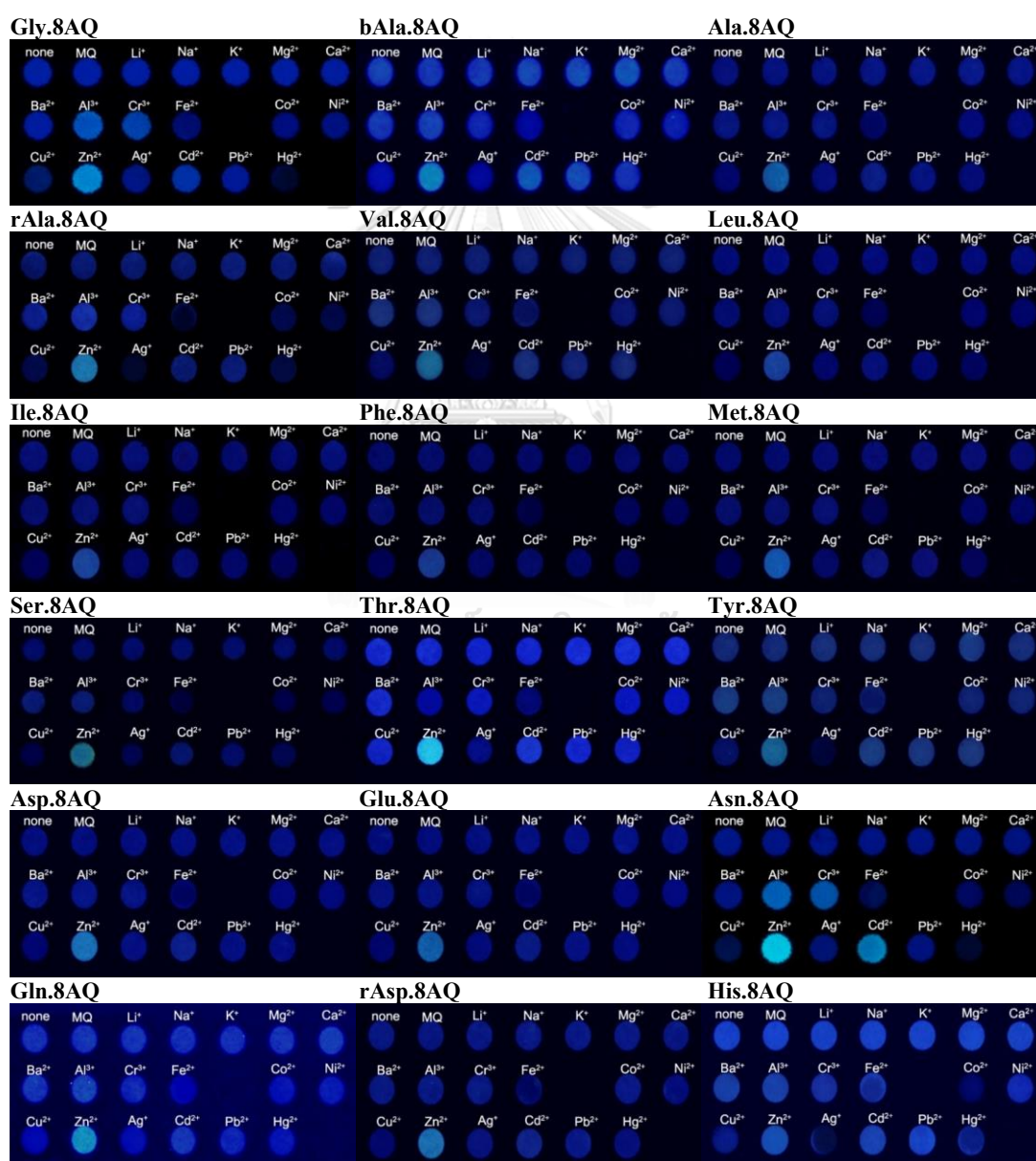


Figure 2.3. Bar graphs representing intensities of each color channel from a) **Asn.8AQ**, b) **Gly.3AQ**, c) **Gly.6AQ**, d) **Gly.8AQ** in responding to Milli-Q water, Cr³⁺, and Zn²⁺ over the period of two weeks.

In this proof-of-concept experiment, we commenced with the screening of the **X** counterpart while keeping the **Y** component to be **8AQ** to allow some comparison with our previous study⁶. The evaluation was performed by observing any fluorescence change when incubated with metal ions including Li^+ , Na^+ , K^+ , Mg^{2+} , Ca^{2+} , Ba^{2+} , Al^{3+} , Cr^{3+} , Fe^{2+} , Co^{2+} , Ni^{2+} , Cu^{2+} , Zn^{2+} , Ag^+ , Cd^{2+} , Pb^{2+} , and Hg^{2+} . After obtaining a preliminary result (Figure 2.4), the **X** components **Gly** and **Asn** were selected for the **Y**-component screening.



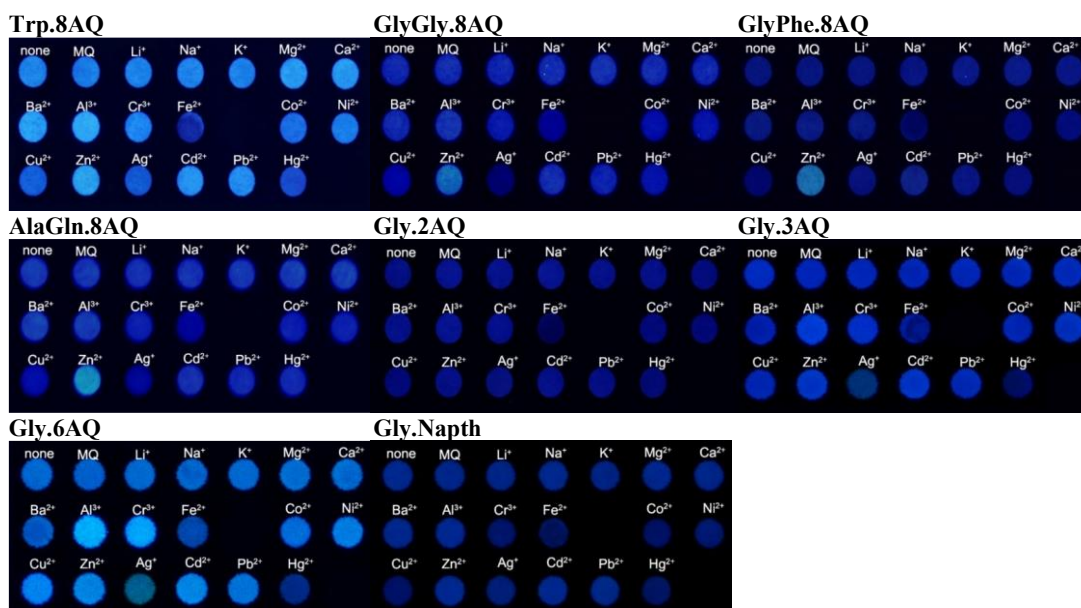


Figure 2.4. Preliminary fluorescence screening of all scaffolds synthesized via macroarray synthesis against selected metal ions.

After compiling obtained results, a set of interesting fluorescent compounds was revealed (Figure 2.5). Interestingly, these scaffolds, generally weak or non-fluorescent in water, showed obvious increase in fluorescence upon binding to certain metal ions such as Zn^{2+} , Al^{3+} , and Cr^{3+} , while some metal ions, *e.g.*, Hg^{2+} , can further decrease the fluorescence intensity of certain fluorophores, likely due to the inherent quenching attributes of Hg^{2+} such as enhanced spin-orbit coupling.^{58, 59} More importantly, the responses of these scaffolds were dependent on specific chemical features present in each scaffold. For example, while the modified surface **Gly.8AQ** exhibited strong fluorescence upon binding with Zn^{2+} (believed to be due to a combination of reasons such as the prevention of non-radiative relaxations, *e.g.*, photoinduced electron transfer from the nitrogen of the $-\text{CH}_2\text{-NH}-$ moiety to the quinoline ring, and the restriction of bond rotation), trivalent Al^{3+} and Cr^{3+} seemed to give better fluorescence increase with **Gly.3AQ** and **Gly.6AQ**, whose aminoquinoline scaffolds are merely regioisomers to that of **Gly.8AQ**. **Asn.8AQ**, on the other hand, showed strong preference towards both Zn^{2+} and Cd^{2+} , the latter of which was never discovered as a metal ion capable of turning on fluorescence of related compounds before. In essence, the ability to obtain such useful information in a relatively short amount of time

clearly underscores the fact that macroarray synthesis is indeed an efficient method in revealing new kinds of fluorescent sensors.

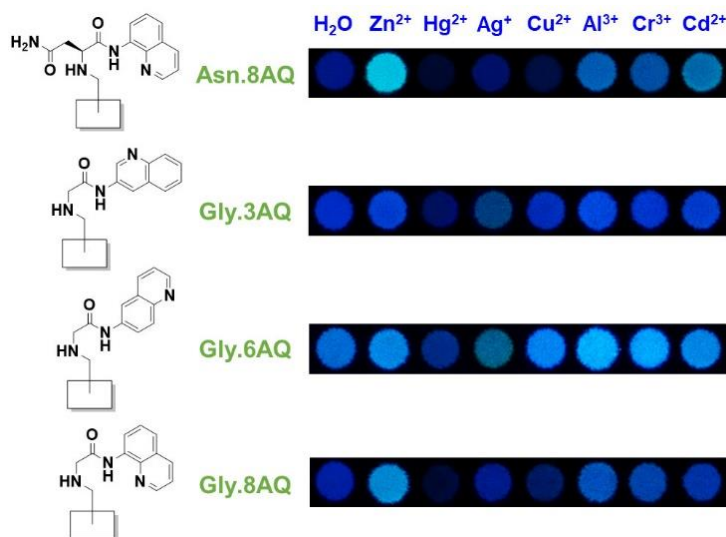


Figure 2.5. Structures and sensing profiles of four selected fluorophores discovered from the macroarray synthesis against a variety of metal ions.

To capitalize on the observed signals, chemometric approaches were used to glean more information. First, all fluorescence signals were captured into a digital camera, which were then processed by the imaging software ImageJ. The percentage of red, green, and blue intensities were calculated, and the resulting data were used to create a multidimensional data set with 180 samples (17 metal ions and a blank \times 10 replicates) and 12 variances (3 sets of %RGB \times 4 fluorophores). Thereafter, the data were analyzed by Linear Discriminant Analysis (LDA) and the resulting score plots for all metal ions are shown in Figure 2.6, with each group representing the sensing capability of the combination of four sensors (**Asn.8AQ**, **Gly.3AQ**, **Gly.6AQ**, **Gly.8AQ**) on each analyte. The LDA score plot showed that most tested ions including Ba²⁺, Al³⁺, Cr³⁺, Fe²⁺, Co²⁺, Ni²⁺, Cu²⁺, Zn²⁺, Ag⁺, Cd²⁺, Pb²⁺, Hg²⁺ can be clearly discriminated by this combined sensing system. Only a handful of group IA and IIA metal ions (Li⁺, Na⁺, K⁺, Mg²⁺, Ca²⁺) could not be distinguished in this system – this is likely due to the well-documented properties of these metal ions such as the harder acid characters and the lack of π -bonding formation capabilities.

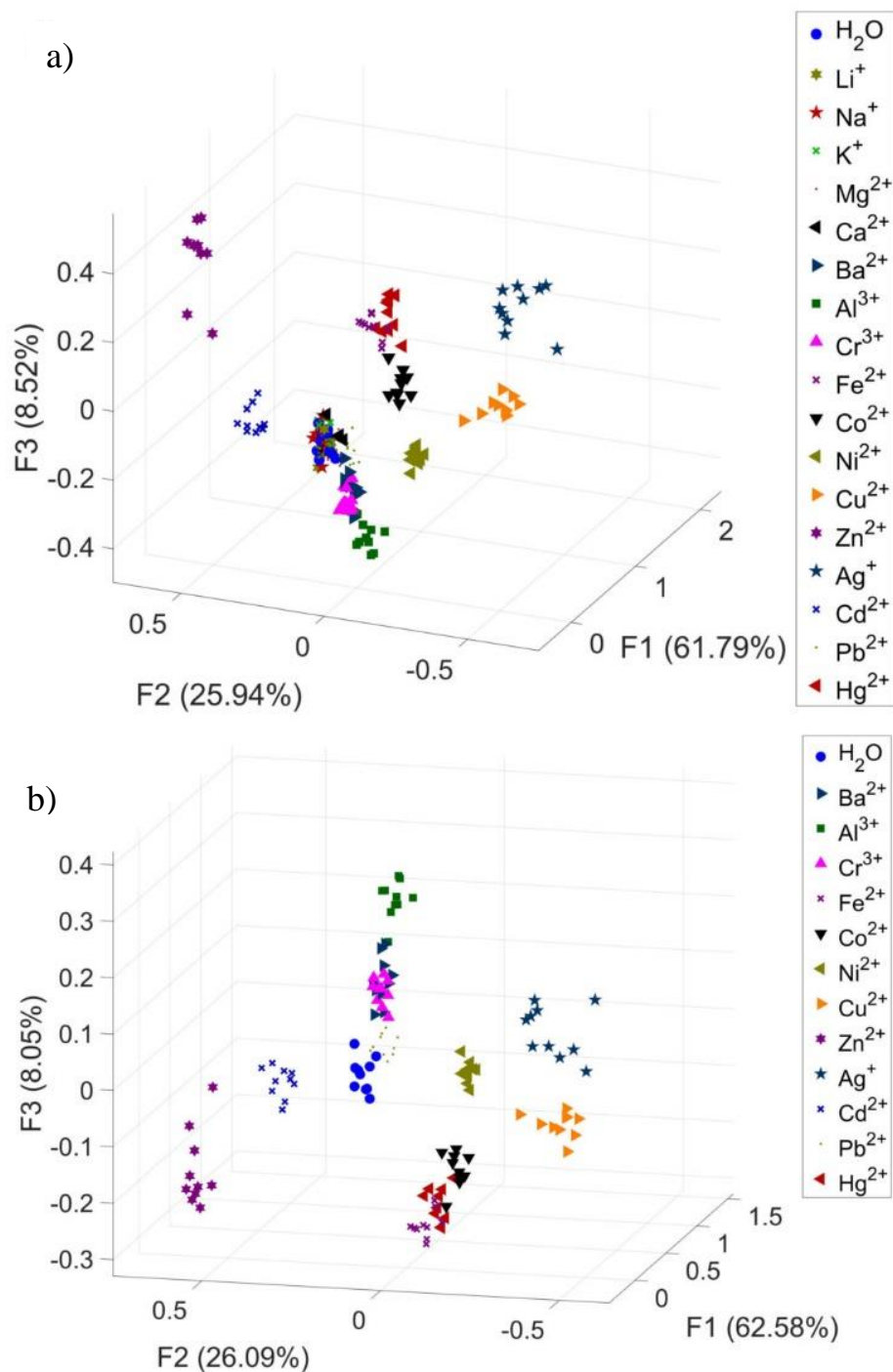


Figure 2.6. Three-dimensional LDA score plots of the combination of four fluorophores (**Asn.8AQ**, **Gly.3AQ**, **Gly.6AQ**, **Gly.8AQ**) in discriminating a) 17 analytes and one blank, and b) 12 analytes with one blank. Ten replicates were performed for each analyte.

The resulting analysis provided classification accuracies of four fluorophores (and their various combinations) for predicting 18 analytes. This is represented as a heat map as shown in Figure A13, where the same colors between each cell to its reference

color on the right panel means the system predicted the metal ion correctly. Any different color means the system predicted it to be some other metal ions as shown exactly in each color. This heat map confirm that the highest classification accuracies was achieved with sensing array containing four fluorophores. In addition, LDA with the Jackknife (Leave-One-Out) approach was performed to investigate the predictive ability of the sensing array on the ions. The Jackknife classification yielded 72.35% accuracy in placing all ions into the sensing system (

Table 2.1), while the successful prediction was raised up to 93.64% with the exclusion of the aforementioned group IA and IIA metal ions (Table 2.2). This is in good agreement with the LDA score plots.

Table 2.1. A Jackknife (leave one out cross-validation) classification table for the ions based on the discrimination performance of the combined sensors (**Asn.8AQ, Gly.3AQ, Gly.6AQ, Gly.8AQ**) in discriminating 17 metal ions and a blank. The prediction accuracy was determined to be 72.35%.

Analytes	H ₂ O	Li ⁺	Na ⁺	K ⁺	Mg ²⁺	Ca ²⁺	Ba ²⁺	Al ³⁺	Cr ³⁺	Fe ²⁺	Co ²⁺	Ni ²⁺	Cu ²⁺	Zn ²⁺	Ag ⁺	Cd ²⁺	Pb ²⁺	Hg ²⁺	%Class.
H ₂ O	0	2	1	4	2	1	0	0	0	0	0	0	0	0	0	0	0	0	0
Li ⁺	1	2	3	1	2	1	0	0	0	0	0	0	0	0	0	0	0	0	20
Na ⁺	1	2	4	2	0	1	0	0	0	0	0	0	0	0	0	0	0	0	40
K ⁺	0	2	1	3	0	4	0	0	0	0	0	0	0	0	0	0	0	0	30
Mg ²⁺	1	3	0	0	3	2	0	0	0	0	0	0	0	0	0	0	1	0	30
Ca ²⁺	0	3	1	2	1	2	0	0	0	0	0	0	0	0	0	0	1	0	20
Ba ²⁺	0	0	0	0	0	0	6	0	2	0	0	0	0	0	0	0	2	0	60
Al ³⁺	0	0	0	0	0	0	1	9	0	0	0	0	0	0	0	0	0	0	90
Cr ³⁺	0	0	0	0	0	0	2	0	8	0	0	0	0	0	0	0	0	0	80
Fe ²⁺	0	0	0	0	0	0	0	0	0	9	0	0	0	0	0	0	0	1	90
Co ²⁺	0	0	0	0	0	0	0	0	0	0	10	0	0	0	0	0	0	0	100
Ni ²⁺	0	0	0	0	0	0	0	0	0	0	0	10	0	0	0	0	0	0	100
Cu ²⁺	0	0	0	0	0	0	0	0	0	0	0	0	10	0	0	0	0	0	100
Zn ²⁺	0	0	0	0	0	0	0	0	0	0	0	0	0	10	0	0	0	0	100
Ag ⁺	0	0	0	0	0	0	0	0	0	0	0	0	0	0	10	0	0	0	100
Cd ²⁺	0	0	0	0	0	0	0	0	0	0	0	0	0	0	0	10	0	0	100
Pb ²⁺	0	0	0	0	1	1	0	0	0	0	0	0	0	0	0	0	8	0	80
Hg ²⁺	0	0	0	0	0	0	0	0	0	1	0	0	0	0	0	0	0	9	90

(%class. = %classifications)

Table 2.2. A Jackknife (leave one out cross-validation) classification table for the ions based on the discrimination performance of the combined sensors (**Asn.8AQ**, **Gly.3AQ**, **Gly.6AQ**, **Gly.8AQ**) in discriminating 12 metal ions and a blank. The prediction accuracy was determined to be 93.64%.

Analytes	H ₂ O	Ba ²⁺	Al ³⁺	Cr ³⁺	Fe ²⁺	Co ²⁺	Ni ²⁺	Cu ²⁺	Zn ²⁺	Ag ⁺	Cd ²⁺	Pb ²⁺	Hg ²⁺	%Class.
H ₂ O	9	0	0	0	0	0	0	0	0	0	0	1	0	90
Ba ²⁺	0	7	0	3	0	0	0	0	0	0	0	0	0	70
Al ³⁺	0	1	9	0	0	0	0	0	0	0	0	0	0	90
Cr ³⁺	0	1	0	8	0	0	0	0	0	0	0	1	0	80
Fe ²⁺	0	0	0	0	10	0	0	0	0	0	0	0	0	100
Co ²⁺	0	0	0	0	0	10	0	0	0	0	0	0	0	100
Ni ²⁺	0	0	0	0	0	0	10	0	0	0	0	0	0	100
Cu ²⁺	0	0	0	0	0	0	0	10	0	0	0	0	0	100
Zn ²⁺	0	0	0	0	0	0	0	0	10	0	0	0	0	100
Ag ⁺	0	0	0	0	0	0	0	0	0	10	0	0	0	100
Cd ²⁺	0	0	0	0	0	0	0	0	0	0	10	0	0	100
Pb ²⁺	0	0	0	0	0	0	0	0	0	0	0	10	0	100
Hg ²⁺	0	0	0	0	0	0	0	0	0	0	0	0	10	100

(%class. = %classifications)

Apart from the multiple detections of metal ions by chemometric approaches, a ready-to-use, paper-based device for detecting a single metal ion with naked-eye observation was also fabricated and evaluated for its sensitivity. Specifically, **Gly.8AQ** was *in-situ* synthesized on paper support as usual, followed by wax printing to generate confined channels for sample dropping. Thereafter, several concentrations of Zn²⁺ ion were dropped to each channel containing covalently bound **Gly.8AQ**, followed by a data collection process (Figure 2.7a-b, numerical data in Table 2.3). The digitized data were then used to create a calibration curve, which then revealed that **Gly.8AQ** gave a good linear response to the Zn²⁺ concentrations between 0-1 μM. At higher concentrations, the responses reached a plateau. Interestingly, the limit of detection (LOD), obtained from the calibration curve, was found to be about 200 nM (13 ppb), which is comparable to several works using more complicated methods in determining Zn²⁺ ion^{60, 61}. In addition, the maximum concentration tested, which gave very clear change by naked eyes, was still well below the minimum tolerable limit in bottled waters based on the Code of Federal Regulations at 5 ppm⁶². This cellulose-bound sensor also offers two additional benefits for sensing application. First, repeating steps of spotting and drying the analyte solution on the detection zone

should increase the amount of the analyte in contact with the sensing unit without washing it away. This was found to be a practical way to boost the sensitivity of the sensor by least 10 times (LOD = 13 nM, Figure 2.7c-d) when the photographic image was analyzed after 10 cycles of spotting and drying steps.

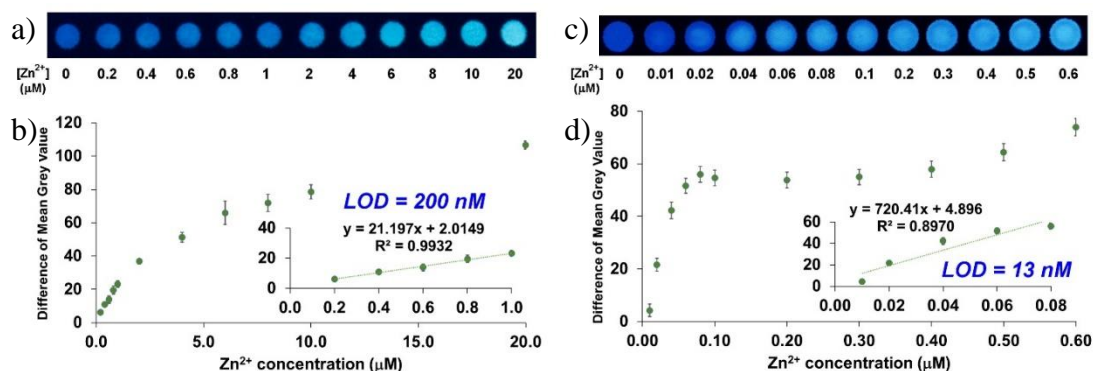


Figure 2.7. Representative images, along with scattered plots, of fluorescence changes of **Gly.8AQ** when incubated with different concentrations of Zn^{2+} ion via one spotting (a, b) and 10-time repeated spotting (c, d) of each solution. Calibration plots are also shown as insets in each graph.

Table 2.3. Numerical data of graphs shown in Figure 2.7.

Single spotting			10-time spotting		
$[\text{Zn}^{2+}]$ (μM)	Difference of Mean Gray Value	SEM	$[\text{Zn}^{2+}]$ (μM)	Difference of Mean Gray Value	SEM
0.20	6.21	0.78	0.00	5.91	2.41
0.40	10.93	1.54	0.01	5.96	2.44
0.60	13.89	2.26	0.02	7.53	3.07
0.80	19.53	2.46	0.04	6.99	2.85
1.00	23.10	1.94	0.06	7.42	3.03
2.00	36.83	1.61	0.08	7.36	3.01
4.00	51.27	3.08	0.10	7.35	3.00
6.00	65.94	7.00	0.20	7.14	2.91
8.00	71.82	5.10	0.30	7.41	3.02
10.00	78.54	4.32	0.40	7.98	3.26
20.00	106.55	2.37	0.50	7.87	3.21

The proof of principle here should also be applicable to improve sensitivity of other cellulose-bound sensors or any dryable surface-bound sensors. Second, a reusability test was conducted to exploit the surface-bound nature of the sensor. By simply incubating the Zn^{2+} -bound sensor with EDTA, a chelator for Zn^{2+} , followed by aqueous washing, the sensor was free and ready to sense Zn^{2+} again. Using this washing process, the cellulose-bound **Gly.8AQ** can be easily reused at least 10 times (Figure 2.8).

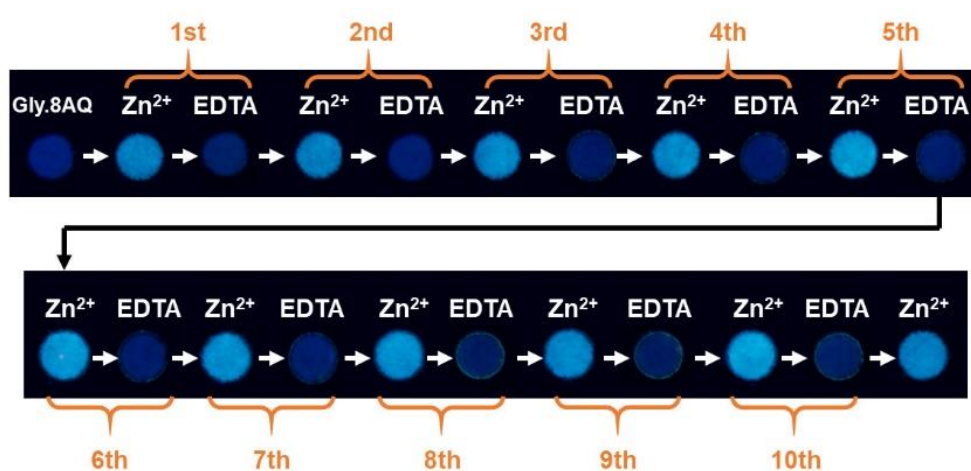


Figure 2.8. Fluorescence responses of **Gly.8AQ** in sensing Zn^{2+} after ten times. The sensor was recovered by sequestering Zn^{2+} with EDTA, a known chelator for Zn^{2+} .

In addition, the same concept was applied to two other prominent examples including **Asn.8AQ** with Zn^{2+} and Cd^{2+} (Figure 2.9), where the determination of LOD could be done in a similar manner.

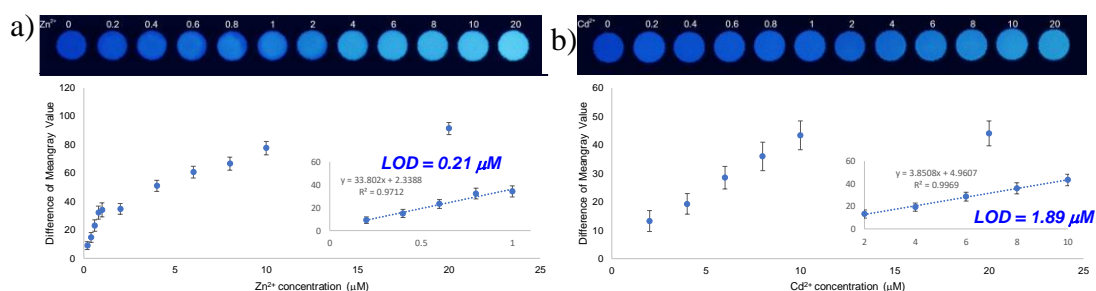


Figure 2.9. Response curves for **Asn.8AQ** in sensing (a) Zn^{2+} and (b) Cd^{2+} .

Taken together, this level of performance is considered to be superior to previous paper-based sensors for Zn²⁺ (Table 2.4). Clearly, all of them showed higher LOD values/working concentrations while only few studies reported the reusability of their sensors. Hence, the whole process very well demonstrated the utility of the macroarray synthesis in expediting the discovery of compounds with great practicality in sensing applications.

Table 2.4. Comparison of paper-based, fluorescent sensors for Zn²⁺ ion.

Reference	Working concentration (μM)	LOD (μM)	Reusability
63	5,000	N. R.	N. R.
64	5	N. R.	EDTA wash demonstrated
65	1	N. R.	N. R.
66	N/A	20	N. R.
67	1,000	N. R.	N. R.
68	200	N. R.	EDTA wash demonstrated
This work	0.01–1.0	0.01 for 10× repeated spotting	EDTA wash, at least 10 cycles

Working concentration is the concentration of Zn²⁺ ion used for demonstration in each study. This value is used for comparison due to the absence of LOD values in these studies. N/A = not applicable; N. R. = not reported.

To further confirm the success of the synthesis, and to indirectly characterize the immobilized molecules on support, selected compounds containing the suggested scaffolds from the results in Figure 2.5 were synthesized, fully characterized by NMR spectroscopy and MS, and studied fluorescence and UV-vis properties. For instance, 2-amino-*N*-(quinolin-8-yl)acetamide (surface-free version of **Gly.8AQ**) did show preferential increase in fluorescence upon binding to Zn²⁺ (Figure 2.10).

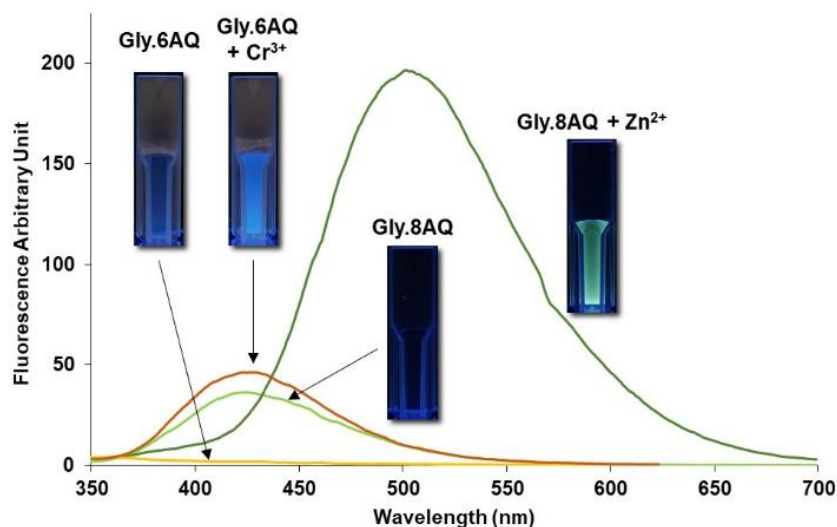


Figure 2.10. Fluorescence spectra of surface-free **Gly.8AQ** (10 μM with/without 50- μM Zn^{2+} - excited at 300 nm) and **Gly.6AQ** (10 μM with/without 50- μM Cr^{3+} - excited at 365 nm). Inset: the images of the cuvettes containing the same solutions (but with 100- μM fluorophores with/without 500- μM metal ions) under the illumination of 365-nm light. Note: the photos of **Gly.6AQ** solutions were taken with 1-s longer exposure time than that of **Gly.8AQ** due to lower fluorescence intensities.

The fluorescence titration in Figure 2.11 also confirmed the gradual decrease of the fluorescence at the emission maximum around 420 nm with concomitant increase in the fluorescence intensity at 500 nm under the higher concentrations of Zn^{2+} . UV-vis titration (Figure 2.12), on the other hand, showed that the absorption maximum around 300 nm was decreased in absorbance with a slight increase in the region around 330-400 nm when the concentrations of Zn^{2+} was increased. On the contrary, it was shown that the fluorescence of 2-amino-*N*-(quinolin-6-yl)acetamide (surface-free version of **Gly.6AQ**) was increased upon incubation with Cr^{3+} .

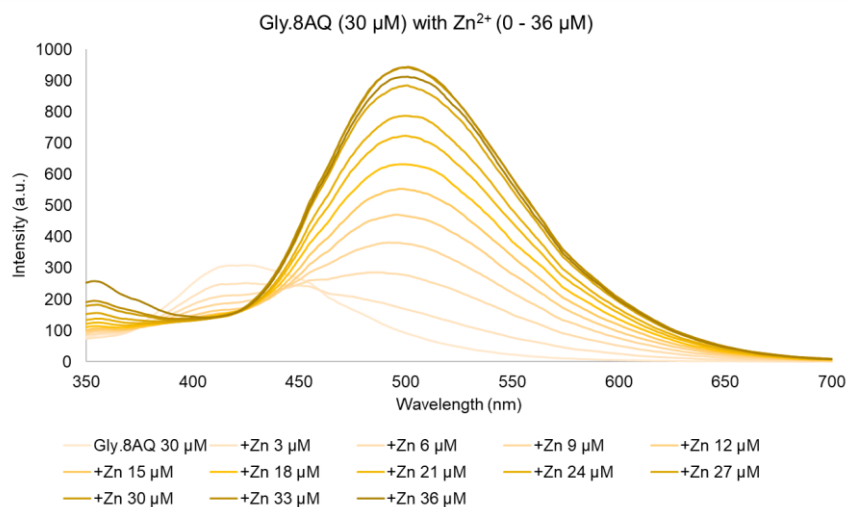


Figure 2.11. Fluorescence titration of **Gly.8AQ** with Zn^{2+} (excited at 300 nm)

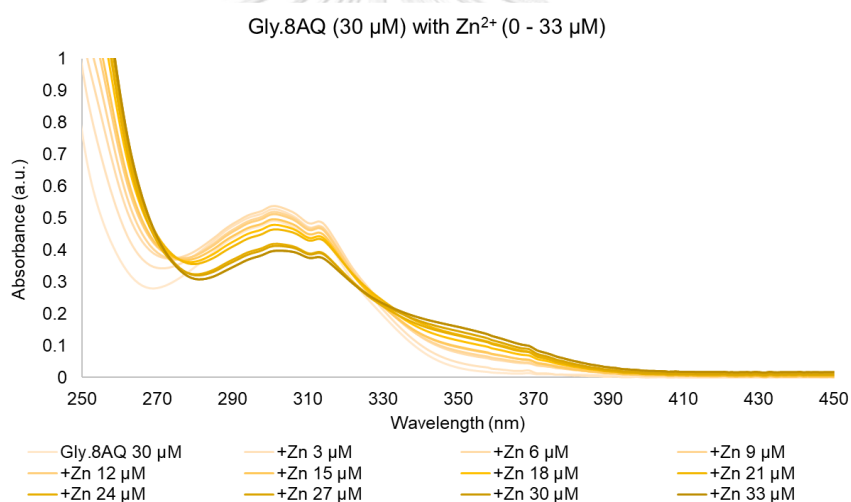


Figure 2.12. UV-vis titration of **Gly.8AQ** with Zn^{2+} .

A similar fluorescence titration (Figure 2.13) revealed that there was a single emission maximum (450 nm) in this case, whose fluorescence intensity was increased in a direct relationship with the increasing Cr^{3+} concentrations. UV-vis titration (Figure 2.14) of this sensor-metal ion pair appeared to be slightly complicated, with a general trend being that the absorption around 270-320 nm was significantly increased with higher Cr^{3+} concentrations.

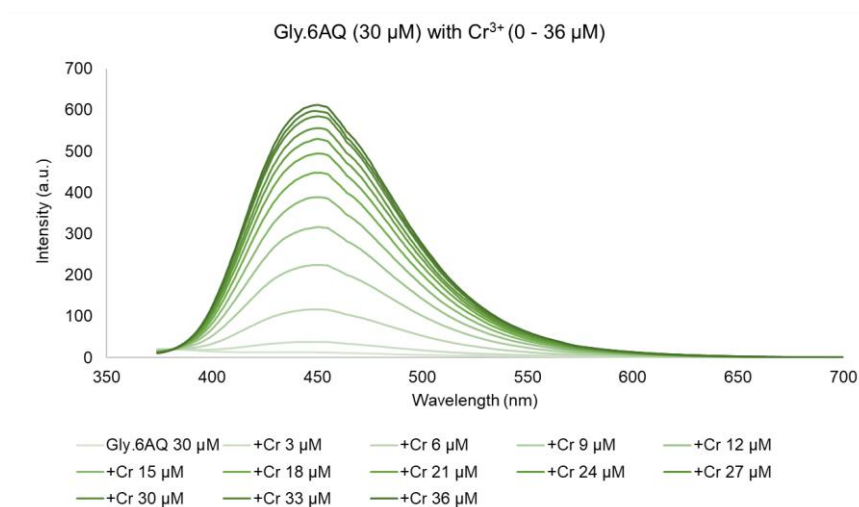


Figure 2.13. Fluorescence titration of **Gly.6AQ** with Cr^{3+} (excited at 365 nm).

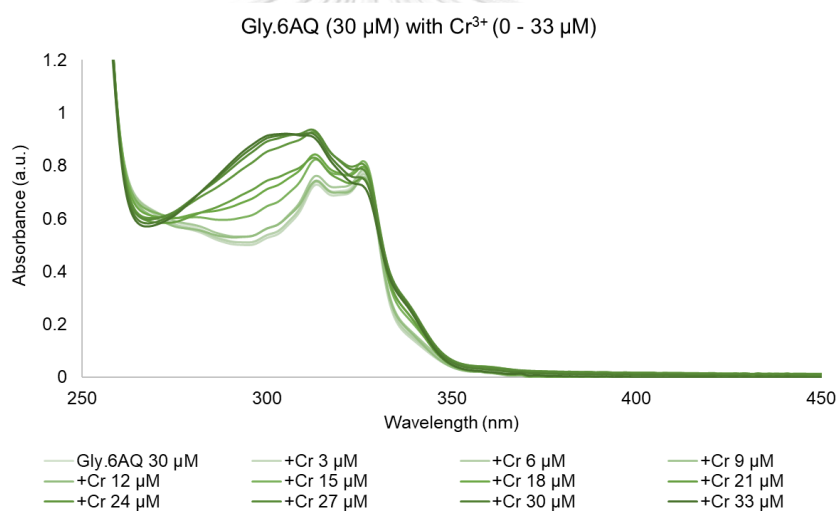


Figure 2.14. UV-vis titration of **Gly.6AQ** with Cr^{3+} .

This behaviour was also found to be similar for the interaction between the same ligand and Al^{3+} ion (Figure 2.15 and Figure 2.16). Interestingly, although surface-free **Gly.8AQ** could give much higher fluorescence intensity when bound to Zn^{2+} than did all other cases, the turn-on ratio (the fluorescence ratio of Cr^{3+} -**Gly.6AQ** complex over free **Gly.6AQ**) was slightly higher than that of **Gly.8AQ** with Zn^{2+} (ca. 25 folds vs 22 folds) due to much lower background in free **Gly.6AQ**. This indicated that both could function well as sensors for their respective metal ion partners and suggested that the synthetic strategy used in this study was an effective one to rapidly evaluate fluorescence properties of a variety of molecular scaffolds.

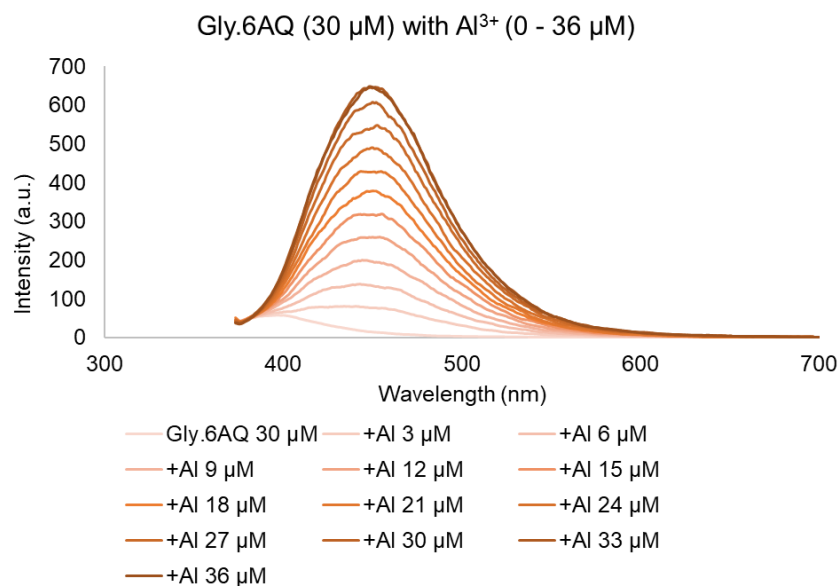


Figure 2.15. Fluorescence titration of **Gly.6AQ** with Al^{3+} (excited at 365 nm).

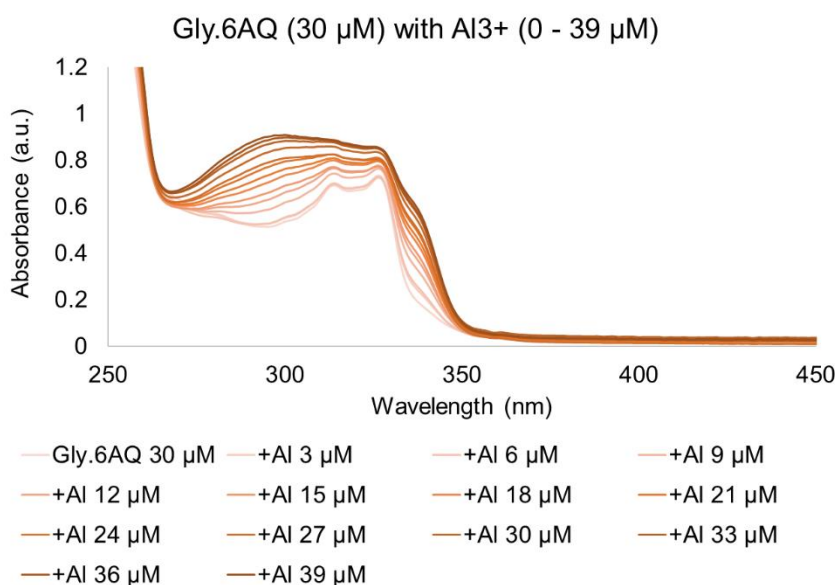


Figure 2.16. UV-vis titration of **Gly.6AQ** with Al^{3+} .

Last but not least, titration experiments via MS and NMR were also conducted to further confirm the binding interactions between selected pairs of ligands and metal ions. For MS titrations, as shown in Figure 2.17, surface-free **Gly.8AQ** exhibited both 1:1 and 2:1 binding modes (ligand:metal ion) when Zn^{2+} ion was sub-stoichiometric amounts, and 1:1 binding seemed to be dominant when the molar ratio was around 1:1.

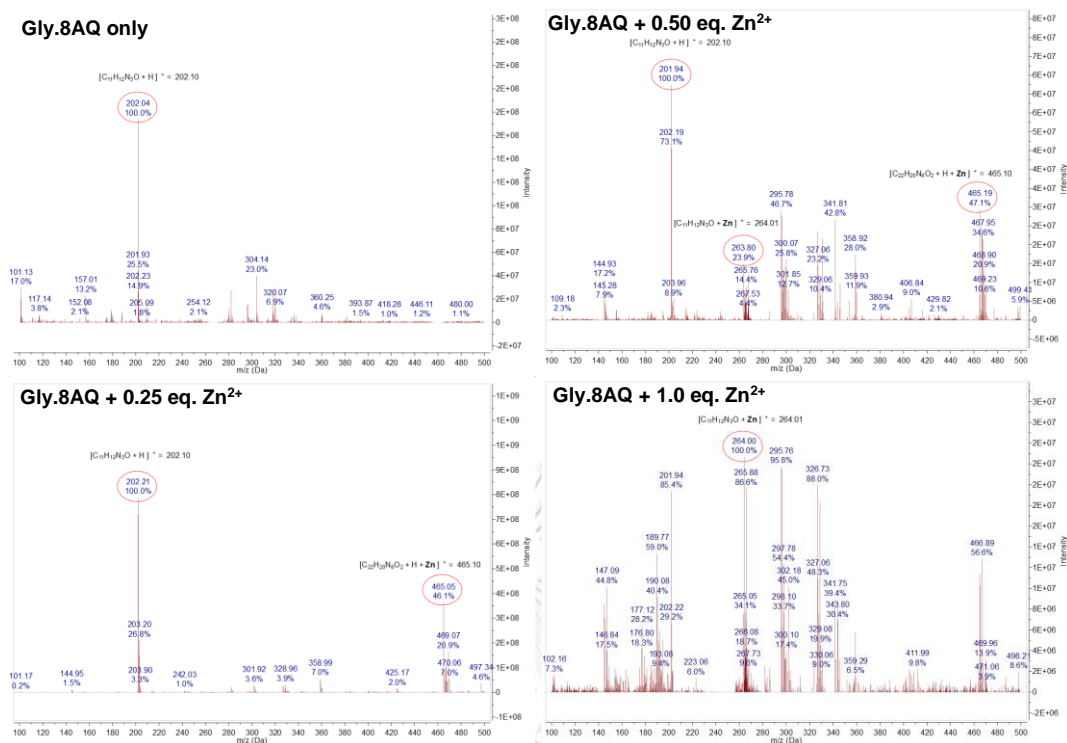


Figure 2.17. MS titration between surface-free **Gly.8AQ** and Zn^{2+} .

On the other hand, **Gly.6AQ** interacted with Cr^{3+} in a more complicated manner, showing only 3:2 binding mode (ligand:metal ion) once the molar ratio reached 1:1 (Figure 2.18).

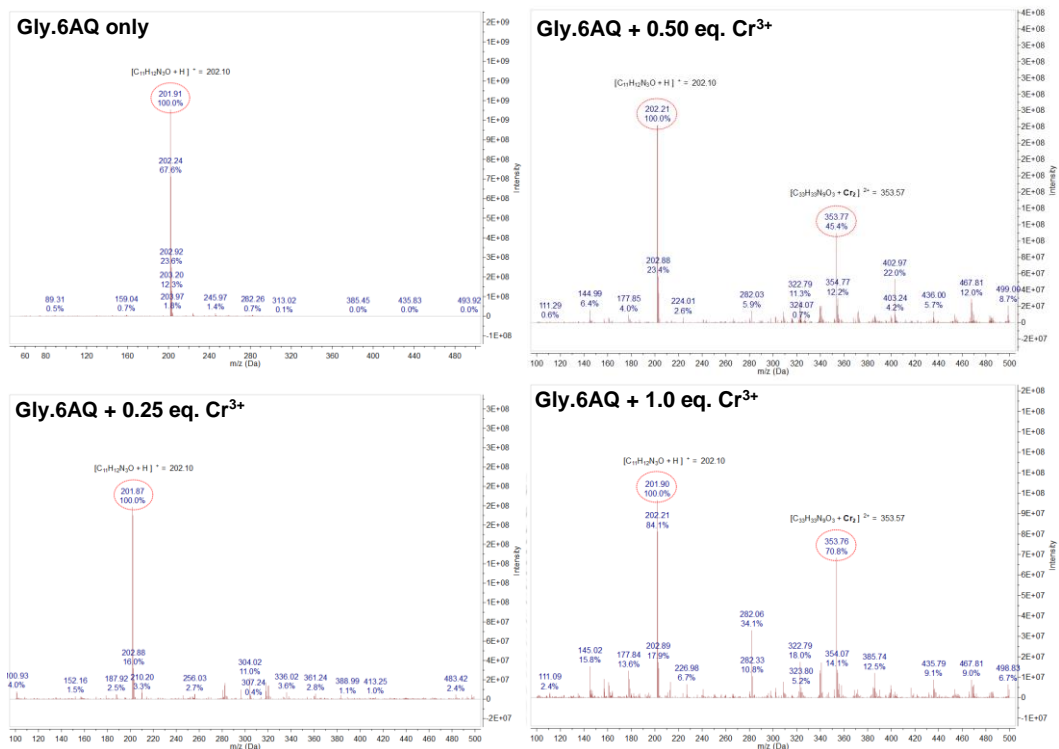


Figure 2.18. MS titration between surface-free **Gly.6AQ** and Cr^{3+} .

For NMR titration, the set of **Gly.8AQ** and Zn^{2+} showed several apparent shifts, with the most notable one being the methylene protons (starting at around 3.5 ppm) when more metal ion was added into the solution (Figure 2.19). All of these evidence clearly pointed out that there were indeed some significant bindings between the ligands and the metal ions used in this work.

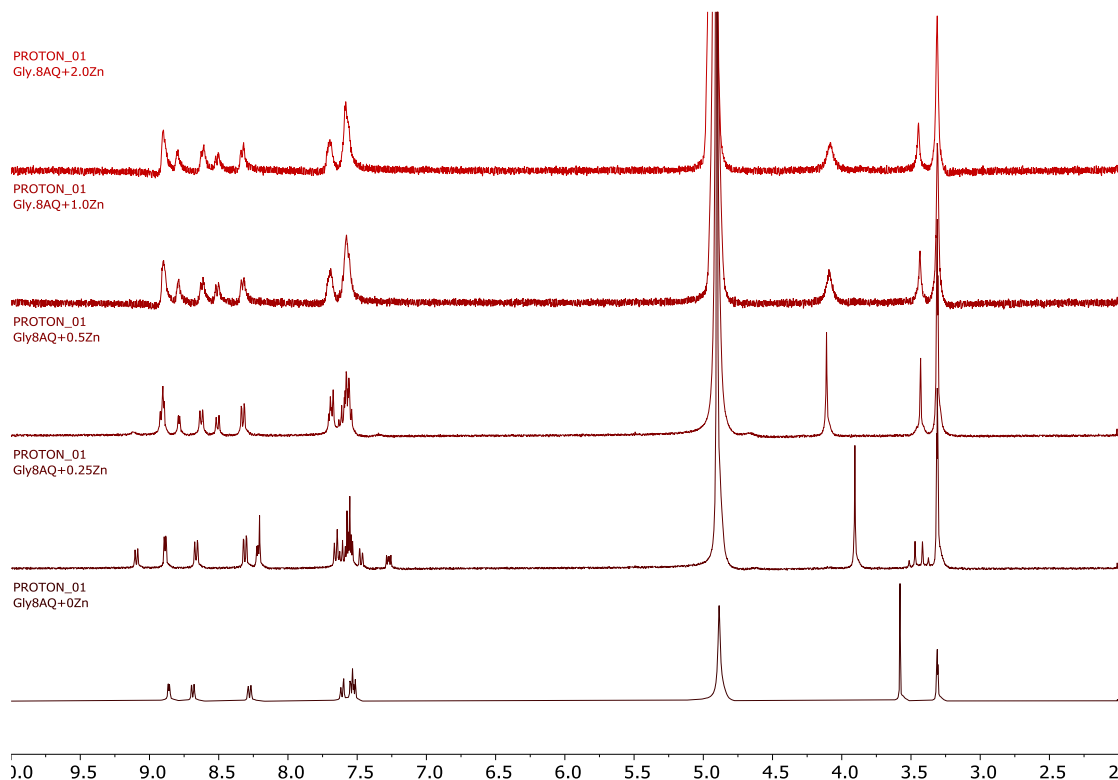


Figure 2.19. NMR titration between surface-free Gly.8AQ and Zn²⁺.

2.4. Conclusions

The macroarray synthesis approach was implemented herein to rapidly generate a variety of fluorophores, which were readily amenable to direct screenings to discover metal ion sensors. Using chemometric approaches, combined fluorophore systems could predict several metal ions with high prediction accuracies, while the fabrication of a single fluorophore to detect Zn²⁺ gave a practical paper-based sensor with great sensitivity and reusability. Lastly, this information could be reversed to yield typical solution-based sensors, hence demonstrating that the synthesis methodology is also a very useful tool for rapid discovery of even larger and more diverse libraries of fluorescent sensors.

CHAPTER III

Synthesis of Quinoline Ligands with Tunable Hydrophobicity for Distance-Based Quantification of Metal Ion on Paper-Based Fluorescent Sensors

Five amidoquinoline derivatives with different *N*-substitution were synthesized and used for the development of paper-based fluorescent sensing platform. In aqueous solution, the quinoline ligands selectively show strong green fluorescence upon binding to Zn^{2+} – this was clearly observed by naked eyes under blacklight irradiation. The paper-based sensor was prepared by depositing an amidoquinoline derivative in a wax-printed channel on filter paper. Developing of a Zn^{2+} sample, deposited below the ligand spot, with an aqueous buffer solution creates an intense green fluorescent line suitable for distance-based quantification. The ligands with a tertiary amino group showed better defined fluorescent line than did those ligands containing primary and secondary amino groups. The linear relationships between the length of the fluorescent lines, measured by naked-eye observation or image processing software, and the amounts of Zn^{2+} can be achieved in the range of 2.5-80 nmol. The hydrophobicity of the ligands increases the dynamic range of detection with an expense of the sensitivity and the detection speed. Importantly, the paper-based sensor was able to quantitatively analyze drinking water, dietary supplement, and fertilizer samples containing 0.04-64% (w/v) Zn^{2+} without multiple dilutions.

3.1. Introduction

Filter paper works as an excellent platform for reagent carrying and fluid transportation due to capillary action from hydrophilic and porous surface of non-woven cellulose fibers. Paper-based sensors are thus very attractive analytical devices for economical on-site chemical analysis of liquid samples.⁶⁹⁻⁷³ Distance-based quantification on paper-based sensors gains considerable attention as it offers simple naked-eye quantification. Currently, this method has been demonstrated with some success for a few analytes^{15, 17, 74-78} including limited number of metal ions.^{18, 79-82} The

development of paper-based sensing platforms with distance-based quantification capability requires not only a selective sensing probe but also suitable interface interaction involving the probe, analyte, stationary phase and mobile phase that is largely remained unexplored.

Zinc ion (Zn^{2+}) is an essential mineral playing crucial roles in living systems and environment.⁸³⁻⁸⁵ Although zinc is generally perceived as a relatively nontoxic element, either an excess or a deficiency of Zn^{2+} can be harmful for microorganisms, plants, animals, and human.⁸⁶⁻⁸⁸ Therefore, Zn^{2+} has been incorporated in dietary supplement for human and micronutrient fertilizer for plants. Recently, we have demonstrated that amidoquinoline is a convenient building block for constructing simple turn-on fluorescent probes for Zn^{2+} .^{6, 89} To apply the quinoline probes in a paper-based sensing platform with distance-based quantification capability, we decided to synthesize and investigate a series of amidoquinoline derivatives containing various alkyl substituted glycine side chain. This new series of quinoline fluorophores should provide systematic modulation of intermolecular interactions among the probe, cellulose substrate, and eluent. The fluorophores were evaluated and optimized for distance-based quantification of Zn^{2+} on paper-based sensing platform. The distance observed by naked eyes correlated well with distance determined by an image processing software. Using these paper-based sensors, the quantitative analysis of real samples containing Zn^{2+} at subpercentage to percentage level gave reliable results without multiple dilutions in the sample preparation.

3.2. Experimental section

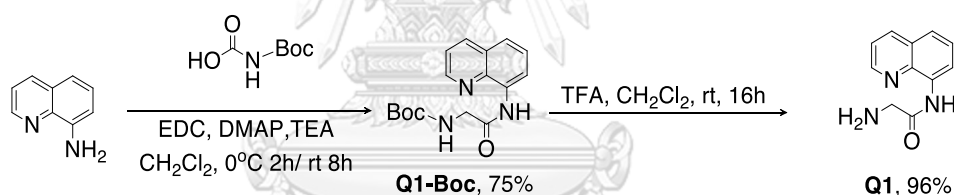
3.2.1. General information

8-Aminoquinoline, pyrrolidine, Boc-glycine, Boc-*N*-methylglycine, *N,N*-dimethylglycine, *N*-ethyl-*N'*-(3-dimethylaminopropyl)carbodiimide and hydrochloride (EDC·HCl) were purchased from TCI Tokyo Chemical Industry (Japan). 4-Dimethylaminopyridine (DMAP), triethylamine (TEA), chloroacetyl chloride, piperidine, ammonium chloride, trifluoroacetic acid (TFA) and sodium bicarbonate were purchased from Sigma Aldrich (USA). In anhydrous reactions, solvents such as dichloromethane and acetonitrile were dried before use. All column chromatography

was run on Merck silica gel 60 (70–230 mesh). Thin layer chromatography (TLC) was performed on Merck F245 silica gel plates. Solvents used for extraction and chromatography such as dichloromethane, hexane and ethyl acetate were commercial grade and distilled before use. All metal ions used in this study were in the form of nitrate salts. All aqueous solutions were made with Milli-Q water from ultrapure water systems with a Millipak 40 filter unit (0.22 μm , Millipore, USA). Whatman grade 1 qualitative filter paper was used for wax printed channel paper platform. The amount of Zn^{2+} in the drinking water, dietary supplement, and fertilizer samples was quantified according to the standard method (ASTM D1691-17) using Agilent 280FS atomic absorption spectrometer. NMR spectra were acquired on a Jeol NMR spectrometer at 500 MHz (^1H) and 125 MHz (^{13}C). The high-resolution mass spectra were obtained from an electrospray ionization MS (micro-TOF, Bruker Daltonics).

3.2.2. Synthetic procedures

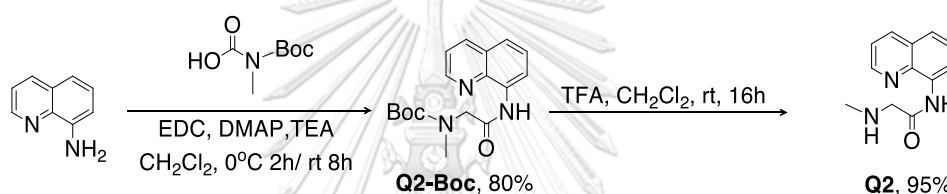
3.2.2.1. 2-amino-*N*-(quinolin-8-yl)acetamide (**Q1**)



8-aminoquinoline (500 mg, 3.47 mmol), DMAP (21.18 mg, 0.17 mmol) and triethylamine (0.97 ml, 0.70 mmol) were dissolved in dry CH_2Cl_2 (30 mL) Boc-glycine (1.22 g, 6.94 mmol) was added to the mixer in ice bath ($\sim 0^\circ\text{C}$) followed by the addition of EDC $\cdot\text{HCl}$ (1.33 g, 6.94 mmol). The reaction mixture was stirred at 0°C for 2 hours and stirred at room temperature for 8 hours. The reaction mixture was extracted with ammonium chloride. The combined organic layer was dried over MgSO_4 , filtered, and concentrated in high vacuum. The crude product was purified by column chromatography using silica gel (70-230 mesh) using 40% ethyl acetate in hexane as an eluent to afford compound **Q1-Boc** (784 mg, 75%) as a white solid. The deprotection of Boc protecting group of **Q1-Boc** (784 mg, 2.60 mmol) was achieved by using trifluoroacetic acid (1.0 mL, 13.3 mmol) in dichloromethane (10 mL). The stirring was continued at room temperature for 3 hours. Solvent and excess TFA were removed under high vacuum and then the reaction mixture was neutralized by

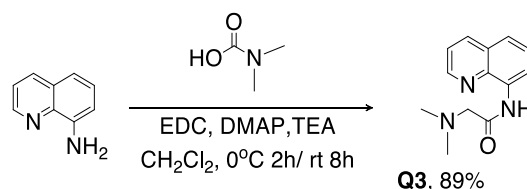
saturated sodium bicarbonate solution followed by an addition of dichloromethane (10 mL). The organic layer was separated and dried over MgSO_4 , filtered, and concentrated in high vacuum. **Q1** was obtained as a yellow solid (502 mg, 96%). ^1H NMR (400 MHz, $\text{DMSO-}d_6$) δ 11.62 (s, 1H), 8.92 (dd, $J = 4.0, 1.1$ Hz, 1H), 8.75 (d, $J = 7.5$ Hz, 1H), 8.39 (d, $J = 8.2$ Hz, 1H), 7.67–7.54 (m, 3H), 3.41 (s, 2H), 2.40 (s, 2H). ^{13}C NMR (101 MHz, $\text{DMSO-}d_6$) δ 172.2, 148.9, 138.1, 136.4, 134.2, 127.8, 127.0, 122.0, 121.5, 115.3, 45.6, 39.5. MS (ESI); m/z calculated for $[\text{C}_{11}\text{H}_{11}\text{N}_3\text{O} + \text{Na}]^+$ is 224.0794; found 224.0796 $[\text{M} + \text{Na}]^+$. The spectra images of ^1H , ^{13}C NMR and HRMS can also be found in Appendix Figure A14-16.

3.2.2.2. 2-(methylamino)-*N*-(quinolin-8-yl)acetamide (**Q2**)



Using a similar procedure in the synthesis of **Q1** but replacing Boc-glycine with Boc-*N*-methylglycine, **Q2** was obtained as a yellow solid (568 mg, 95% yield). ^1H NMR (500 MHz, $\text{DMSO-}d_6$) δ 11.31 (s, 1H), 8.93 (dd, $J = 4.2, 1.7$ Hz, 1H), 8.73 (dd, $J = 7.7, 1.4$ Hz, 1H), 8.40 (dd, $J = 8.3, 1.7$ Hz, 1H), 7.69 – 7.55 (m, 3H), 3.34 (s, 2H), 2.40 (s, 3H). ^{13}C NMR (126 MHz, $\text{DMSO-}d_6$) δ 171.1, 149.7, 138.6, 137.1, 134.6, 128.4, 127.6, 122.7, 122.2, 116.0, 56.2, 37.1. MS (ESI); m/z calculated for $[\text{C}_{12}\text{H}_{13}\text{N}_3\text{O} + \text{H}]^+$ is 216.1131; found 216.1132 $[\text{M} + \text{H}]^+$. The spectra images of ^1H , ^{13}C NMR and HRMS can also be found in Appendix Figure A17-19.

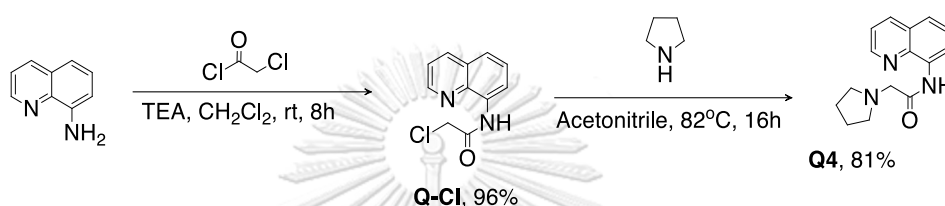
3.2.2.3. 2-(dimethylamino)-*N*-(quinolin-8-yl)acetamide (**Q3**)



Using a similar procedure in the synthesis of **Q1** but replacing Boc-glycine with *N,N*-dimethylglycine without Boc deprotection, **Q3** was obtained as a brown solid (708 mg, 89% yield). ^1H NMR (500 MHz, $\text{DMSO-}d_6$) δ 11.02 (s, 1H), 8.94 (dd, $J =$

4.3, 1.7 Hz, 1H), 8.71 (dd, $J = 7.7, 1.4$ Hz, 1H), 8.41 (dd, $J = 8.3, 1.7$ Hz, 1H), 7.70 – 7.61 (m, 2H), 7.59 (t, $J = 7.9$ Hz, 1H), 3.21 (s, 2H), 2.37 (s, 6H). ^{13}C NMR (126 MHz, DMSO- d_6) δ 168.9, 149.3, 138.0, 136.6, 134.0, 127.9, 127.0, 122.2, 121.9, 115.6, 64.0, 45.7. MS (ESI); m/z calculated for $[\text{C}_{13}\text{H}_{15}\text{N}_3\text{O} + \text{H}]^+$ is 230.1288; found 230.1289 $[\text{M} + \text{H}]^+$. The spectra images of ^1H , ^{13}C NMR and HRMS can also be found in Appendix Figure A20-22.

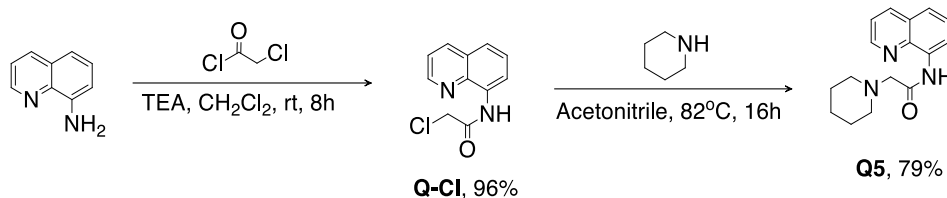
3.2.2.4. 2-(pyrrolidin-1-yl)-*N*-(quinolin-8-yl)acetamide (**Q4**)



8-aminoquinoline (500 mg, 3.47 mmol) and triethylamine (0.58 ml, 4.16 mmol) were dissolved in dry CH_2Cl_2 (30 mL). Chloroacetyl chloride (0.55 ml, 6.94 mmol) was gradually added to the solution mixer. The reaction mixture was stirred at room temperature for 8 hours followed by extraction with water. The organic layer was dried over MgSO_4 , filtered, and concentrated in high vacuum. The crude product was purified by column chromatography using silica gel (70-230 mesh) using 10% ethyl acetate in hexane as an eluent to afford compound **Q-Cl** (735 mg, 96%) as a white solid. The substitution of pyrrolidine group of **Q-Cl** (735 mg, 3.33 mmol) was achieved by using pyrrolidine (0.56 mL, 6.66 mmol) in acetonitrile (10 mL). The solution mixture was refluxed at 82°C for 16 hours. Solvent and excess pyrrolidine were removed under high vacuum and the reaction mixture was neutralized by saturated ammonium chloride solution followed by an addition of dichloromethane (30 mL). The organic layer was separated and dried over MgSO_4 , filtered, and concentrated in high vacuum. **Q4** was obtained as a yellow oil (689 mg, 81%). ^1H NMR (500 MHz, DMSO- d_6) δ 11.12 (s, 1H), 8.91 (dd, $J = 4.0, 1.6$ Hz, 1H), 8.67 (d, $J = 7.4$ Hz, 1H), 8.40 (dd, $J = 8.2, 1.6$ Hz, 1H), 7.67 (d, $J = 8.2$ Hz, 1H), 7.64 – 7.55 (m, 2H), 3.38 (s, 2H), 2.68 (q, $J = 4.5, 3.0$ Hz, 4H), 1.86 – 1.80 (m, 4H). ^{13}C NMR (126 MHz, DMSO- d_6) δ 169.7, 149.8, 138.6, 137.1, 134.5, 128.4, 127.6, 122.8, 122.3, 116.1, 60.2, 54.4, 24.2. MS (ESI); m/z calculated for $[\text{C}_{15}\text{H}_{17}\text{N}_3\text{O} + \text{H}]^+$ is 256.1444;

found 256.1446 $[M + H]^+$. The spectra images of ^1H , ^{13}C NMR and HRMS can also be found in Appendix Figure A23-25.

3.2.2.5. 2-(piperidin-1-yl)-*N*-(quinolin-8-yl)acetamide (**Q5**)



Using a similar procedure in the synthesis of **Q4** but replacing pyrrolidine with piperidine, **Q5** was obtained as a brown oil (482 mg, 79% yield). ^1H NMR (500 MHz, $\text{DMSO-}d_6$) δ 11.36 (s, 1H), 8.93 (dd, $J = 4.2, 1.7$ Hz, 1H), 8.66 (dd, $J = 7.2, 1.2$ Hz, 1H), 8.41 (dd, $J = 8.3, 1.7$ Hz, 1H), 7.69 – 7.55 (m, 3H), 1.68 (p, $J = 5.6$ Hz, 4H), 1.48 (q, $J = 6.0$ Hz, 2H). ^{13}C NMR (126 MHz, $\text{DMSO-}d_6$) δ 169.6, 149.7, 138.6, 137.1, 134.6, 128.4, 127.6, 122.8, 122.3, 115.9, 63.1, 54.8, 26.4, 24.0. MS (ESI); m/z calculated for $[\text{C}_{16}\text{H}_{19}\text{N}_3\text{O} + \text{H}]^+$ is 270.1601; found 270.1603 $[M + H]^+$. The spectra images of ^1H , ^{13}C NMR and HRMS can also be found in Appendix Figure A26-28.

3.2.3. Measurement of photophysical properties

Absorption spectra were obtained from aqueous solution samples using a 1.4 mL quartz cell with 1 cm optical path length and recorded in the wavelength range of 200–1000 nm at ambient temperature. Each sample was prepared from a stock solution of the compound in methanol and diluted to the desired concentration with aqueous Tris-HCl buffer pH 7.4. All final solutions contained less than methanol (1%, v/v). The fluorescence spectra were acquired from the aqueous solution samples using an excitation wavelength at 340 nm and recorded in the wavelength range of 350–700 nm.

3.2.4. Preparation of the paper-based fluorescent sensing platform and analysis performance

The layout of the sensing platform consisting of unwaxed channels with 1.5-mm wide and 56-mm long was printed on a Whatman Grade 1 filter paper by a wax printer (Xerox ColorQube 8870). The printed channels were heated in an oven at 150 °C for 90 seconds for melting the wax and creating hydrophobic barriers in the paper

sheet. The ligand and metal ion samples were deposited from 0.5 μL of their solutions at the loading zone of a channel on the filter paper. The loaded paper-based sensor was dipped vertically into an aqueous solution in a closed chamber for chromatographic development. For naked-eye quantification, the distance of a fluorescent line travelling in the channel was observed against a ruler scale. For image analysis, the images were captured by using a digital camera (Panasonic DMC-GF7) with the following camera setting: ISO-3200, f/5.6, and 1/250 s exposure time in a cover box under a 365-nm UV light ambient (TCP-20.LM Vilber Lourmat illuminator, Germany). The mean grey value of the image was extracted from the center area covering $\sim 70\%$ width of the channel to avoid color interference from the wax barrier, using the ImageJ program (<http://imagej.nih.gov/ij/>). The mean gray values were plotted against the pixel positions, starting from 0.50 cm above the ligand loading spot. The distance was then determined from a boundary of the fluorescence line having a threshold value of $10\times$ standard deviation (SD) of the mean gray value of the pure ligand (blank). The limits of detections were calculated from $3\times\text{SD}$ (of the shortest observed distance)/slope (of the calibration line).

3.3. Results and Discussion

To systematically modulate the intermolecular interactions among the sensing probe, cellulose substrate, and the eluent, the structures of amidoquinoline ligands **Q1-Q5** (Figure 3.1) were designed to have different alkyl substituents on the terminal amino group of the glycine side chain. This variation provides tuning of hydrogen bonding and hydrophobicity of the sensing probes. The target probes were synthesized, evaluated for metal ion sensing properties, and developed into paper-based sensors for quantitative analysis of Zn^{2+} in real samples.

3.3.1. Synthesis and characterization

The target amidoquinoline derivatives (**Q1-Q5**) were successfully synthesized from amide coupling reactions and *N*-alkylation according to Figure 3.1. The coupling of 8-aminoquinoline with glycine derivatives in the presence of TEA, DMAP and EDC gave Boc-protected precursors **Q1-Boc**, **Q2-Boc** and the target compound **Q3** in high yields. The deprotection of Boc group with TFA gave **Q1** and **Q2** in excellent

yields. The condensation of 8-aminoquinoline with chloroacetyl chloride gave precursors **Q-Cl** followed by nucleophilic substitutions with pyrrolidine and piperidine cleanly gave **Q4** and **Q5**, respectively. The chemical structures and purity of **Q1-Q5** were confirmed by ^1H , ^{13}C NMR and MS (Figure A14-A28). Clean ^1H NMR spectra of **Q2-Q5** showed similar pattern of aromatic proton signals to that of **Q1** reported in our previous work.⁶ The additional ^1H signals of the aliphatic protons in **Q2-Q5** were located in the range of 1.0-4.0 ppm.

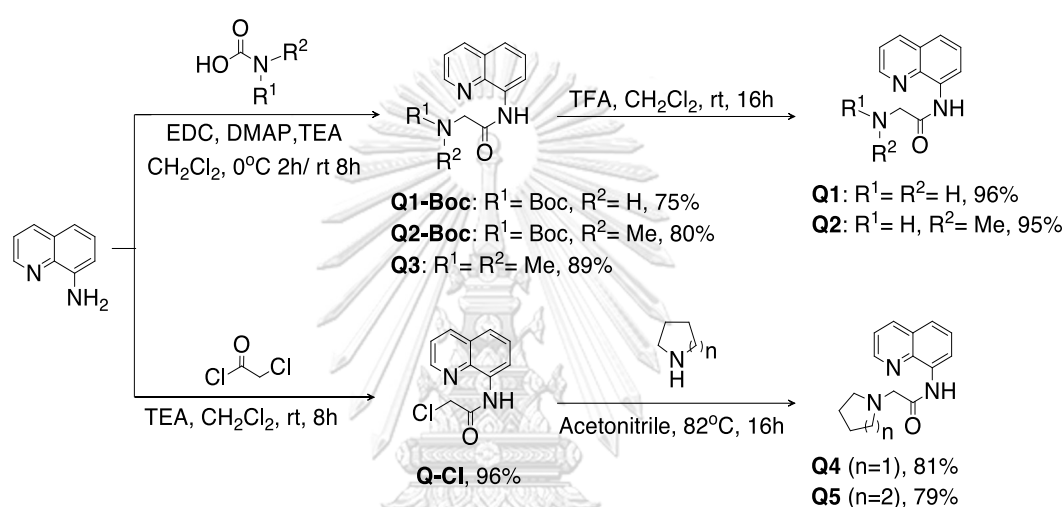


Figure 3.1. Synthesis scheme of target aminoquinoline derivatives (**Q1-Q5**)

3.3.2. Metal ion sensing study

The fluorescence responses of **Q1-Q5** to various metal ions (Li^+ , Na^+ , K^+ , Mg^{2+} , Ca^{2+} , Ba^{2+} , Al^{3+} , Cr^{3+} , Fe^{2+} , Co^{2+} , Ni^{2+} , Cu^{2+} , Zn^{2+} , Ag^+ , Cd^{2+} , Pb^{2+} and Hg^{2+}) were tested in Tris-HCl buffer solution pH 7.4. In the aqueous solution, all ligands showed low fluorescence that was considerably enhanced in the presence of only Zn^{2+} . The strong blue-green fluorescence was clearly observed by naked eye and the fluorescence spectra showed strong emission peak at $\lambda_{\text{em}} \sim 500$ nm with over 10 times of the enhancement ratio (I/I_0) (Figure 3.2).

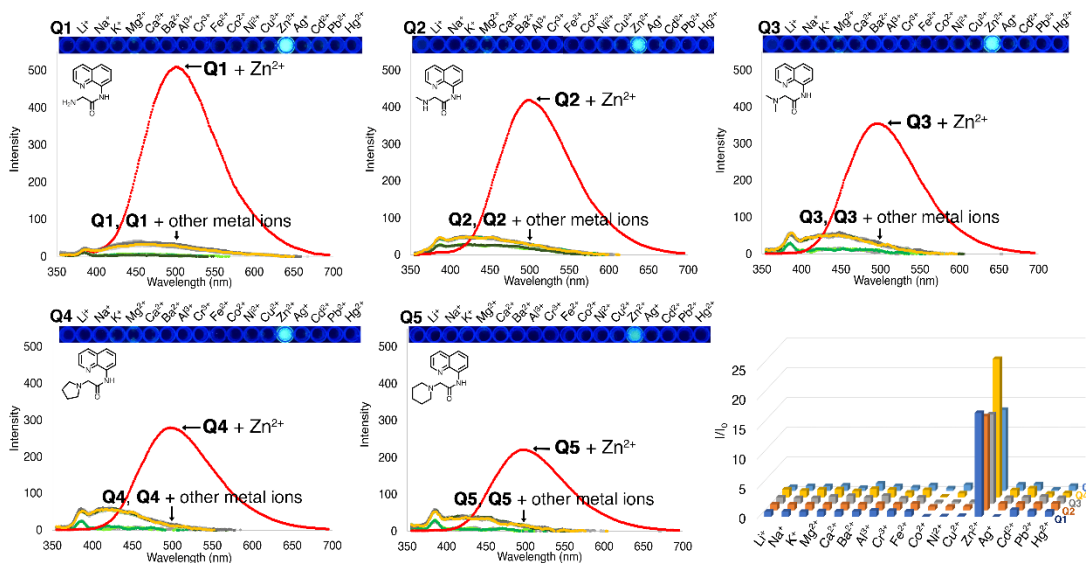


Figure 3.2. Fluorescence spectra and photographic images of **Q1-Q5** (10 μM in 20 mM Tris-HCl solution) tested with various metal ions (100 μM) and their fluorescence intensity enhancement ratios (I/I_0 measured @500 nm, excited @340 nm).

The pH dependence of the fluorescence response of the ligands toward Zn^{2+} in aqueous media was also studied. All compounds showed no pH dependence of the emission intensity in the pH range of 4.0-9.0. In the presence of Zn^{2+} , the emission intensity (@500 nm) was enhanced starting from pH ~ 6.5 reaching the maximum plateau at the pH range of 7.4-8.0 and gradually dropped at higher pH (Figure 3.3). The initial rise of the fluorescence enhancement signifies the stronger complexation between the ligand and Zn^{2+} at higher pH that is promoted by the deprotonation of the amidic proton.^{33, 90-92} The fluorescence drop at the pH higher than 8.0 is likely due to the competitive formation of $\text{Zn}(\text{OH})_2$.

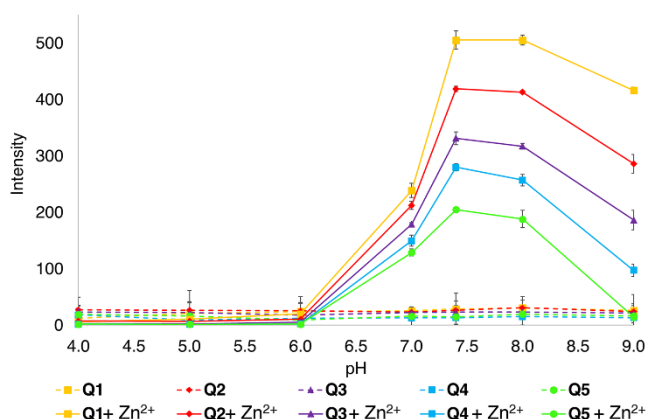


Figure 3.3. Fluorescence intensity (@500 nm) of **Q1-Q5** solution (10 μM in 20 mM Tris-HCl buffer solution) in the absence (—) and presence (---) of Zn^{2+} (100 μM) at various pH.

The 1:1 complexation constants (K_a) between the ligand and Zn^{2+} were determined from host-guest UV titration data using the BindFit v0.5 online tools (supramolecular.org).⁹³ Interestingly, the Zn^{2+} complexation constants with the ligands containing cyclic amine (**Q4** and **Q5**) were relatively lower than those with other ligands (Figure 3.4), probably due to geometrical constraint of the ring that reduce the chelation of the amino lone pair to the metal ion..

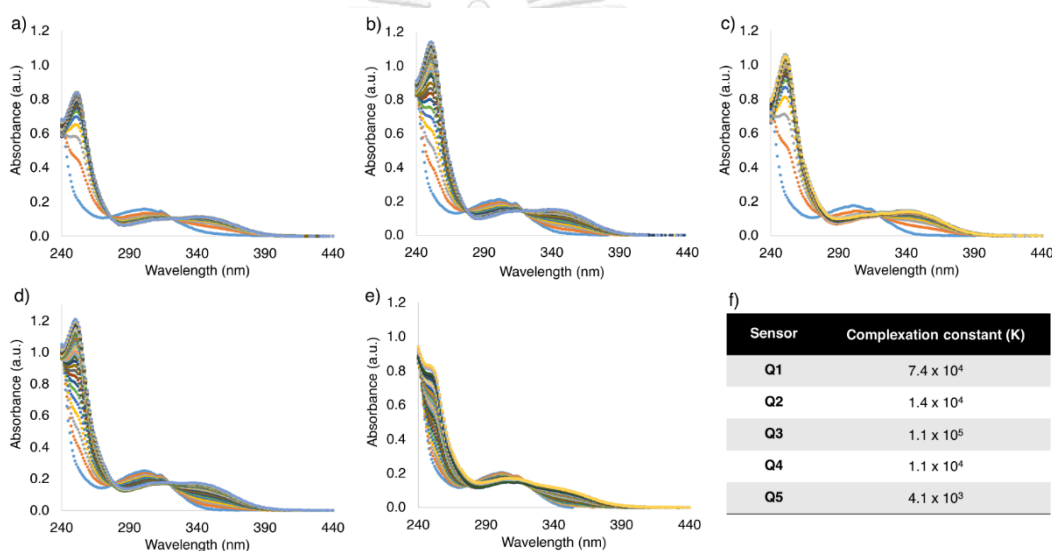


Figure 3.4. Absorption spectra of (a) **Q1**, (b) **Q2**, (c) **Q3**, (d) **Q4** and (e) **Q5** (40 μM) with gradual increment of Zn^{2+} concentration (0-800 μM) in Tris-HCl solution (20 mM) and (f) association constants of **Q1-Q5** with Zn^{2+} .

3.3.3. Preparation and optimization of paper-based sensors

In the preparation of a paper-based sensing platform, **Q4** was selected as an initial probe model for optimization due to its lowest background fluorescence. The sensing platform was produced by wax-printing to generate channel pattern on filter paper and heated to create wax barrier (Figure 3.5a). An ethanolic solution of the ligand **Q4** was deposited at the lower end of the channel. To test the sensing properties, a solution of each metal ion was deposited just below the ligand spot. The paper-based platform was then dipped into a Tris-HCl buffer solution (pH 7.4) in a closed chamber where the solution was allowed to elute upward until the solvent front reached the top of the

platform (Figure 3.5b). After air drying (Figure 3.5c), strong blue-green fluorescent line was observed under blacklight illumination selectively in the channel of Zn^{2+} (Figure 3.5d) – this is consistent with the selectivity observed in the solution test.

For quantification of Zn^{2+} via distance measurement, the length of the fluorescent line was either observed by naked eye against a ruler scale or evaluated from the photographic image by ImageJ processing software (Figure 3.5e). The mean gray values of pixels were plotted as a function of the distance. The length of the fluorescence line was determined from the distance that the mean gray value of the pixels equal to the threshold value set at 10 times of noises (SD of blank signals).

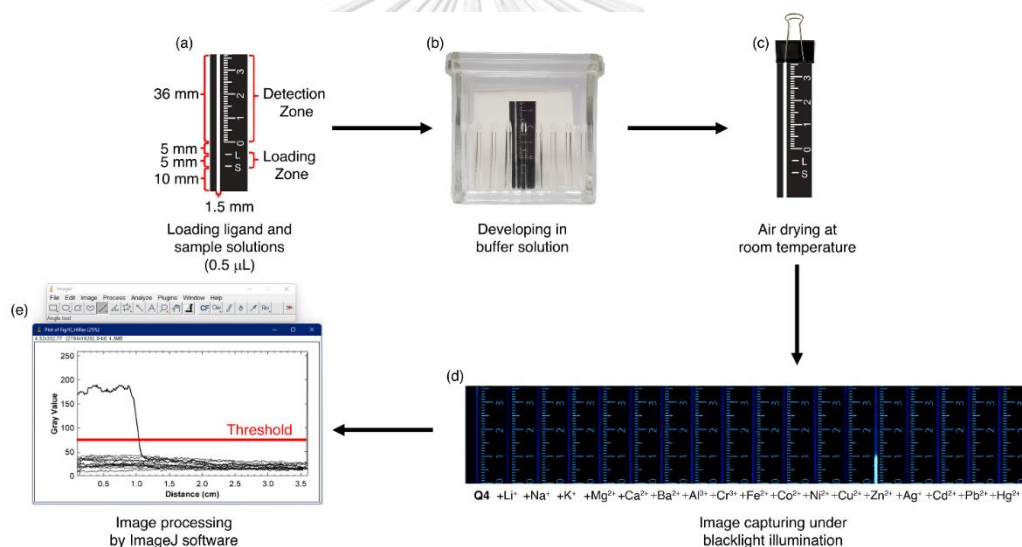


Figure 3.5. Experimental process for distance-based quantification of Zn^{2+} by paper-based sensor, a) drawing of paper-based channel sensing platform showing deposited point for ligand (L) and sample (S), (b) photographic image of paper-based sensor dipped into a Tris-HCl buffer solution (pH 7.4) in a closed chamber, (c) drying method of paper-based sensor after the solvent was reached the top of the platform (d) photographic images under black light illumination of paper-based sensor **Q4** (100 nmol) tested with various metal ions (20 nmol) eluted with Tris-HCl buffer solution pH 7.4 (0.20 M).

All 5 synthesized ligands were comparatively evaluated on a paper-based sensing platform. **Q1** and **Q2** showed little dependence to the amount of Zn^{2+} tested (Figure 3.6). Moreover, the fluorescent lines of **Q1** appeared to be separated into 2 sections. **Q3**, **Q4** and **Q5** showed fluorescent line with the length dependence to the amount of

Zn^{2+} . The results clearly indicated the superiority of the ligands containing tertiary amine (**Q3**, **Q4** and **Q5**) over the primary amine ligand (**Q1**) and secondary amine ligand (**Q2**) as distance-based fluorescent sensors. The hydrophilicity and hydrogen bonding present in the primary or secondary amine of the ligands are largely responsible for the fast and non-uniform elution of both the free ligands and their complexes. Being more hydrophobic, the tertiary amine ligands (**Q3-Q5**) tended to adsorb more strongly to the filter paper that only their zinc complexes can be eluted. The hydrophobic ligand also exhibited shorter fluorescent line that affected the dynamic range of the sensor in Zn^{2+} quantification.

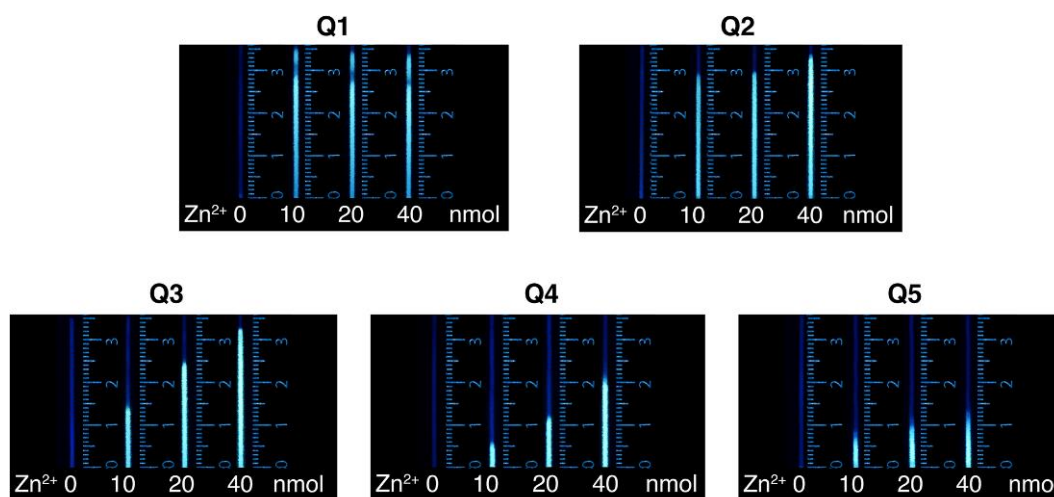


Figure 3.6. Photographic images of **Q1-Q5** (100 nmol) deposited on wax barrier printed filter paper channel tested with various amounts of Zn^{2+} deposited from $Zn(NO_3)_2$ solutions eluted with Tris-HCl buffer pH 7.4 solution (0.20 M). Images were taken under black light illumination.

To evaluate the effect of the ligand amount on the sensor performance, various amounts of **Q4** were used for the preparation of the sensor. With 1 nmol of **Q4**, the fluorescent lines appeared relatively weak and the gray value profiles were irregular probably due to the insufficient amount of ligand for complete complexation with Zn^{2+} . When the amount of the ligand increased, the fluorescent lines became stronger and the gray value profiles became more consistent (Figure 3.7). Nevertheless, it is important to note that increasing the ligand amount generally requires longer time to complete the elution. For further optimization, 100 nmol of **Q4** was used as it

produced the most consistent gray value profiles within acceptable elution time (less than 30 min).

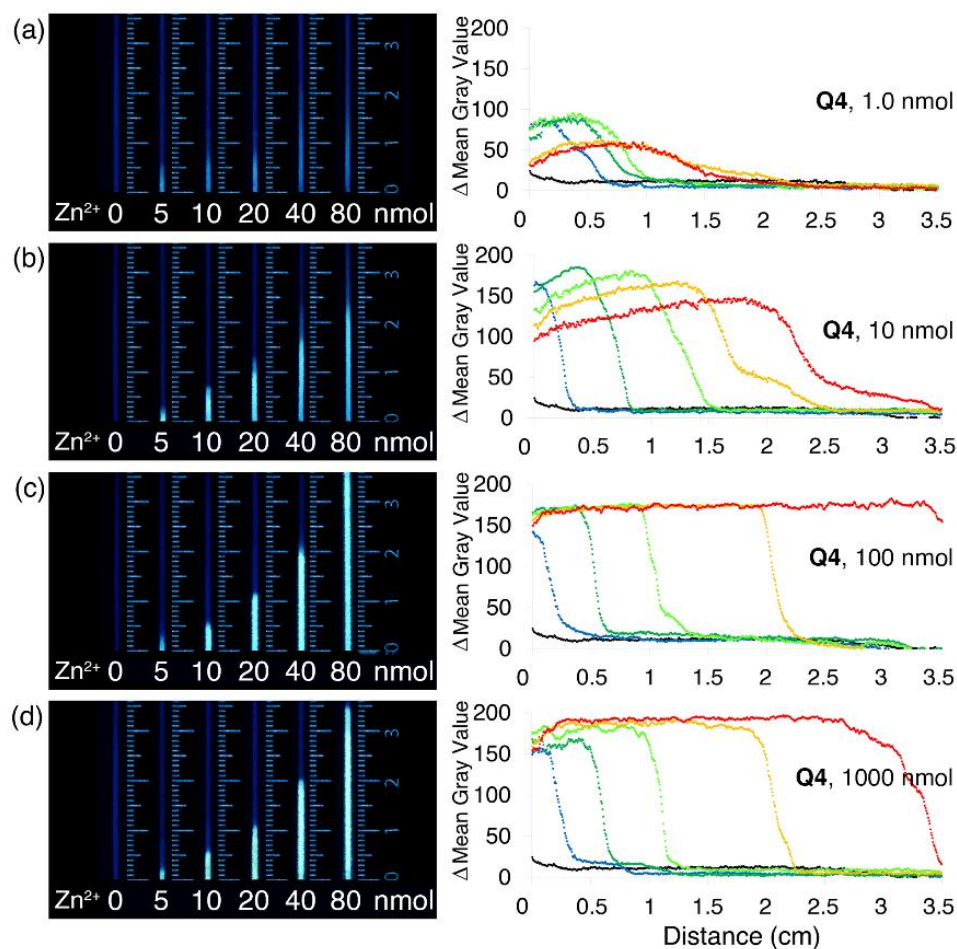


Figure 3.7. Photographic images under black light illumination of **Q4** paper-based channel sensors tested with various amounts of Zn^{2+} (• 0, • 5, • 10, • 20, • 40, • 80 nmol) and their mean gray values measured at various distances along the channel. Deposited amounts of **Q4** are a) 1.0, b) 10, c) 100 and d) 1000 nmol. Mean gray values were averaged from 10 pixels across each channel of 3 sensor replicates.

For further optimization, the sensor was evaluated for its performance in different pH ranging from 5.0 to 8.0. At the pH lower than 7.0, the fluorescence lines and gray value profiles were rather irregular (Figure 3.8). The most uniform fluorescent line and gray value profile was obtained at pH 7.4. At pH 8.0, the fluorescent lines were considerably shortened probably due to the formation of $\text{Zn}(\text{OH})_2$. The effects of pH observed in these paper-based sensing platform are consistent with the results observed in solution described in the previous section.

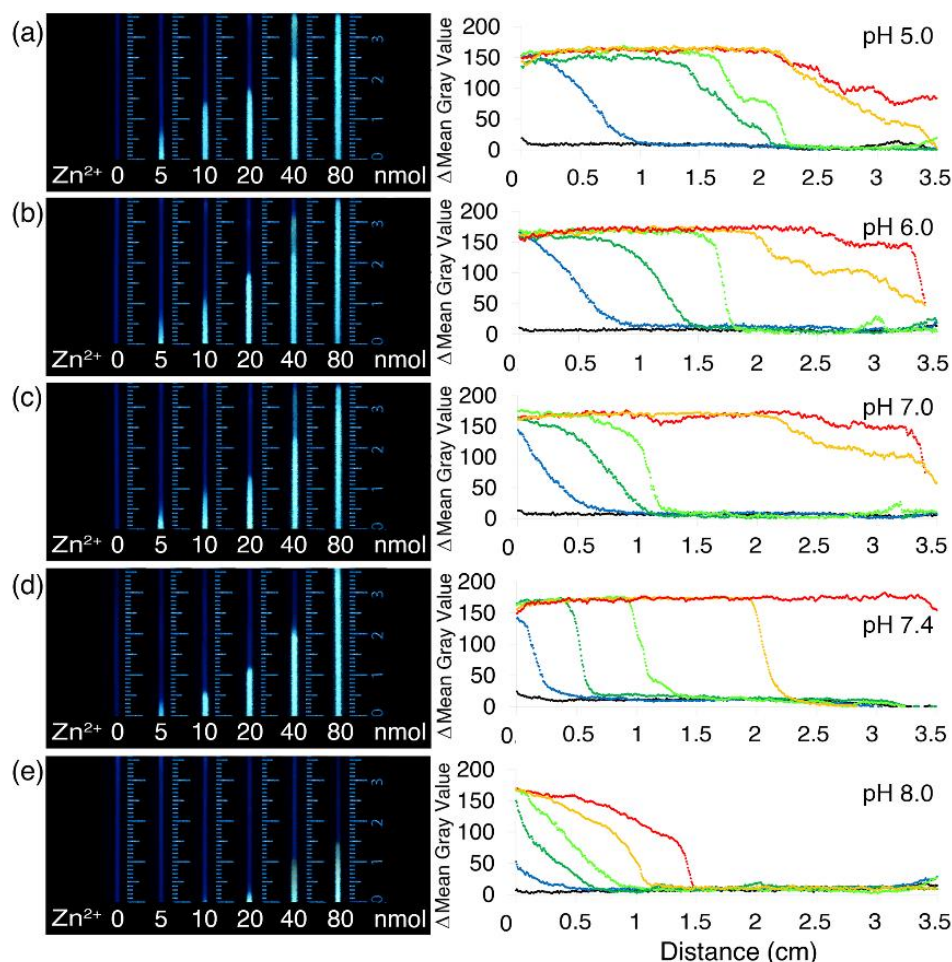


Figure 3.8. Photographic images under black light illumination of **Q4** (100 nmol) paper-based channel sensors tested with various amounts of Zn^{2+} (• 0, • 5, • 10, • 20, • 40, • 80 nmol) and their mean gray values measured at various distances along the channel. Eluent pH were a) 5.0, b) 6.0, c) 7.0 d) 7.4 and e) 8.0. Mean gray values were averaged from 10 pixels across each channel of 3 replicates.

To evaluate the effect of channel width, the sensing channels were created with varied widths and tested for Zn^{2+} sensing. Interestingly, increasing the channel width from 1.5 to 4.5 mm insignificantly affected the length of fluorescent lines indicating that the quantitative analysis has a good toleration to the channel width variation (Figure 3.9). However, the wider channels slightly deteriorate the fluorescence uniformity in the channel and the gray value profiles, especially at higher concentration of Zn^{2+} . In this work, the most uniform fluorescent line was obtained with the narrowest channel having the width of 1.5 mm.

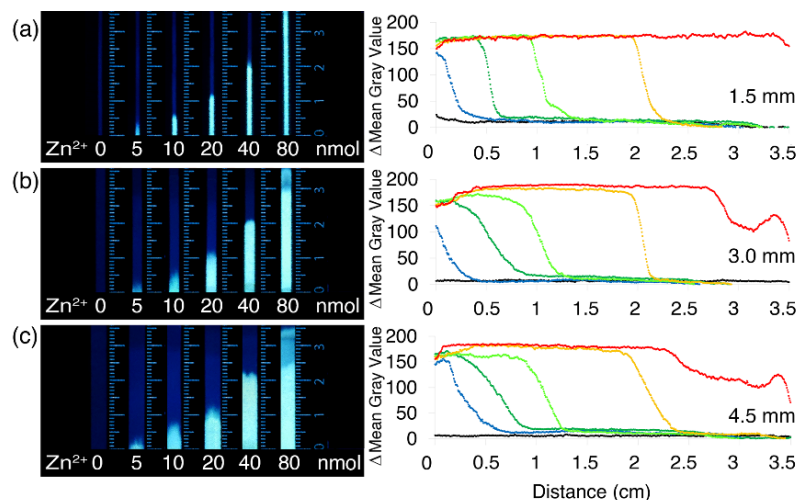


Figure 3.9. Photographic images under black light illumination of **Q4** paper-based channel sensors tested with various amounts of Zn^{2+} (\bullet 0, \bullet 5, \bullet 10, \bullet 20, \bullet 40, \bullet 80 nmol) and their mean gray values plotted as a function distance along the channel. Channel width are a) 1.5 mm, b) 3.0 mm and c) 4.5 mm. Mean gray values were averaged from 10 pixels across each channel of 3 sensor replicates.

Next, **Q3-Q5** were evaluated for sensitivity and applicability for distance-based quantification of Zn^{2+} using optimal sensing condition presented above. The fluorescence distances observed by naked eye and those determined by image analysis were virtually equal as shown in the scattered plots (Figure 3.10). The results indicate that the distance-based quantification with these sensors can be performed either by naked eye observation or image analysis.

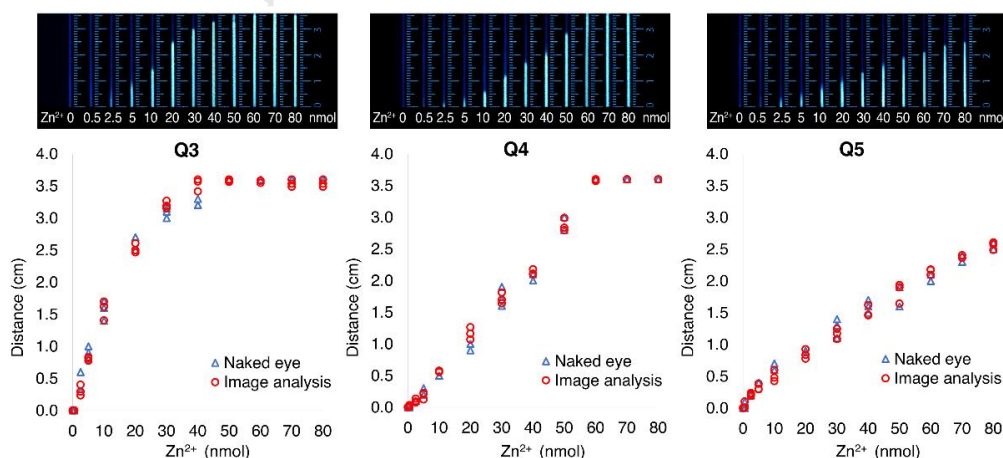


Figure 3.10. The scatter plots of fluorescent distance observed by naked eye against a ruler scale (Δ) and image analysis using a threshold line at the 10 times of noises (\square), 3 replicates.

Ligands **Q3**, **Q4** and **Q5** showed different linear ranges between the distance and the amount of Zn^{2+} , 0-30, 0-60 and 0-70 nmol, respectively (Figure 3.11). The detection limits for **Q3**, **Q4** and **Q5**, determined from $3 \times SD$ (of the shortest observed distance)/slope (of the calibration line) were 1.87, 1.32 and 1.57 nmol, respectively. Interestingly, the more hydrophobic ligand increased the dynamic linear range of Zn^{2+} quantification. Adjusting hydrophobicity of the ligands can thus be used to tune the dynamic range of the sensors.

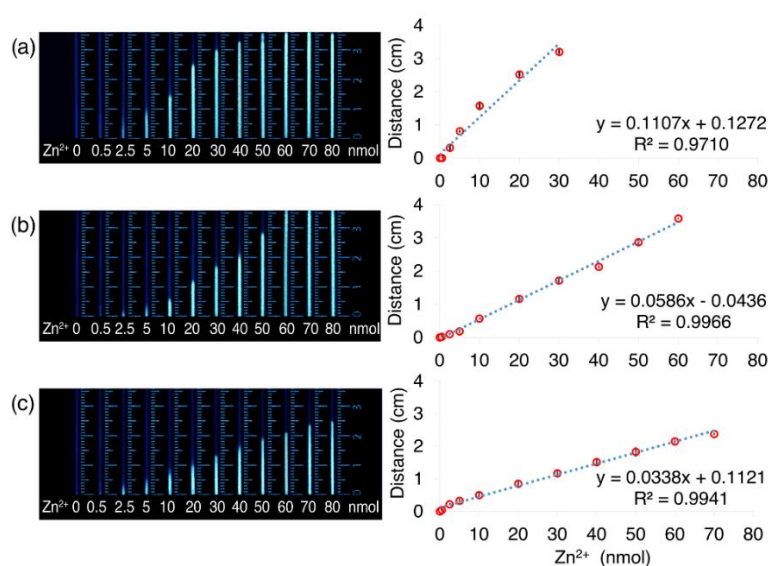


Figure 3.11. Photographic images under black light illumination of a) **Q3**, b) **Q4** and c) **Q5** (100 nmol) paper-based channel sensors tested with various amounts of Zn^{2+} eluted with Tris-HCl buffer pH 7.4 solution (0.20 M) and their calibration plots obtained from fluorescent distance that have mean gray value more than threshold level ($10 \times SD$ of mean gray value of controlled images, $n = 10$) 3 replicates.

3.3.4. Real sample analysis

To demonstrate the applicability of our paper-based sensor for real samples, the amounts of Zn^{2+} in drinking water, dietary supplement, and micronutrient fertilizer were determined by these paper-based sensors in comparison with a standard method (ASTM D1691-17) using atomic absorption spectroscopy (AAS). As shown in Table 3.1, the amounts of Zn^{2+} in drinking water were below the detection limit of the paper-based distance channel sensors. Therefore, known amounts of Zn^{2+} were spiked into these samples. The analysis by both AAS and our sensors gave high recovery (93-97%). For the real samples, the analysis results of a dietary supplement and a

fertilizer by the AAS and paper-based channel sensors were in good agreement confirmed by the paired sample *t*-tests at the 95% confidence level ($t_{\text{calculated}}$ of **Q3**, **Q4** and **Q5** = 1.57, 0.55, 1.42, respectively $< t_{\text{critical}} = 2.02$). It is important to note that the analysis of the samples with high content of Zn^{2+} such as dietary supplement and fertilizer by AAS requires multiple dilutions while these samples can be analyzed by the paper-based sensors without or with single dilution. These paper-based sensors are thus convenient and reliable tools for on-site quantification of Zn^{2+} at subpercentage-percentage levels.

Table 3.1. Determination of Zn^{2+} with distance-based sensor (**Q3-Q5**) in real samples.

Sample	% (w/v) of Zn^{2+} (mean \pm SD)				
	Spike	AAS	Image analysis		
			Q3	Q4	Q5
Drinking water	-	$< 1 \times 10^{-5}$	BD*	BD*	BD*
Drinking water	0.040 0	0.0385 ± 0.0002 96.3% recovery	0.0387 ± 0.0030 96.8% recovery	0.0388 ± 0.0023 97.0% recovery	0.0373 ± 0.0130 93.3% recovery
Drinking water	38.00	35.97 ± 0.06 94.7% recovery	37.0 ± 0.9 97.4% recovery	36.2 ± 4.1 95.3% recovery	37.0 ± 1.9 97.3% recovery
Dietary Supplement	-	0.0506 ± 0.0001	0.0511 ± 0.0020	0.0525 ± 0.0033	0.0504 ± 0.0138
Fertilizer	-	63.31 ± 0.14	OD*	63.1 ± 0.4	64.4 ± 0.8

*Note: BD = Below detection limit, OD = Over detection limit.

3.4. Conclusion

The amidoquinoline derivatives containing *N*-substituted glycine side chain were successfully synthesized and demonstrated as a selective turn-on fluorescent probe for Zn^{2+} . In the paper-based channel sensor, the ligands containing *N,N*-disubstituted glycine side chain showed more uniform fluorescent line than did the unsubstituted and monosubstituted glycine side chain. Three *N,N*-disubstituted ligands deposited on wax-printed filter paper gave sensors with reliable distance-based quantification of Zn^{2+} . The dynamic range of detection could be increased, with an expense of the sensitivity and detection speed, by increasing the hydrophobicity of the ligands. The quantification can be done conveniently by either simple distance measurement or

image processing software. Using these paper-based sensors, the quantitative analysis of real samples containing 0.04-100% (w/v) Zn^{2+} gave reliable results without multiple dilutions in the sample preparation.



CHAPTER IV

CONCLUSION

In this dissertation, new series of amidoquinoline derivatives were synthesized and investigated for fluorescence sensing properties to expand the set of the fluorescent probes from our previous quinoline platform. This work includes two topics i.e., 1) macroarray synthesis on filter paper for rapid discovery and structure-property relationships of metal ion fluorescent sensors, 2) synthesis of quinoline ligands with tunable hydrophobicity for distance-based quantification of metal ion on paper-based fluorescent sensors.

In the first topic, a parallel solid-state synthesis on filter paper was used for rapid synthesis of over 20 amidoquinoline derivatives. Using this technique, multiple compounds could be simultaneously synthesized. The purification of multiple products was also easily achieved by simultaneous washing of unreacted materials and byproducts without complex deconvolution. The probes covalently bound on the cellulose surface was used as an array of functional substrate-supported sensors which offer rapid sensing screening, reusability, and enhanced sensitivity for metal ion identification and quantitative analysis of Zn^{2+} .

In the second topic, a series of 5 amidoquinolines with tunable hydrophobicity were synthesized. The synthesized compounds were studied as sensing probes in both aqueous solution and on paper-based platform. The paper-based sensors were also developed for distance-based quantification of metal ion. The distance of the fluorescent lines created in the sensor was directly related to the amount of the metal ion. The linear dynamic ranges of the sensors were depended on the hydrophobicity of the amidoquinoline probes. The distance-based quantification of Zn^{2+} in drinking water, dietary supplement, and fertilizer samples by these paper-based sensors gave the results comparable with the standard method using the atomic absorption spectroscopy.

APPENDIX

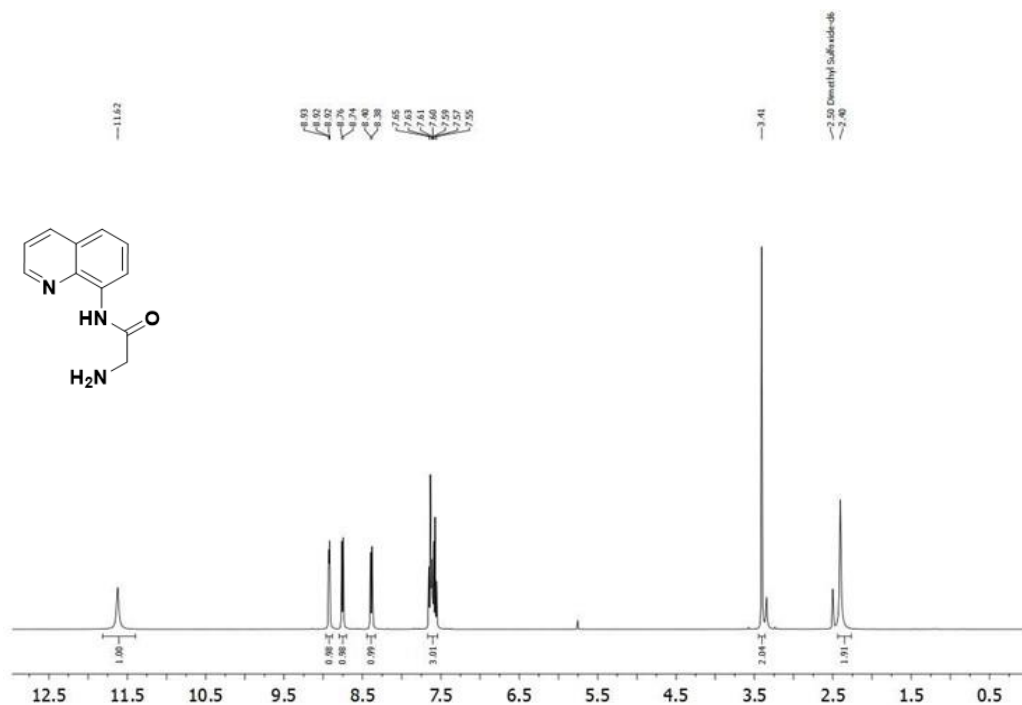


Figure A1. ¹H NMR spectrum of 2-amino-*N*-(quinolin-8-yl)acetamide (Gly.8AQ) in DMSO-*d*₆.

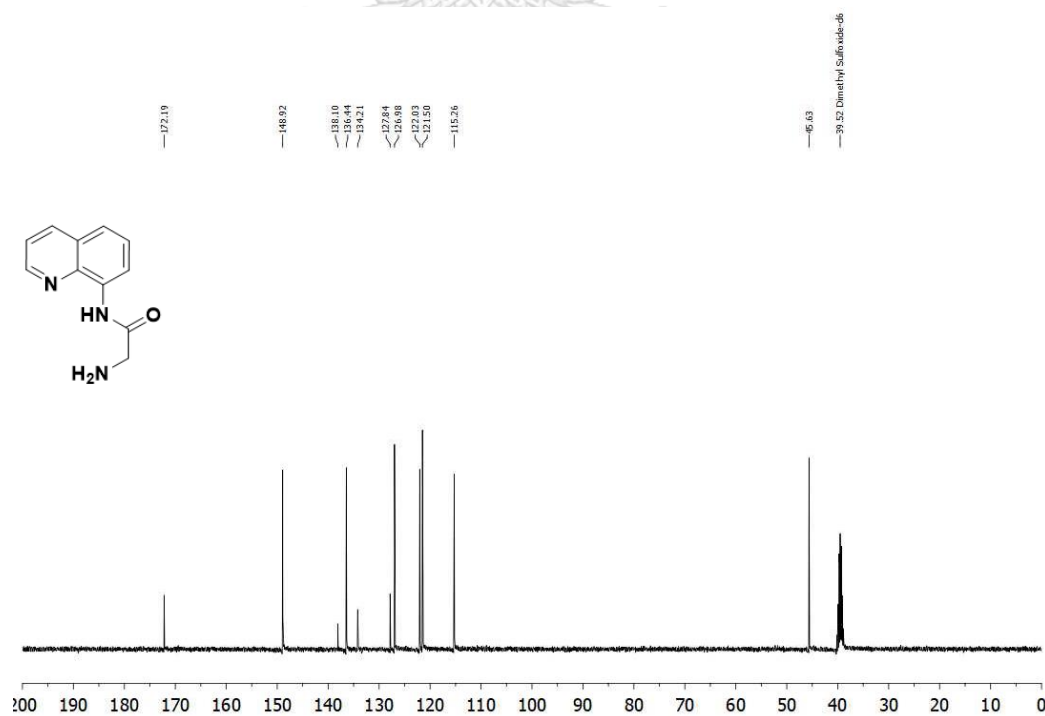


Figure A2. ¹³C NMR spectrum of 2-amino-*N*-(quinolin-8-yl)acetamide (Gly.8AQ) in DMSO-*d*₆.

Mass Spectrum List Report

Analysis Info		Acquisition Date	8/10/2018 10:59:35 AM
Analysis Name	D:\Data\Data Service\180810_pos_Glycine-8AQ.d	Operator	CU.
Method	NV_pos_0.3min_profile_1segment_lowNubulizerDrygas.m	Instrument / Ser#	micrOTOF-Q II 10335
Sample Name	180810_pos_Glycine-8AQ		
Comment			

Acquisition Parameter

Source Type	ESI	Ion Polarity	Positive	Set Nebulizer	0.4 Bar
Focus	Not active	Set Capillary	4000 V	Set Dry Heater	200 °C
Scan Begin	50 m/z	Set End Plate Offset	-500 V	Set Dry Gas	4.0 l/min
Scan End	1500 m/z	Set Collision Cell RF	150.0 Vpp	Set Divert Valve	Waste

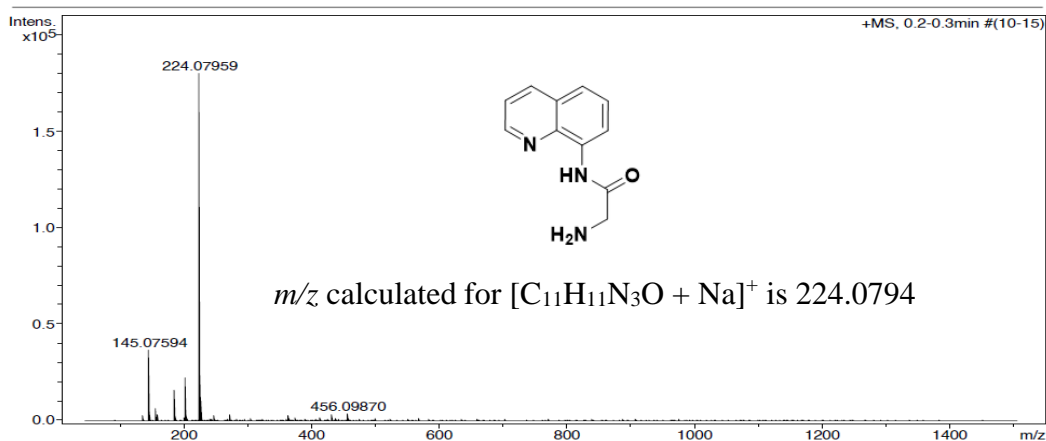


Figure A3. HRMS (ESI) spectrum of 2-amino-*N*-(quinolin-8-yl)acetamide (Gly.8AQ).

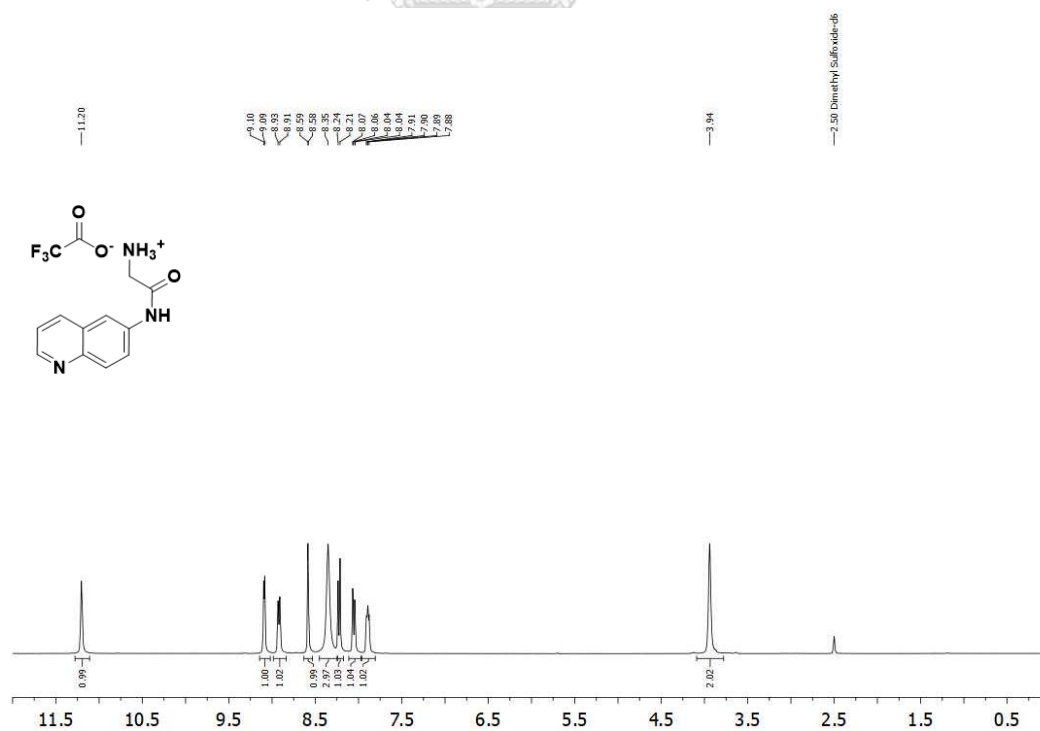


Figure A4. 1H NMR spectrum of 2-amino-*N*-(quinolin-6-yl)acetamide (unbound, TFA salt of Gly.6AQ) in $DMSO-d_6$.

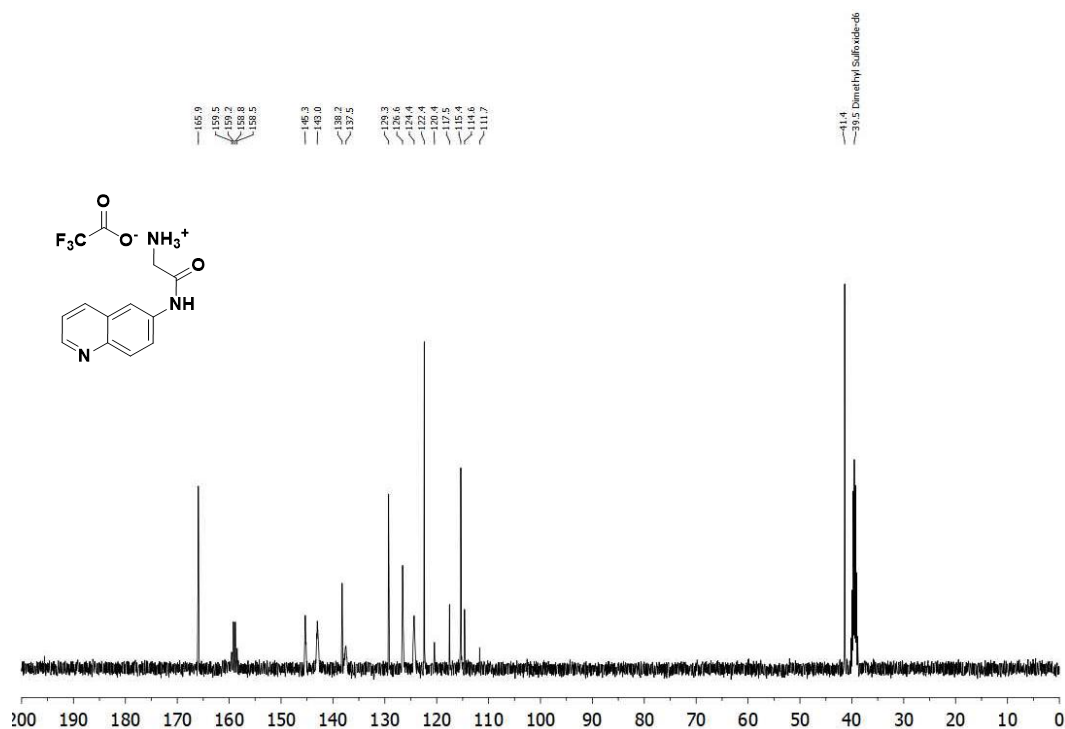


Figure A5. ^{13}C NMR spectrum of 2-amino-*N*-(quinolin-6-yl)acetamide (unbound, TFA salt of Gly.6AQ) in $\text{DMSO-}d_6$.

Mass Spectrum List Report

Analysis Info		Acquisition Date	
Analysis Name	D:\Data\Data Service\180810_pos_Glycine-6AQ.d	8/10/2018 9:57:05 AM	
Method	NV_pos_0.3min_profile_1segment_lowNubulizerDrygas.m	Operator	CU
Sample Name	180810_pos_Glycine-6AQ	Instrument / Ser#	micrOTOF-Q II 10335
Comment			
Acquisition Parameter			
Source Type	ESI	Ion Polarity	Positive
Focus	Not active	Set Capillary	4000 V
Scan Begin	50 m/z	Set End Plate Offset	-500 V
Scan End	1500 m/z	Set Collision Cell RF	150.0 Vpp
		Set Nebulizer	0.4 Bar
		Set Dry Heater	200 °C
		Set Dry Gas	4.0 l/min
		Set Divert Valve	Waste

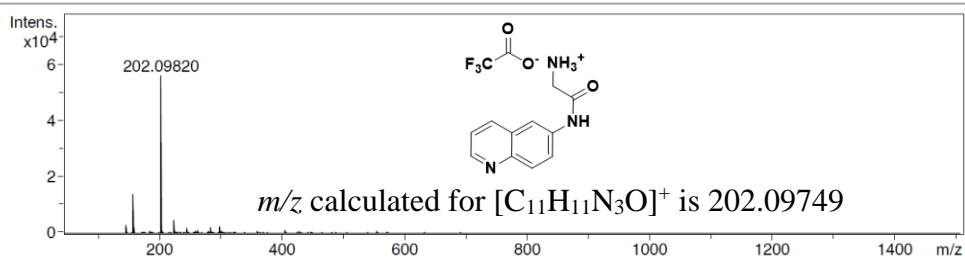


Figure A6. HRMS (ESI) spectrum of 2-amino-*N*-(quinolin-6-yl)acetamide (unbound, TFA salt of Gly.6AQ).

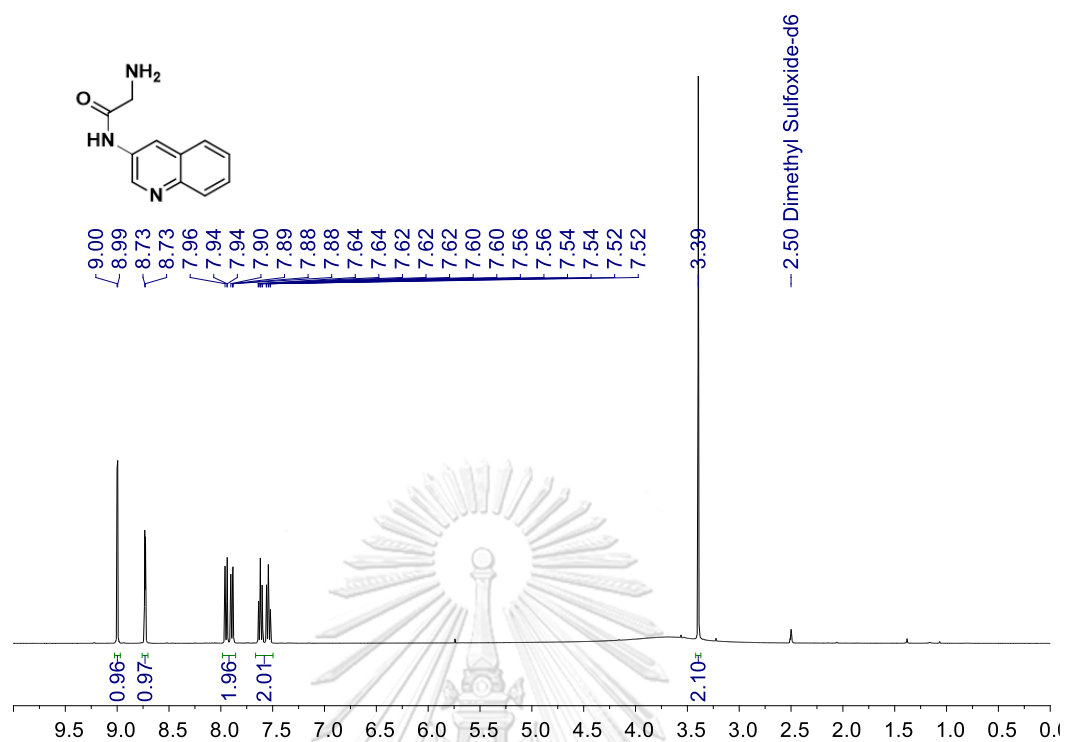


Figure A7. ¹H NMR spectrum of 2-amino-*N*-(quinolin-3-yl)acetamide (**Gly.3AQ**) in DMSO-*d*₆.

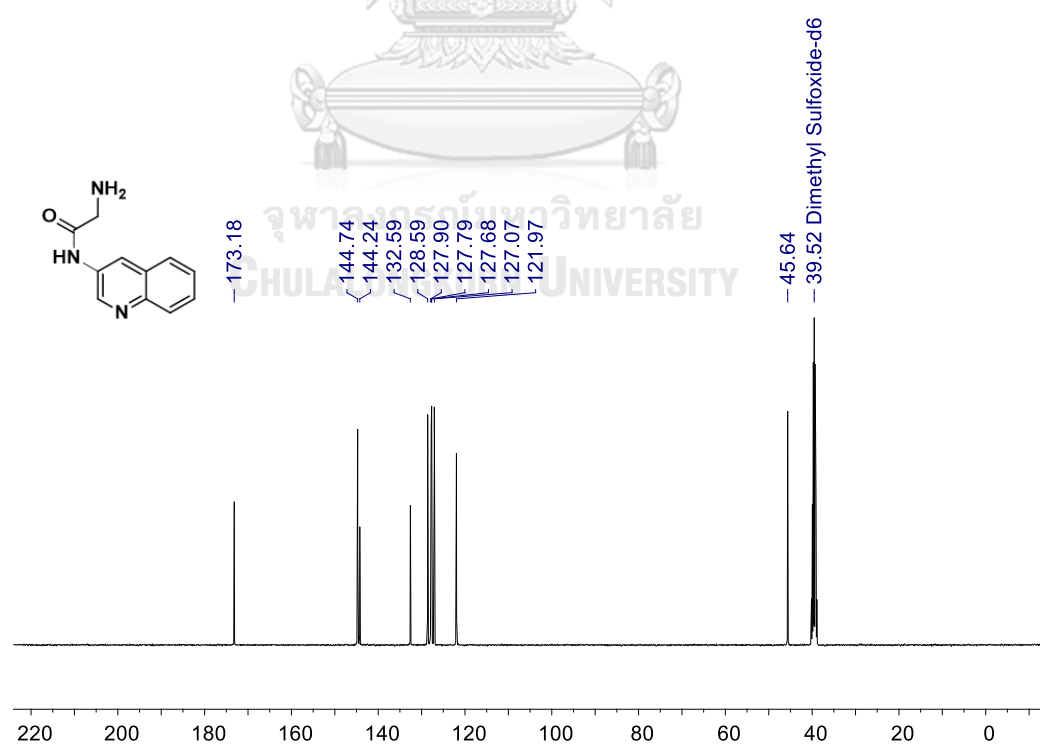


Figure A8. ¹³C NMR spectrum of 2-amino-*N*-(quinolin-3-yl)acetamide (**Gly.3AQ**) in DMSO-*d*₆.

Mass Spectrum List Report

Analysis Info

Analysis Name OSAP27052019002_1.d
 Method Tune_low_90_04092017.m
 Sample Name Gly.3AQ
 Gly.3AQ

Acquisition Date 5/27/2019 12:10:25 PM
 Operator Administrator
 Instrument micrOTOF 72

Acquisition Parameter

Source Type ESI
 Scan Range n/a
 Scan Begin 50 m/z
 Scan End 3000 m/z

Ion Polarity Positive
 Capillary Exit 120.0 V
 Hexapole RF 90.0 V
 Skimmer 1 70.0 V
 Hexapole 1 25.0 V

Set Corrector Fill 50 V
 Set Pulsar Pull 337 V
 Set Pulsar Push 337 V
 Set Reflector 1300 V
 Set Flight Tube 9000 V
 Set Detector TOF 2295 V

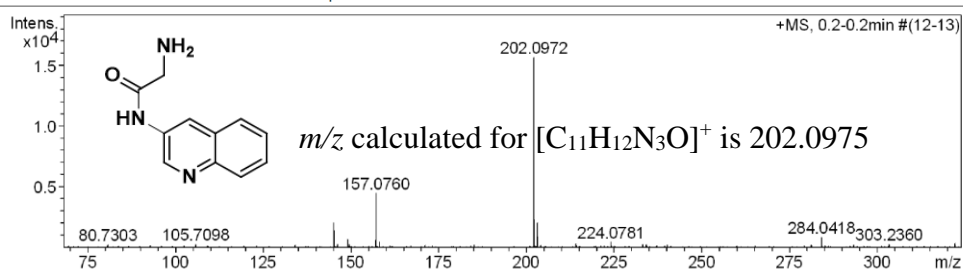


Figure A9. HRMS (ESI) spectrum of 2-amino-*N*-(quinolin-3-yl)acetamide (Gly.3AQ).

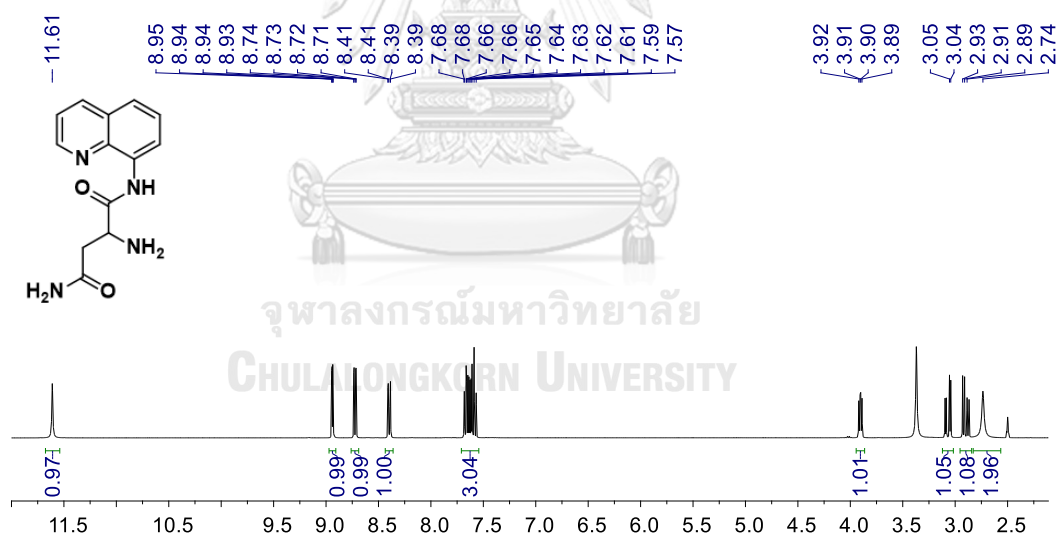


Figure A10. 1H NMR spectrum of 2-amino-*N*-(quinolin-8-yl)succinamide (Asn.8AQ) in $DMSO-d_6$.

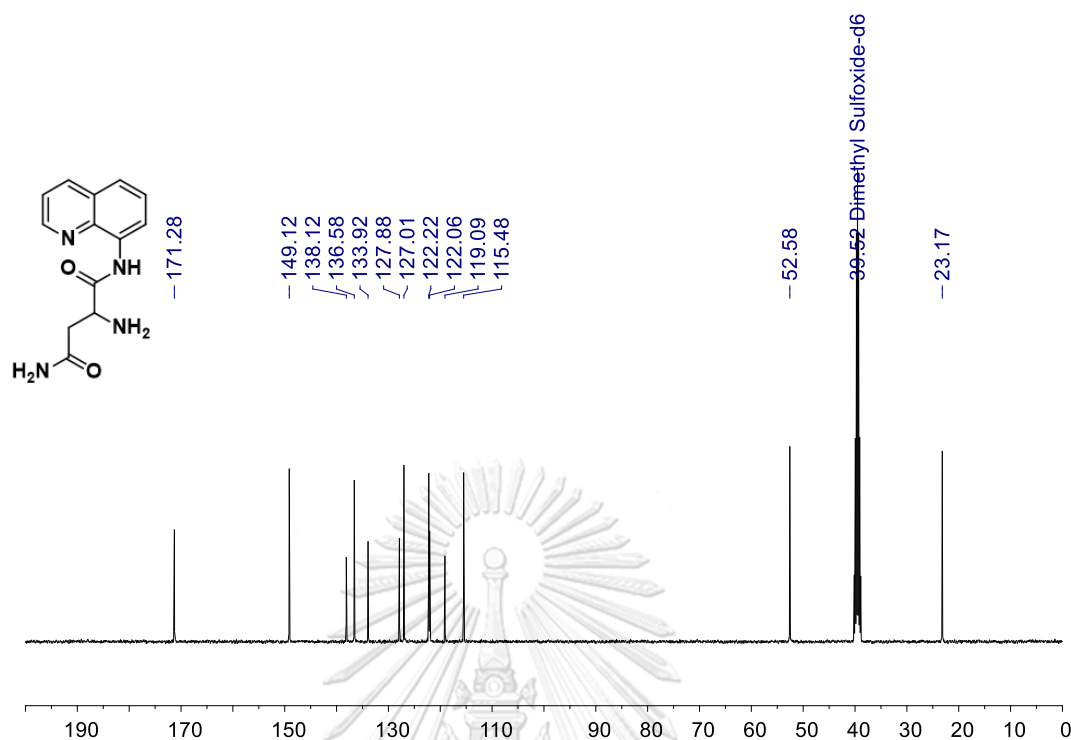


Figure A11. ¹³C NMR spectrum of 2-amino-*N*-(quinolin-8-yl)succinamide (Asn.8AQ) in DMSO-*d*₆.

Mass Spectrum List Report

Analysis Info			
Analysis Name	OSAP27052019001.d	Acquisition Date	5/27/2019 12:03:53 PM
Method	Tune_low_90_04092017.m	Operator	Administrator
Sample Name	Asn.8AQ	Instrument	micrOTOF 72
	Asn.8AQ		
Acquisition Parameter			
Source Type	ESI	Ion Polarity	Positive
Scan Range	n/a	Capillary Exit	120.0 V
Scan Begin	50 m/z	Hexapole RF	90.0 V
Scan End	3000 m/z	Skimmer 1	70.0 V
		Hexapole 1	25.0 V
		Set Corrector Fill	50 V
		Set Pulsar Pull	337 V
		Set Pulsar Push	337 V
		Set Reflector	1300 V
		Set Flight Tube	9000 V
		Set Detector TOF	2295 V

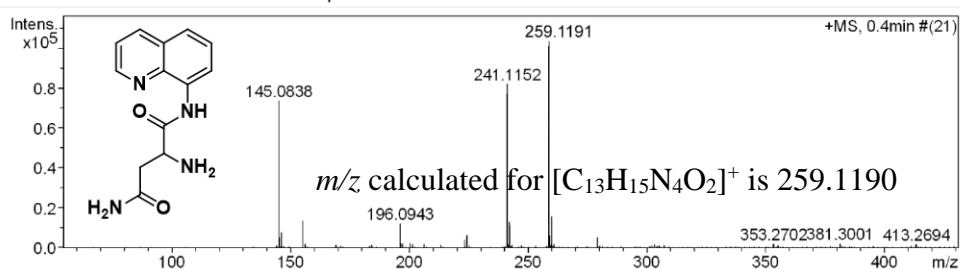


Figure A12. HRMS (ESI) spectrum of 2-amino-*N*-(quinolin-8-yl)succinamide (Asn.8AQ) in DMSO-*d*₆.

1 = Asn.8AQ, 2 = Gly.3AQ, 3 = Gly.6AQ, 4 = Gly.8AQ

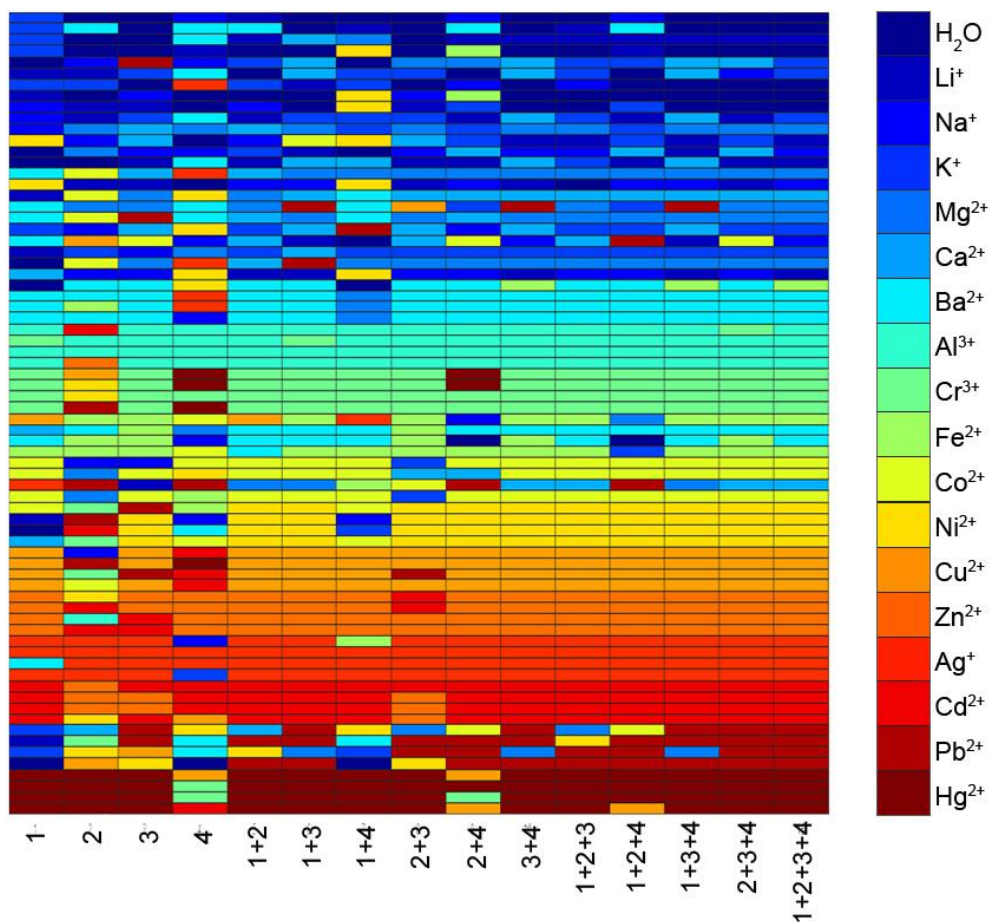
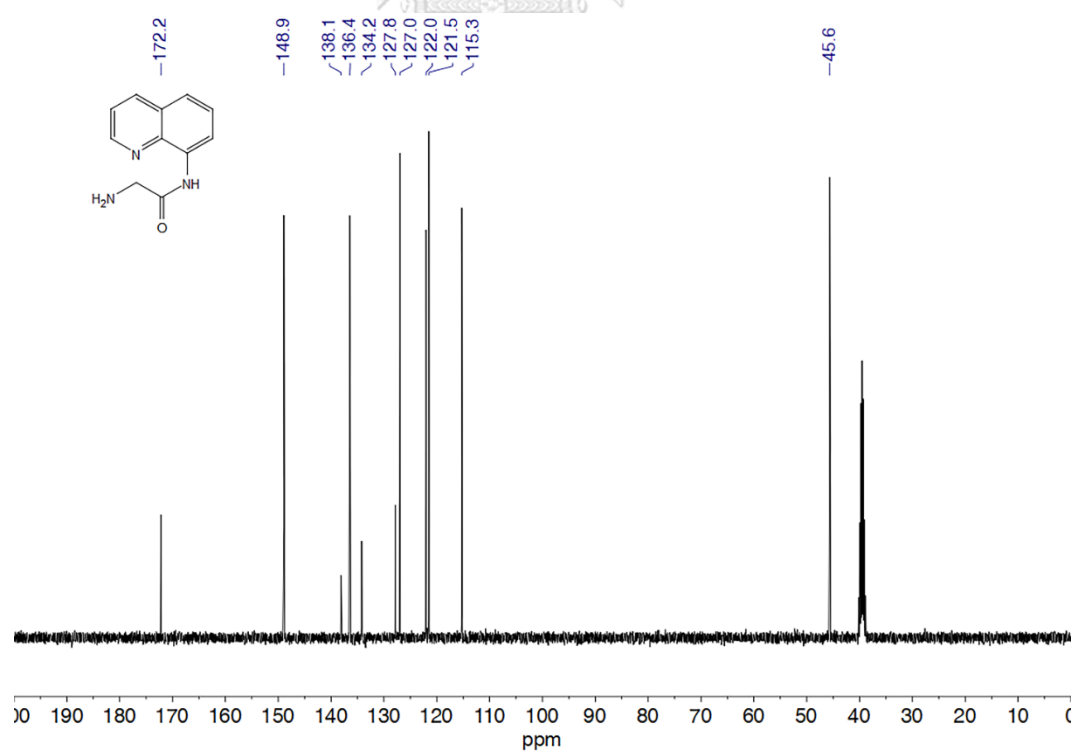
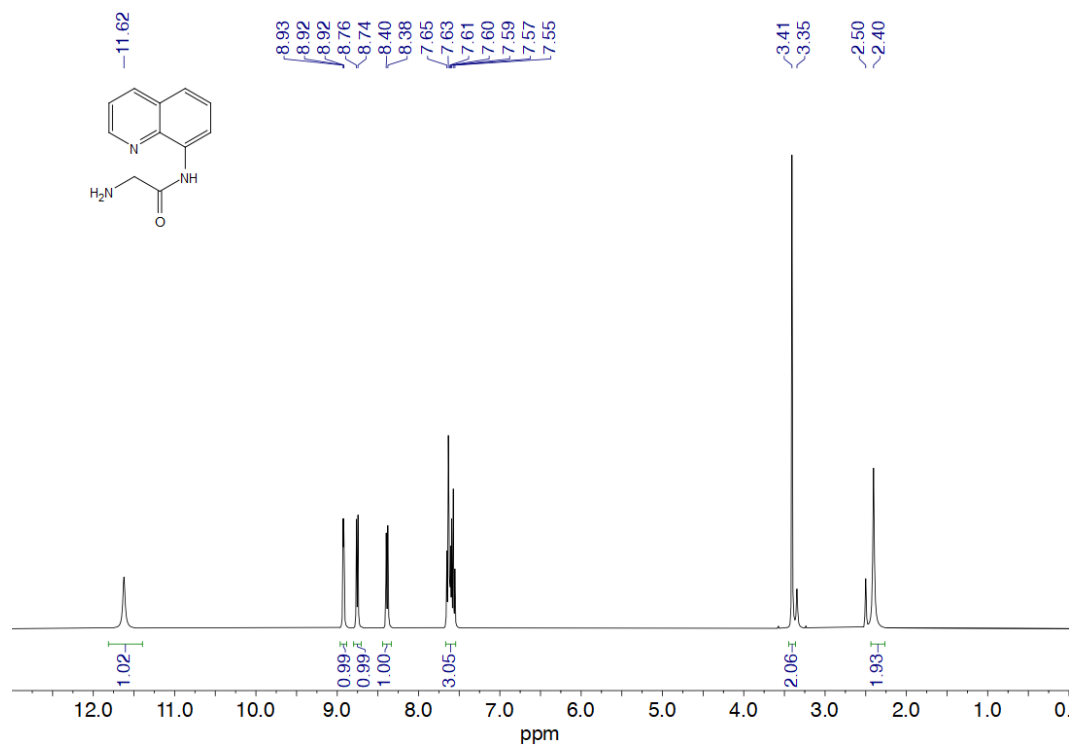


Figure A13. A heat map showing classification accuracies of four fluorophores (and their various combinations) for predicting 18 analytes, where the same colors between each cell to its reference color on the right panel means the system predicted the metal ion correctly. Any different color means the system predicted it to be some other metal ions as shown exactly in each color.



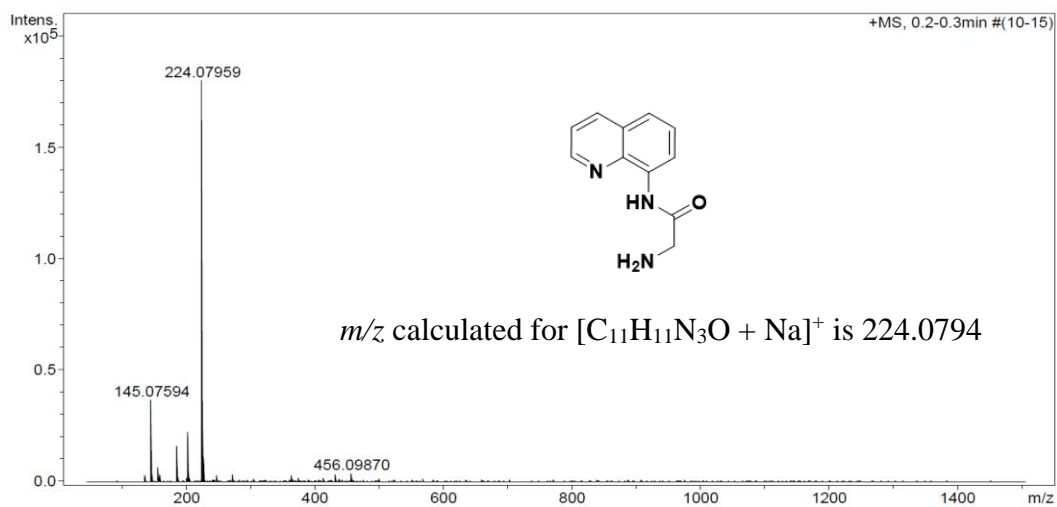


Figure A16. HRMS (ESI) spectrum of 2-amino-*N*-(quinolin-8-yl)acetamide (**Q1**).

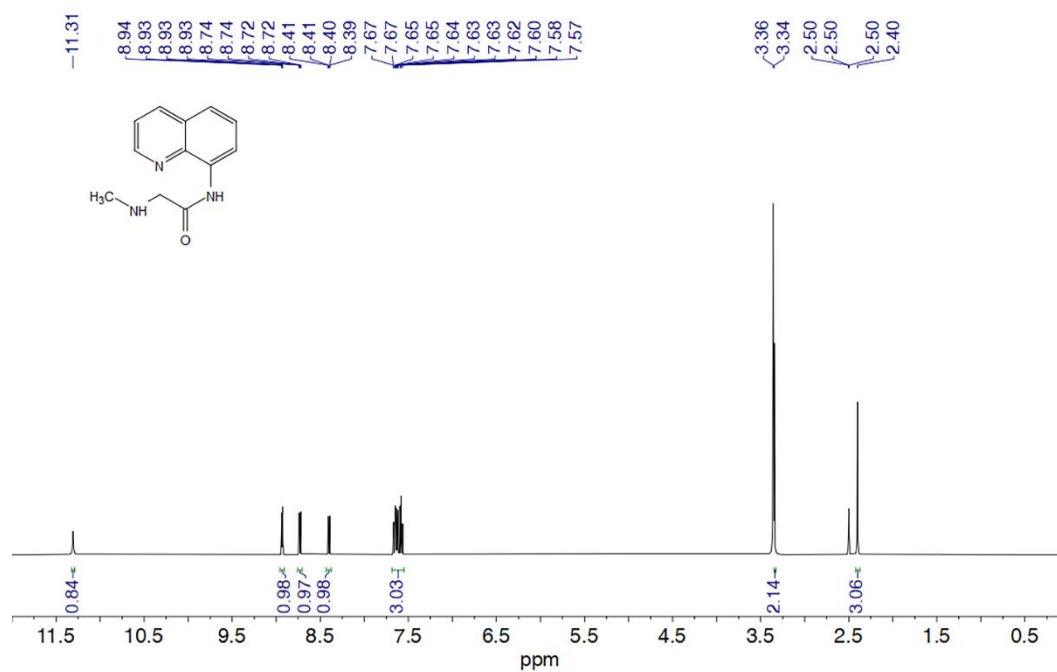


Figure A17. ¹H NMR spectrum of 2-(methylamino)-*N*-(quinolin-8-yl)acetamide (**Q2**) in DMSO-*d*₆.

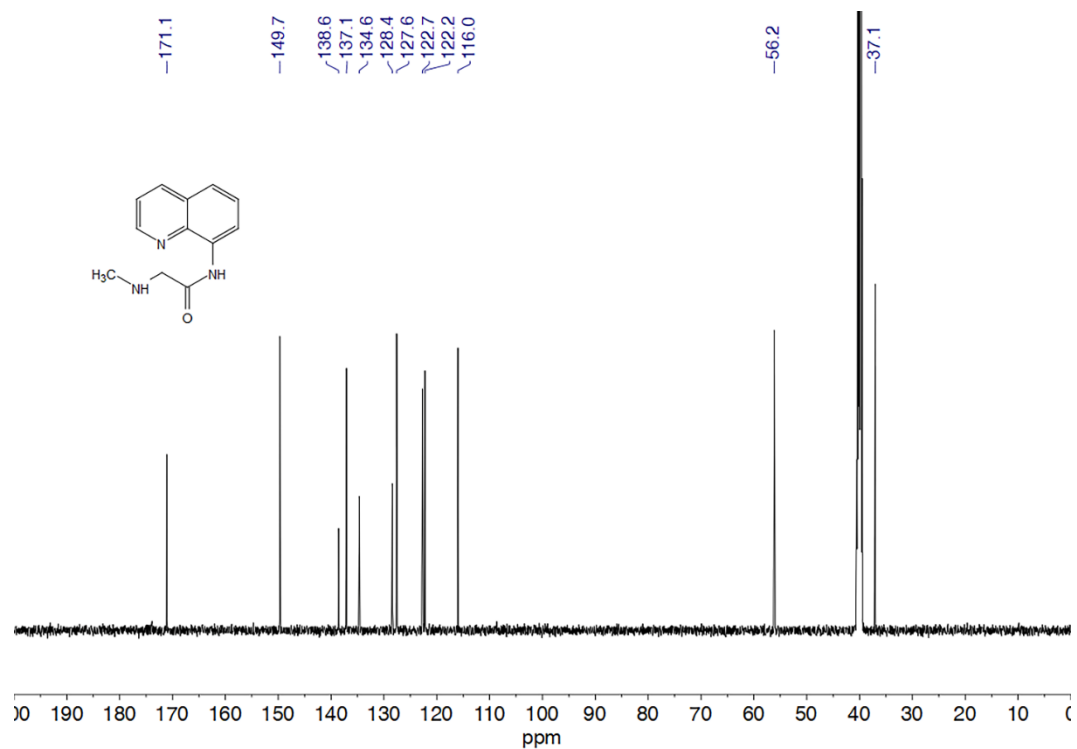


Figure A18. ^{13}C NMR spectrum of 2-(methylamino)-*N*-(quinolin-8-yl)acetamide (Q2) in $\text{DMSO-}d_6$.

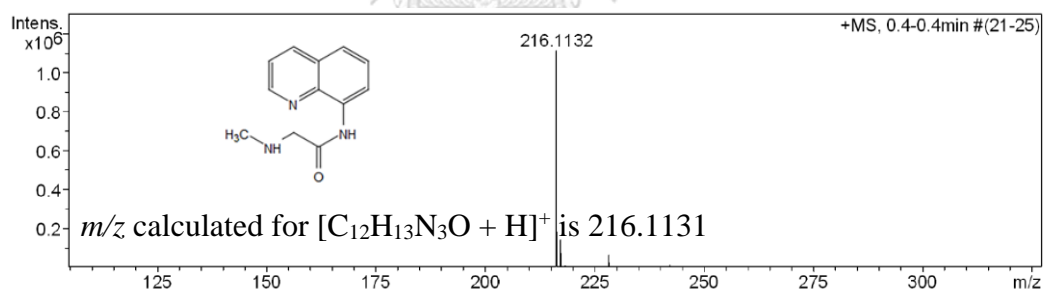


Figure A19. HRMS (ESI) spectrum of 2-(methylamino)-*N*-(quinolin-8-yl)acetamide (Q2).

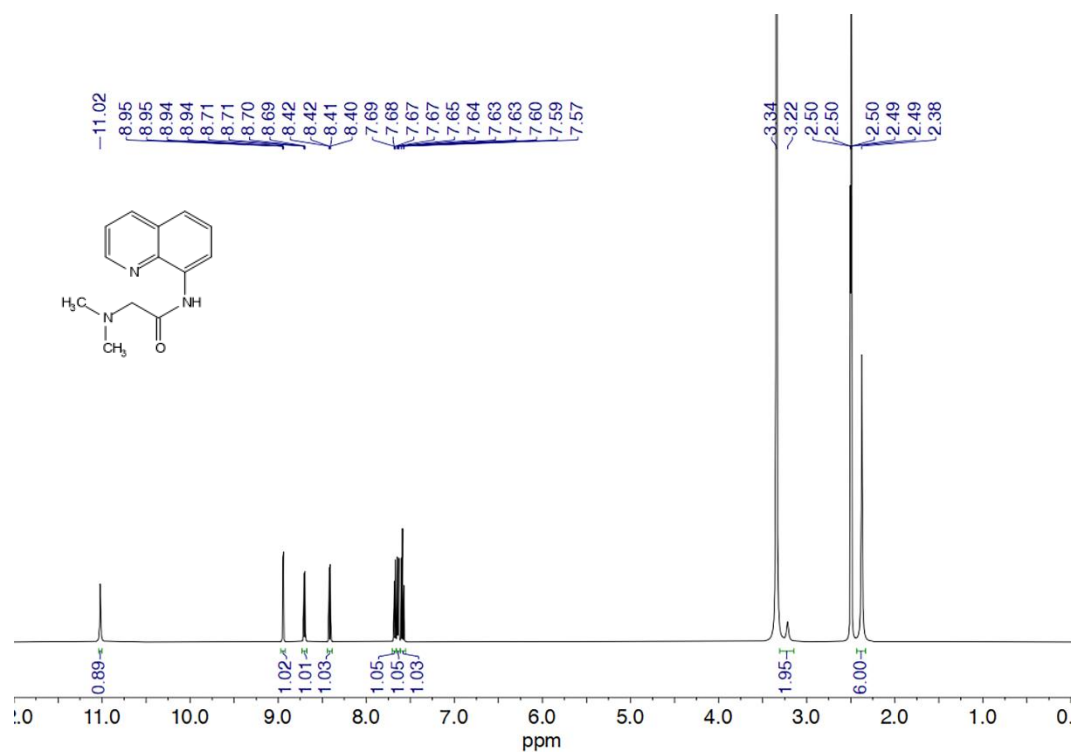


Figure A20. ¹H NMR spectrum of 2-(dimethylamino)-*N*-(quinolin-8-yl)acetamide (Q3) in DMSO-*d*₆.

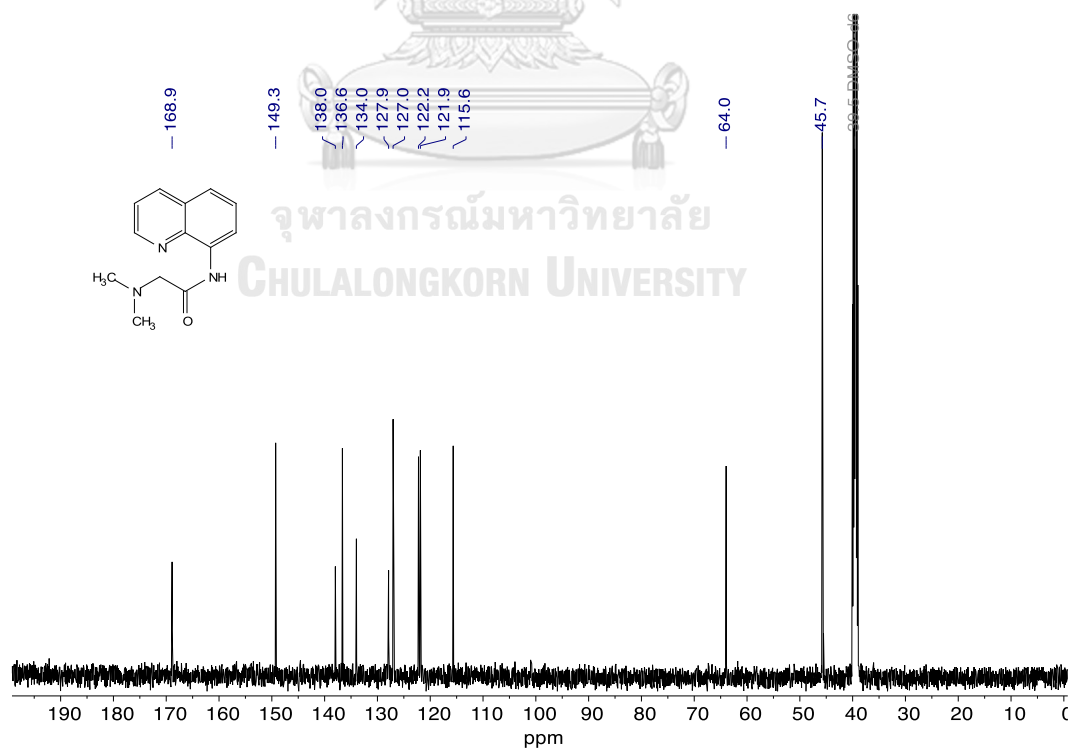


Figure A21. ¹³C NMR spectrum of 2-(dimethylamino)-*N*-(quinolin-8-yl)acetamide (Q3) in DMSO-*d*₆.

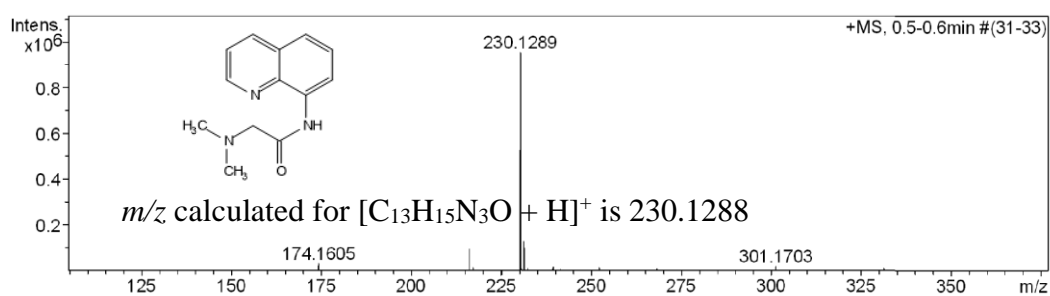


Figure A22. HRMS (ESI) spectrum of 2-(dimethylamino)-*N*-(quinolin-8-yl)acetamide (**Q3**).

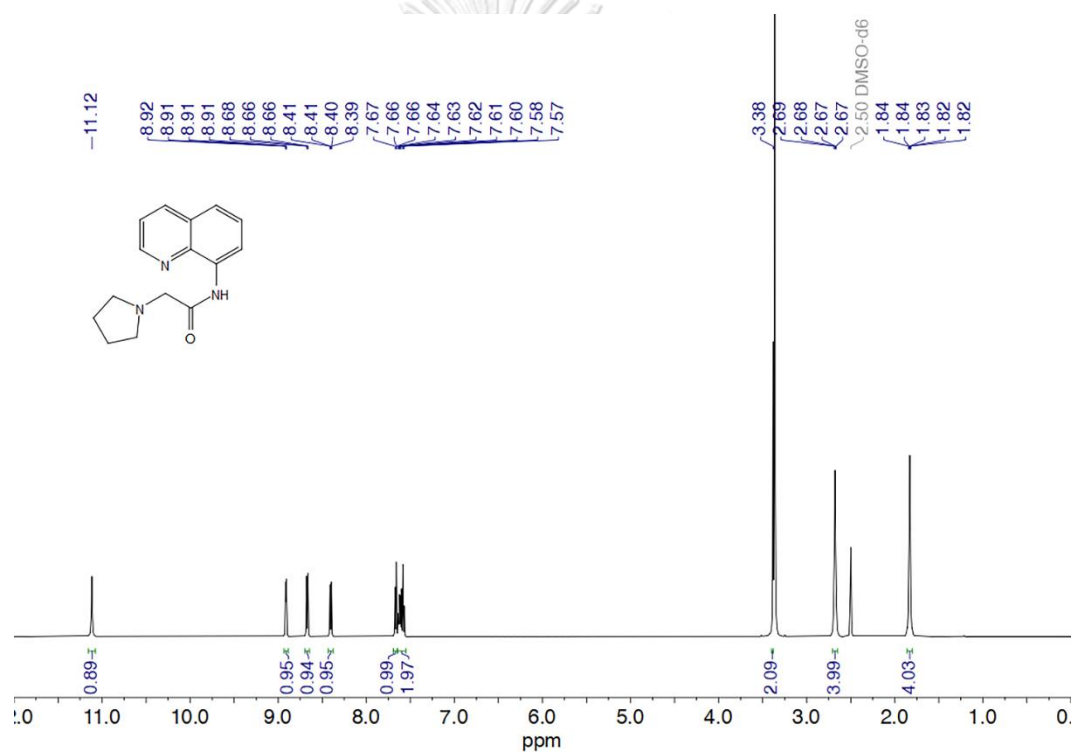


Figure A23. ¹H NMR spectrum of 2-(pyrrolidin-1-yl)-*N*-(quinolin-8-yl)acetamide (**Q4**) in DMSO-*d*₆.

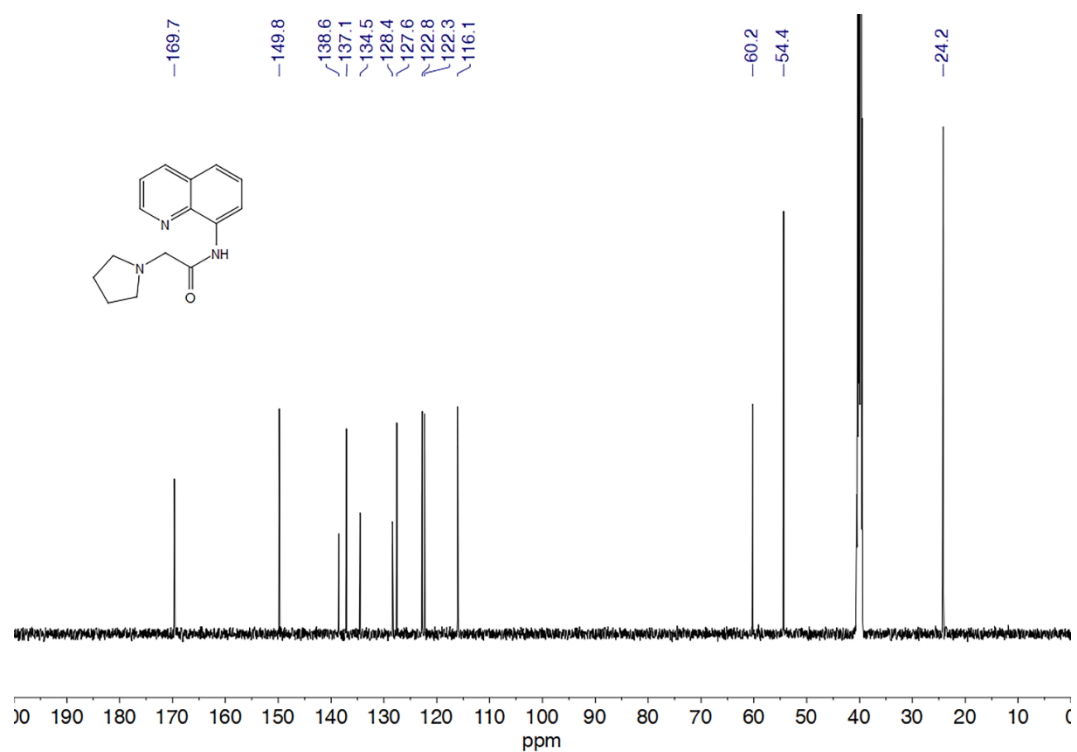


Figure A24. ^{13}C NMR spectrum of 2-(pyrrolidin-1-yl)-*N*-(quinolin-8-yl)acetamide (**Q4**) in $\text{DMSO-}d_6$.

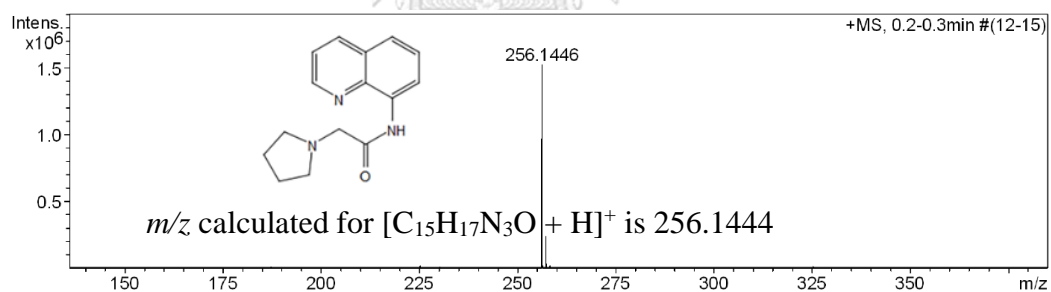


Figure A25. HRMS (ESI) spectrum of 2-(pyrrolidin-1-yl)-*N*-(quinolin-8-yl)acetamide (**Q4**).

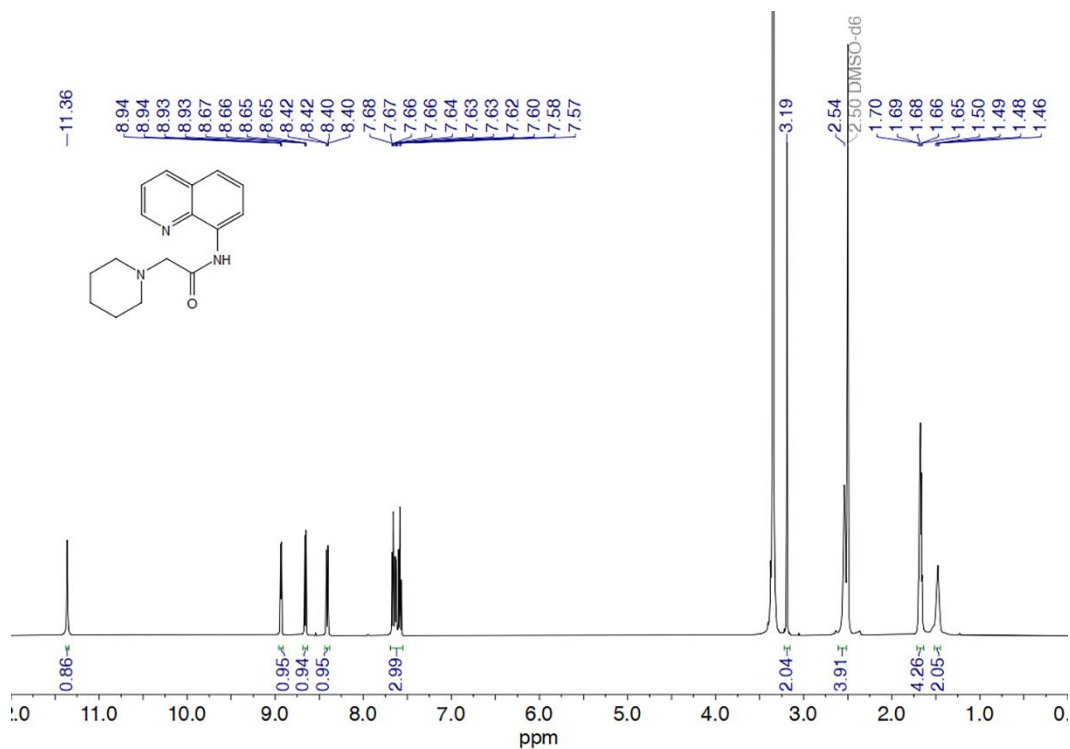


Figure A26. ¹H NMR spectrum of 2-(piperidin-1-yl)-N-(quinolin-8-yl)acetamide (Q5) in DMSO-d₆.

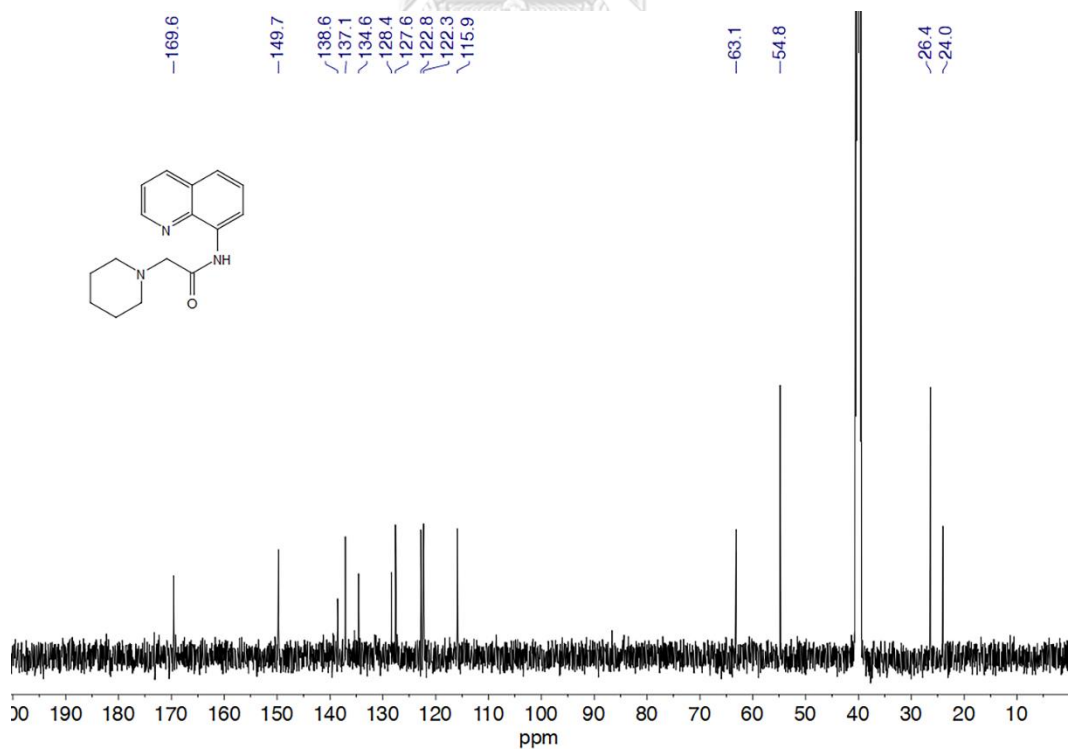


Figure A27. ¹³C NMR spectrum of 2-(piperidin-1-yl)-N-(quinolin-8-yl)acetamide (Q5) in DMSO-d₆.

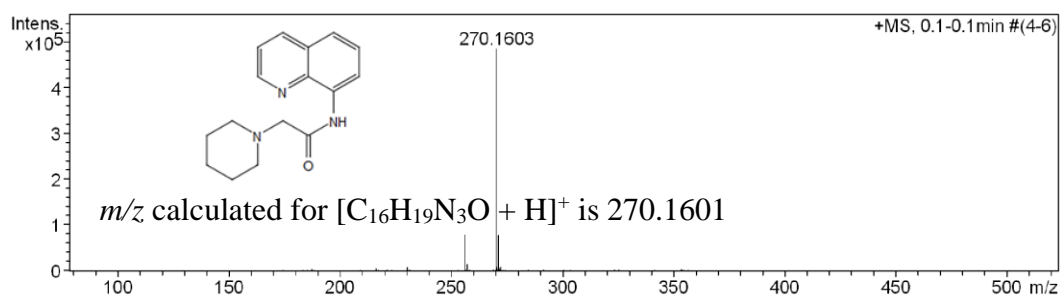


Figure A28. HRMS (ESI) spectrum of 2-(piperidin-1-yl)-*N*-(quinolin-8-yl)acetamide (Q5).



REFERENCES

1. Bett, S., What is the Jablonski diagram? <http://quora.com/What-is-the-Jablonski-diagram>, 2014.
2. Gunnlaugsson, T.; Ali, H. D. P.; Glynn, M.; Kruger, P. E.; Hussey, G. M.; Pfeffer, F. M.; dos Santos, C. M. G.; Tierney, J., Fluorescent photoinduced electron transfer (PET) sensors for anions; from design to potential application. *Journal of Fluorescence* **2005**, *15* (3), 287-299.
3. Druzhinin, S. I.; Mayer, P.; Stalke, D.; von Bülow, R.; Noltemeyer, M.; Zachariasse, K. A., Intramolecular charge transfer with 1-*tert*-butyl-6-cyano-1,2,3,4-tetrahydroquinoline (NTC6) and other aminobenzonitriles. a comparison of experimental vapor phase spectra and crystal structures with calculations. *Journal of the American Chemical Society* **2010**, *132* (22), 7730-7744.
4. Dong, Z.; Jin, J.; Zhao, W.; Geng, H.; Zhao, P.; Li, R.; Ma, J., Quinoline group grafted carbon nanotube fluorescent sensor for detection of Cu²⁺ ion. *Applied Surface Science* **2009**, *255* (23), 9526-9530.
5. Ma, Y.; Wang, F.; Kambam, S.; Chen, X., A quinoline-based fluorescent chemosensor for distinguishing cadmium from zinc ions using cysteine as an auxiliary reagent. *Sensors and Actuators B: Chemical* **2013**, *188*, 1116-1122.
6. Boonkitpatarakul, K.; Smata, A.; Kongnukool, K.; Srisurichan, S.; Chainok, K.; Sukwattanasinitt, M., An 8-aminoquinoline derivative as a molecular platform for fluorescent sensors for Zn(II) and Cd(II) ions. *Journal of Luminescence* **2018**, *198*, 59-67.
7. Zhu, Y.; Xu, X.; Brault, N. D.; Keefe, A. J.; Han, X.; Deng, Y.; Xu, J.; Yu, Q.; Jiang, S., Cellulose paper sensors modified with zwitterionic poly(carboxybetaine) for sensing and detection in complex media. *Analytical Chemistry* **2014**, *86* (6), 2871-2875.
8. Dong, S.; Cho, H. J.; Lee, Y. W.; Roman, M., Synthesis and cellular uptake of folic acid-conjugated cellulose nanocrystals for cancer targeting. *Biomacromolecules* **2014**, *15* (5), 1560-1567.
9. Sirvio, J.; Hyvakkö, U.; Liimatainen, H.; Niinimäki, J.; Hormi, O., Periodate oxidation of cellulose at elevated temperatures using metal salts as cellulose activators. *Carbohydrate Polymers* **2011**, *83* (3), 1293-1297.
10. Noor, M. O.; Krull, U. J., Paper-based solid-phase multiplexed nucleic acid hybridization assay with tunable dynamic range using immobilized quantum dots as donors in fluorescence resonance energy transfer. *Analytical Chemistry* **2013**, *85* (15), 7502-7511.
11. Kumari, S.; Chauhan, G. S., New cellulose-lysine schiff-base-based sensor-adsorbent for mercury ions. *ACS Applied Materials & Interfaces* **2014**, *6* (8), 5908-5917.
12. Mello, J. V.; Finney, N. S., Reversing the discovery paradigm: a new approach to the combinatorial discovery of fluorescent chemosensors. *Journal of the American Chemical Society* **2005**, *127* (29), 10124-10125.
13. Martinez, A. W.; Phillips, S. T.; Whitesides, G. M.; Carrilho, E., Diagnostics for the developing world: microfluidic paper-based analytical devices. *Analytical Chemistry* **2010**, *82* (1), 3-10.
14. Zuk, R. F.; Ginsberg, V. K.; Houts, T.; Rabbie, J.; Merrick, H.; Ullman, E. F.;

- Fischer, M. M.; Sizto, C. C.; Stiso, S. N.; Litman, D. J., Enzyme immunochromatography quantitative immunoassay requiring no instrumentation. *Clinical Chemistry* **1985**, *31* (7), 1144-1150.
15. Cate, D. M.; Dungchai, W.; Cunningham, J. C.; Volckens, J.; Henry, C. S., Simple, distance-based measurement for paper analytical devices. *Lab on a Chip* **2013**, *13* (12), 2397-2404.
 16. Cate, D. M.; Noblitt, S. D.; Volckens, J.; Henry, C. S., Multiplexed paper analytical device for quantification of metals using distance-based detection. *Lab on a Chip* **2015**, *15* (13), 2808-2818.
 17. Phoonsawat, K.; Ratnarathorn, N.; Henry, C. S.; Dungchai, W., A distance-based paper sensor for the determination of chloride ions using silver nanoparticles. *Analyst* **2018**, *143* (16), 3867-3873.
 18. Nguyen, M. P.; Kelly, S. P.; Wydallis, J. B.; Henry, C. S., Read-by-eye quantification of aluminum (III) in distance-based microfluidic paper-based analytical devices. *Analytica Chimica Acta* **2020**, *1100*, 156-162.
 19. El-Kady, A. A.; Abdel-Wahhab, M. A., Occurrence of trace metals in foodstuffs and their health impact. *Trends in Food Science & Technology* **2018**, *75*, 36-45.
 20. Khalid, S.; Shahid, M.; Natasha; Bibi, I.; Sarwar, T.; Shah, A. H.; Niazi, N. K., A review of environmental contamination and health risk assessment of wastewater use for crop irrigation with a focus on low and high-income countries. *International Journal of Environmental Research and Public Health* **2018**, *15* (5).
 21. Planchart, A.; Green, A.; Hoyo, C.; Mattingly, C. J., Heavy metal exposure and metabolic syndrome: evidence from human and model system studies. *Current Environmental Health Reports* **2018**, *5* (1), 110-124.
 22. Vaananen, K.; Leppanen, M. T.; Chen, X. P.; Akkanen, J., Metal bioavailability in ecological risk assessment of freshwater ecosystems: From science to environmental management. *Ecotoxicology and Environmental Safety* **2018**, *147*, 430-446.
 23. Rull-Barrull, J.; d'Halluin, M.; Le Grogne, E.; Felpin, F.-X., Chemically-modified cellulose paper as smart sensor device for colorimetric and optical detection of hydrogen sulfate in water. *Chemical Communications* **2016**, *52* (12), 2525-2528.
 24. Martinez, A. W.; Phillips, S. T.; Butte, M. J.; Whitesides, G. M., Patterned paper as a platform for inexpensive, low-volume, portable bioassays. *Angewandte Chemie International Edition* **2007**, *46* (8), 1318-1320.
 25. Yetisen, A. K.; Akram, M. S.; Lowe, C. R., Paper-based microfluidic point-of-care diagnostic devices. *Lab Chip* **2013**, *13* (12), 2210-2251.
 26. Carter, K. P.; Young, A. M.; Palmer, A. E., Fluorescent sensors for measuring metal ions in living systems. *Chemical Reviews* **2014**, *114* (8), 4564-4601.
 27. Li, M.; Li, X.; Xiao, H.-N.; James, T. D., Fluorescence sensing with cellulose-based materials. *ChemistryOpen* **2017**, 685-696.
 28. Valeur, B.; Leray, I., Design principles of fluorescent molecular sensors for cation recognition. *Coordination Chemistry Reviews* **2000**, *205* (1), 3-40.
 29. Xu, Z.; Xiao, Y.; Qian, X.; Cui, J.; Cui, D., Ratiometric and selective fluorescent sensor for Cu^{II} based on internal charge transfer (ICT). *Organic Letters* **2005**, *7* (5), 889-892.
 30. Wang, J.; Qian, X., A series of polyamide receptor based pet fluorescent sensor molecules: positively cooperative Hg²⁺ ion binding with high sensitivity. *Organic Letters* **2006**, *8* (17), 3721-3724.

31. Chang, K.-C.; Su, I.-H.; Senthilvelan, A.; Chung, W.-S., Triazole-modified calix[4]crown as a novel fluorescent on-off switchable chemosensor. *Organic Letters* **2007**, *9* (17), 3363-3366.
32. Panda, D.; Datta, A., The role of the ring nitrogen and the amino group in the solvent dependence of the excited-state dynamics of 3-aminoquinoline. *J Chem Phys* **2006**, *125* (5), 054513.
33. Xue, L.; Liu, C.; Jiang, H., Highly sensitive and selective fluorescent sensor for distinguishing cadmium from zinc ions in aqueous media. *Organic Letters* **2009**, *11* (7), 1655-1658.
34. Cao, X. W.; Lin, W. Y.; He, L. W., A near-infrared fluorescence turn-on sensor for sulfide anions. *Organic Letters* **2011**, *13* (17), 4716-4719.
35. Liu, Z. P.; Zhang, C. L.; Wang, X. Q.; He, W. J.; Guo, Z. J., Design and synthesis of a ratiometric fluorescent chemosensor for cu(ii) with a fluorophore hybridization approach. *Organic Letters* **2012**, *14* (17), 4378-4381.
36. Ma, Y.; Chen, H. Y.; Wang, F.; Kambam, S.; Wang, Y.; Mao, C.; Chen, X. Q., A highly sensitive and selective ratiometric fluorescent sensor for Zn²⁺ ion based on ICT and FRET. *Dyes Pigments* **2014**, *102*, 301-307.
37. Vongnam, K.; Muangnoi, C.; Rojsitthisak, P.; Sukwattanasinitt, M.; Rashatasakhon, P., A highly selective turn-on fluorescent sensor for glucosamine from amidoquinoline-naphthalimide dyads. *Biosensors and Bioelectronics* **2016**, *86*, 472-476.
38. Liu, J. R.; Maisonia-Besset, A.; Wenzel, B.; Canitrot, D.; Baufond, A.; Chezal, J. M.; Brust, P.; Moreau, E., Synthesis and in vitro evaluation of new fluorinated quinoline derivatives with high affinity for PDE5: Towards the development of new PET neuroimaging probes. *European Journal of Medicinal Chemistry* **2017**, *136*, 548-560.
39. Zhang, Y.; Guo, X. F.; Si, W. X.; Jia, L. H.; Qian, X. H., Ratiometric and water-soluble fluorescent zinc sensor of carboxamidoquinoline with an alkoxyethylamino chain as receptor. *Organic Letters* **2008**, *10* (3), 473-476.
40. Zhu, J. F.; Yuan, H.; Chan, W. H.; Lee, A. W. M., A FRET fluorescent chemosensor SPAQ for Zn²⁺ based on a dyad bearing spiropyran and 8-aminoquinoline unit. *Tetrahedron Letters* **2010**, *51* (27), 3550-3554.
41. Pal, P.; Rastogi, S. K.; Gibson, C. M.; Aston, D. E.; Branen, A. L.; Bitterwolf, T. E., Fluorescence sensing of zinc(ii) using ordered mesoporous silica material (MCM-41) functionalized with *N*-(quinolin-8-yl)-2-[3-(triethoxysilyl)propylamino]acetamide. *ACS Appl. Mater. Interfaces* **2011**, *3* (2), 279-286.
42. Zhou, X. B.; Lu, Y. G.; Zhu, J. F.; Chan, W. H.; Lee, A. W. M.; Chan, P. S.; Wong, R. N. S.; Mak, N. K., Ratiometric fluorescent Zn²⁺ chemosensor constructed by appending a pair of carboxamidoquinoline on 1,2-diaminocyclohexane scaffold. *Tetrahedron* **2011**, *67* (19), 3412-3419.
43. Zhang, Y.; Guo, X. F.; Jia, L. H.; Xu, S. C.; Xu, Z. H.; Zheng, L. B.; Qian, X. H., Substituent-dependent fluorescent sensors for zinc ions based on carboxamidoquinoline. *Dalton Transactions* **2012**, *41* (38), 11776-11782.
44. Dong, Z. P.; Guo, Y. P.; Tian, X.; Ma, J. T., Quinoline group based fluorescent sensor for detecting zinc ions in aqueous media and its logic gate behaviour. *Journal of Luminescence* **2013**, *134*, 635-639.

45. Goswami, S.; Das, A. K.; Aich, K.; Manna, A.; Maity, S.; Khanra, K.; Bhattacharyya, N., Ratiometric and absolute water-soluble fluorescent tripodal zinc sensor and its application in killing human lung cancer cells. *Analyst* **2013**, *138* (16), 4593-4598.
46. Lee, H. G.; Lee, J. H.; Jang, S. P.; Hwang, I. H.; Kim, S. J.; Kim, Y.; Kim, C.; Harrison, R. G., Zinc selective chemosensors based on the flexible dipicolylamine and quinoline. *Inorganica Chimica Acta* **2013**, *394*, 542-551.
47. Ma, Y.; Wang, F.; Kambam, S.; Chen, X. Q., A quinoline-based fluorescent chemosensor for distinguishing cadmium from zinc ions using cysteine as an auxiliary reagent. *Sensors and Actuators B: Chemical* **2013**, *188*, 1116-1122.
48. Dong, Z.; Le, X.; Zhou, P.; Dong, C.; Ma, J., An "off-on-off" fluorescent probe for the sequential detection of Zn²⁺ and hydrogen sulfide in aqueous solution. *New Journal of Chemistry* **2014**, *38* (4), 1802-1808.
49. Pradhan, A. B.; Mandal, S. K.; Banerjee, S.; Mukherjee, A.; Das, S.; Khuda Bukhsh, A. R.; Saha, A., A highly selective fluorescent sensor for zinc ion based on quinoline platform with potential applications for cell imaging studies. *Polyhedron* **2015**, *94*, 75-82.
50. Mello, J. V.; Finney, N. S., Reversing the discovery paradigm: A new approach to the combinatorial discovery of fluorescent chemosensors. *Journal of the American Chemical Society* **2005**, *127* (29), 10124-10125.
51. Blackwell, H. E., Hitting the SPOT: small-molecule macroarrays advance combinatorial synthesis. *Current Opinion in Chemical Biology* **2006**, *10* (3), 203-212.
52. Hilpert, K.; Winkler, D. F. H.; Hancock, R. E. W., Peptide arrays on cellulose support: SPOT synthesis, a time and cost efficient method for synthesis of large numbers of peptides in a parallel and addressable fashion. *Nature Protocols* **2007**, *2* (6), 1333-1349.
53. Volkmer, R., Synthesis and application of peptide arrays: quo vadis SPOT technology. *Chembiochem* **2009**, *10* (9), 1431-1442.
54. Bowman, M. D.; Jeske, R. C.; Blackwell, H. E., Microwave-accelerated SPOT-synthesis on cellulose supports. *Organic Letters* **2004**, *6* (12), 2019-2022.
55. Lin, Q.; O'Neill, J. C.; Blackwell, H. E., Small molecule macroarray construction via Ugi four-component reactions. *Organic Letters* **2005**, *7* (20), 4455-4458.
56. Bowman, M. D.; Jacobson, M. M.; Blackwell, H. E., Discovery of fluorescent cyanopyridine and deazalumazine dyes using small molecule macroarrays. *Organic Letters* **2006**, *8* (8), 1645-1648.
57. Praneenararat, T.; Geske, G. D.; Blackwell, H. E., Efficient synthesis and evaluation of quorum-sensing modulators using small molecule macroarrays. *Organic Letters* **2009**, *11* (20), 4600-4603.
58. Descalzo, A. B.; Martínez-Mañez, R.; Radeaglia, R.; Rurack, K.; Soto, J., Coupling selectivity with sensitivity in an integrated chemosensor framework: design of a Hg²⁺-responsive probe, operating above 500 nm. *Journal of the American Chemical Society* **2003**, *125* (12), 3418-3419.
59. Rurack, K., Flipping the light switch 'ON' – the design of sensor molecules that show cation-induced fluorescence enhancement with heavy and transition metal ions. *Spectrochimica Acta Part A: Molecular and Biomolecular Spectroscopy* **2001**, *57* (11), 2161-2195.

60. Ressalan, S.; Iyer, C. S. P., Review of spectrofluorimetric methods for the determination of copper, nickel and zinc. *Rev. Anal. Chem.* **2004**, *23* (3), 159-232.
61. Pohl, P., Determination of metal content in honey by atomic absorption and emission spectrometries. *TrAC, Trends Anal. Chem.* **2008**, *28* (1), 117-128.
62. eCFR - Code of Federal Regulations; Bottled water. https://www.ecfr.gov/cgi-bin/text-idx?SID=a345042f6bd438d7949b0270596b60fd&mc=true&node=se21.2.165_1110&rgn=div8 (accessed 21 August 2018).
63. Udhayakumari, D.; Saravanamoorthy, S.; Ashok, M.; Velmathi, S., Simple imine linked colorimetric and fluorescent receptor for sensing Zn²⁺ ions in aqueous medium based on inhibition of ESIPT mechanism. *Tetrahedron Letters* **2011**, *52* (36), 4631-4635.
64. Hu, J.-H.; Sun, Y.; Qi, J.; Li, Q.; Wei, T.-B., A new unsymmetrical azine derivative based on coumarin group as dual-modal sensor for CN⁻ and fluorescent "OFF-ON" for Zn²⁺. *Spectrochimica Acta Part A: Molecular and Biomolecular Spectroscopy* **2017**, *175*, 125-133.
65. Diao, H.; Guo, L.; Liu, W.; Feng, L., A novel polymer probe for Zn(II) detection with ratiometric fluorescence signal. *Spectrochimica Acta Part A: Molecular and Biomolecular Spectroscopy* **2018**, *196*, 274-280.
66. Wen, X.; Wang, Q.; Fan, Z., Highly selective turn-on fluorogenic chemosensor for Zn(II) detection based on aggregation-induced emission. *Journal of Luminescence* **2018**, *194*, 366-373.
67. Pang, B.-j.; Li, C.-r.; Yang, Z.-y., A novel chromone and rhodamine derivative as fluorescent probe for the detection of Zn(II) and Al(III) based on two different mechanisms. *Spectrochimica Acta Part A: Molecular and Biomolecular Spectroscopy* **2018**, *204*, 641-647.
68. Chae, J. B.; Yun, D.; Kim, S.; Lee, H.; Kim, M.; Lim, M. H.; Kim, K.-T.; Kim, C., Fluorescent determination of zinc by a quinoline-based chemosensor in aqueous media and zebrafish. *Spectrochimica Acta Part A: Molecular and Biomolecular Spectroscopy* **2019**, *219*, 74-82.
69. Noh, H.; Phillips, S. T., Fluidic timers for time-dependent, point-of-care assays on paper. *Analytical Chemistry* **2010**, *82* (19), 8071-8078.
70. Phillips, S. T.; Thom, N. K., Three-dimensional, paper-based microfluidic devices containing internal timers for running time-based diagnostic assays. in *microfluidic diagnostics: Methods and Protocols*, Jenkins, G.; Mansfield, C. D., Eds. Humana Press: Totowa, NJ, 2013; pp 185-196.
71. Mako, T. L.; Levenson, A. M.; Levine, M., Ultrasensitive detection of nitrite through implementation of *N*-(1-naphthyl)ethylenediamine-grafted cellulose into a paper-based device. *ACS Sensors* **2020**, *5* (4), 1207-1215.
72. Lou, Y.; Chen, W.; Gan, Y.; Zhou, Y.; Ye, H.; Huan, W.; Zhang, Y., Lateral flow analysis of Pb (II) in green tea integrated with ionic imprinted paper-based chip. *Microchemical Journal* **2022**, *176*, 107235.
73. Mehrotra, S.; Rai, P.; Sharma, S. K., A quick and simple paper-based method for detection of furfural and 5-hydroxymethylfurfural in beverages and fruit juices. *Food Chemistry* **2022**, *377*, 131532.
74. Wang, J.; Li, W.; Ban, L.; Du, W.; Feng, X.; Liu, B.-F., A paper-based device with an adjustable time controller for the rapid determination of tumor biomarkers. *Sensors and Actuators, B: Chemical* **2018**, *254*, 855-862.

75. Wang, R.; Du, X.; Zhai, J.; Xie, X., Distance and color change based hydrogel sensor for visual quantitative determination of buffer concentrations. *ACS Sensors* **2019**, *4* (4), 1017-1022.
76. Phoonsawat, K.; Dungchai, W., Highly sensitive, selective and naked-eye detection of bromide and bromate using distance-based paper analytical device. *Talanta* **2021**, *221*, 121590.
77. Mirzaei, Y.; Gholami, A.; Bordbar, M. M., A distance-based paper sensor for rapid detection of blood lactate concentration using gold nanoparticles synthesized by *Satureja hortensis*. *Sensors and Actuators, B: Chemical* **2021**, *345*, 130445.
78. Vaquer, A.; Barón, E.; de la Rica, R., Wearable analytical platform with enzyme-modulated dynamic range for the simultaneous colorimetric detection of sweat volume and sweat biomarkers. *ACS Sensors* **2021**, *6* (1), 130-136.
79. Pratiwi, R.; Nguyen, M. P.; Ibrahim, S.; Yoshioka, N.; Henry, C. S.; Tjahjono, D. H., A selective distance-based paper analytical device for copper(II) determination using a porphyrin derivative. *Talanta* **2017**, *174*, 493-499.
80. Hofstetter, J. C.; Wydallis, J. B.; Neymark, G.; Reilly Iii, T. H.; Harrington, J.; Henry, C. S., Quantitative colorimetric paper analytical devices based on radial distance measurements for aqueous metal determination. *Analyst* **2018**, *143* (13), 3085-3090.
81. Shibata, H.; Hiruta, Y.; Citterio, D., Fully inkjet-printed distance-based paper microfluidic devices for colorimetric calcium determination using ion-selective optodes. *Analyst* **2019**, *144* (4), 1178-1186.
82. Lai, H.; Li, Z.; Zhu, S.; Cai, L.; Xu, C.; Zhou, Q., Naked-eye detection of aluminum in gastric drugs on a paper-based analytical device. *Journal of Chemical Education* **2020**, *97* (1), 295-299.
83. Xie, X. M.; Smart, T. G., A physiological role for endogenous zinc in rat hippocampal synaptic neurotransmission. *Nature* **1991**, *349* (6309), 521-4.
84. Vallee, B. L.; Falchuk, K. H., The biochemical basis of zinc physiology. *Physiological Reviews* **1993**, *73* (1), 79-118.
85. Berg, J. M.; Shi, Y., The galvanization of biology: a growing appreciation for the roles of zinc. *Science* **1996**, *271* (5252), 1081-1085.
86. Solomons, N. W., Competitive mineral-mineral interaction in the intestine. In *Nutritional Bioavailability of Zinc*, AMERICAN CHEMICAL SOCIETY: 1983; Vol. 210, pp 247-271.
87. Prasad, A. S., Zinc: The biology and therapeutics of an ion. *Annals of Internal Medicine* **1996**, *125* (2), 142-143.
88. Hambidge, M., Human zinc deficiency. *Journal of Nutrition* **2000**, *130* (5), 1344S-1349S.
89. Hojitsiriyant, J.; Chaibuth, P.; Boonkitpatarakul, K.; Ruangpornvisuti, V.; Palaga, T.; Chainok, K.; Sukwattanasinitt, M., Effects of amino proton and denticity of quinoline-pyridine based dyes on Cd²⁺ and Zn²⁺ fluorescence sensing properties. *Journal of Photochemistry and Photobiology A: Chemistry* **2021**, *415*, 113307.
90. Lu, C.; Xu, Z.; Cui, J.; Zhang, R.; Qian, X., Ratiometric and highly selective fluorescent sensor for cadmium under physiological pH range: A new strategy to discriminate cadmium from zinc. *Journal of Organic Chemistry* **2007**, *72* (9), 3554-3557.
91. Canovese, L.; Visentin, F.; Chessa, G.; Levi, C.; Dolmella, A., Synthesis, stability

- constant determination, and structural study of some complexes of a zinc triad containing pyridyl-amine-quinoline and pyridyl-thio-quinoline. *European Journal of Inorganic Chemistry* **2007**, 2007 (23), 3669-3680.
92. Canovesi, L.; Visentin, F.; Chessa, G.; Levi, C.; Nikolov, P., Luminescent complexes of the zinc triad with *N*-substituted 8-amino-quinoline ligands: Synthesis and comparative study on the stability constants and related photophysical properties. *Inorganica Chimica Acta* **2009**, 362 (11), 3925-3933.
93. Hibbert, D. B.; Thordarson, P., The death of the Job plot, transparency, open science and online tools, uncertainty estimation methods and other developments in supramolecular chemistry data analysis. *Chemical Communications* **2016**, 52 (87), 12792-12805.





จุฬาลงกรณ์มหาวิทยาลัย
CHULALONGKORN UNIVERSITY

VITA

NAME Apiwat Promchat

DATE OF BIRTH 10 October 1991

PLACE OF BIRTH Songkhla

INSTITUTIONS ATTENDED Chulalongkorn university

HOME ADDRESS 85 Soi.5 Karnjanavanit Road Korhong Hatyai Songkhla

PUBLICATION Promchat, A., Wongravee, K., Sukwattanasinitt, M., Praneenararat, T. Rapid Discovery and Structure-Property Relationships of Metal-Ion Fluorescent Sensors via Macroarray Synthesis. *Sci Rep* 9, 10390 (2019). <https://doi.org/10.1038/s41598-019-46783-8>

Promchat, A., Praneenararat, T., Sukwattanasinitt, M. Paper-based Fluorescent Sensing Platform Prepared with Tunable Quinoline Ligands for Distance-based Quantification of Zn²⁺. *ACS Sensor* (Submitted)